Prediction of ground vibrations induced by impact driving of dolphin piles in Caland Canal

by

A. Mihalache

to obtain the degree of Master of Science
at the Delft University of Technology,
to be defended publicly on Tuesday December 20, 2016 at 11:00 AM.

Student number:	4420209	
Project duration:	January, 2016 - December, 2016	
Thesis committee:	Prof. Dr. M. A. Hicks,	TU Delft
	Dr. Ir. W. Broere,	TU Delft
	Dr. F. Pisanò,	TU Delft
	Dr. Ir. R. Spruit,	Municipality of Rotterdam
	Ing D. Zandbergen,	Municipality of Rotterdam

TU Delft Delft University of Technology

Gemeente Rotterdam

Preface

This thesis has been performed to conclude the Msc degree in Geo-Engineering at the Faculty of Civil Engineering & Geosciences of TU Delft. This study has been carried out at Public Works of Rotterdam. The completion of this research would not have been possible without the support of several people.

I would like to thank the members of the graduation committee for their valuable guidance throughout the process of completing this thesis. I wish to express my appreciation to my supervisors Rodriaan Spruit and Don Zandbergen, for their feedback and encouragement, for guiding me in the practical aspects and for sharing their knowledge. Special thanks are given to the company for giving me the chance to be involved in this project and to all the employees for providing a great workplace.

I would like to express my gratitude to the Delft University of Technology for offering me the Infrastructures & Mobility DIMI Scholarship, providing me the means and the opportunity to obtain this degree.

Finally, I would like to thank my family and friends for their patience and unconditional support during my thesis.

A. Mihalache
Delft, December 2016

Abstract

Modeling pile driving is a complex process, including vibrations generated from the driving hammer, propagating further through the pile and transfered to the surroundings at the pile-soil interface. The vibrations propagating through the ground interact with structures, potentially causing damage to both underground and structures at surface level or potentially disturbing their inhabitants. Prediction models of ground vibrations focus on estimating the vibrations at ground surface level. The prediction of vibration amplitude at different depths can be more useful at sites with sensitive ground conditions. A model predicting these subsurface vibrations, easily applicable in engineering practice is currently not available or not validated. One of the impediments in developing a model for predicting ground vibrations at different depths is the lack of field data for validation.

The purpose of this thesis is to find a prediction model for ground vibrations at different depths below the surface level. The study is focused on vibrations induced by impact driving of open ended steel tubular piles. A literature study was conducted to gain theoretical knowledge on pile driving and ground vibrations. The model developed by Massarsch and Fellenius [15] was found in the literature and although it predicts ground vibrations at surface level, the adaptation of the model for predicting vibrations at different depths was studied. Vibration measurements from the field test performed in the Caland Canal have been analyzed. The soil profile at the site consists of sandy clay and clay layers overlying a dense sand layer. First, large diameter dolphin piles were driven by a vibratory hammer. When the pile toe reached the dense sand layer, the driving process was changed to impact hammering in order to change the characteristics of the vibrations transmitted through the soil. The pile driving was extensively monitored and particle velocities were recorded by 3D geophones placed up to depths of NAP -22 m (9.50 m embedment depth).

The prediction model of Massarsch and Fellenius [15] makes a distinction between the velocities of different wave types emitted from piles during impact driving. These waves are the shear waves propagating with a cylindrical wave front along the pile shaft and compression waves emitted at the pile toe, propagating with a spherical wave front. Surface waves resulting from wave reflection at ground surface are not considered in this thesis, as this research focuses on vibrations at different depths. Wave velocities are calculated from the hammer input energy, taking into account ground conditions and considering the vibration transmission efficacy which defines the amount of energy transmitted at the pile-soil interface. The model is adapted for open ended tubular piles. Due to the large diameter of the dolphin piles and the present soil conditions, the soil plugging effect and its contribution to dynamic soil resistance at the pile toe are ignored. Dynamic soil resistance at the pile toe is considered the source of spherical waves, while the soil resistance along the pile shaft is the source of cylindrical waves. The ratio between the pile cross section and the total area delimited by the external diameter is taken into account when calculating the dynamic soil resistance at the pile toe, resulting particle velocities of spherical waves smaller than unity. Therefore the cylindrical waves propagating from the pile shaft are considered the main source of ground vibrations.

The results of the prediction model have been compared to vibration values measured in the field test. The predicted vibration amplitudes are a good approximation of the vibration levels measured in the sandy clay and clay layers. The predicted vibrations are of higher magnitude compared to the amplitude of vibrations recorded by the sensors placed in the dense sand layer.

Contents

1 Introduction

1.1. Background

Ground vibrations are generated by natural phenomena such as earthquakes or by human activities. Vibrations from human activities can arise from different sources, including construction works, traffic, machines and explosions. The intensity of man-made vibrations depends on the source of vibrations and is generally lower than the intensity of an earthquake shaking. This thesis is limited to vibrations induced by pile driving. Vibrations are generated by the vibratory hammer or impact hammer and transmitted to the pile. At the soil-pile interface, the vibrations propagate into the surrounding soil, leading to changes of soil properties such as the arrangement of grains, changes of soil density and changes of the stress state. The propagation of vibrations through the soil is a complex process and it is difficult to describe the soil behaviour around the pile.

To predict vibrations at surface level, different models have been developed, focusing on the impact of vibrations emitted from sheet pile driving and pile driving in urban areas. Most of the research was conducted in urban area because of the damage the vibrations can cause to adjacent buildings, from either ground shaking or from settlements of the soil under the foundations. The goal of the prediction models for surface waves is to help indicate the difference between tolerable levels of vibrations and vibrations that cause damage to the structures in the proximity of pile driving. Several prediction models are summarized by Deckner [6] and the conclusion of the mentioned research was that the models are not reliable. The overestimation of the environmental impact of ground vibrations induced by pile driving can lead to higher costs and the choice of construction method could be limited.

Electronic monitoring systems have been developed and sensors placed in the ground, on the driving hammer or on the pile can measure different parameters such as the amplitude of vibrations. The information available from the monitoring system can be used to control the driving process or it can be post-processed and used to verify the anticipated level of vibrations.

The prediction model developed by Massarsch and Fellenius [15] is presented in the literature review and represents a starting point of the research in this thesis. The model has been adapted to open ended tubular piles and assumptions are made in order to predict the vibrations at different depths. The vibration velocity measurements from the field test at Caland Canal provide empirical data for the verification of the prediction model.

1.2. Problem statement

The degree of uncertainty related to prediction of the soil behaviour increases in case of vibratory pile driving in slopes. Factors of safety are used to cover the uncertainties when assessing slope stability during pile driving. As a consequence, the calculations will not be favorable for driving piles in slopes at certain sites, while the experience shows that in the past such projects were possible.

No easy to apply prediction model for vibrations below ground level is available. For projects such as the construction of new dolphin configurations in the Caland Canal, the ground vibrations caused by pile driving are expected to exceed safety values and the slope stability could be compromised. The riverbank slope stability was maintained during the installation of dolphin piles in the Caland Canal, but not for every project of pile driving in sensitive soil conditions there is the possibility of extensive monitoring of real-time ground vibrations and accelerations development, at different depths and at different distances from the pile.

1.3. Main objective

The main objective of the research is to develop a prediction model that can be easily used for estimating the level of vibrations due to pile driving. The research is focused on the vibrations transmitted in the ground and not at the surface level.

Another important aspect of the research is related to vibrations monitoring equipment and the processing of measurement data. The experience of working with the dataset recorded during the field study at Caland Canal can give indications of how to make the data recording more efficient for future vibration monitoring projects. The post processing of the measurement data is compared with the output of the real-time monitoring system developed by the Municipality of Rotterdam in order to check its accuracy. Measurements of vibration velocities recorded during pile driving, not only at the surface level, but at different depths, can be valuable for further research regarding the transfer of vibrations and the interaction of the elements in the hammer-pile-soil system.

The current research is limited to a simplified prediction model, assuming the soil an elastic medium and not considering the plastic/elasto-plastic zone in the proximity of the pile.

1.4. Research questions

From the above mentioned objective, the following questions are defined:

- How can ground vibrations induced by pile driving be predicted at different depths?
- How can an existing prediction model for surface ground vibrations be modified to calculating vibrations at different depths below the surface level?
- What are the parameters that will influence the prediction model?

1.5. Outline master thesis

In this section the structure of the report is summarized. The research starts with a literature review presented in **Chapter 2**. The literature review aims to provide background knowledge of basic dynamics. Vibratory driving and impact driving techniques are also presented. The last section of Chapter 2 summarizes the prediction model of Massarsch and Fellenius [15]. **Chapter 3** provides information about the field study, regarding the driving equipment, the site conditions and the monitoring equipment. **Chapter 4** shows the results of the vibration measurements interpretation. **Chapter 5** provides the results of the vibrations prediction model presented in the literature review. The conclusions and the recommendations for future research are summarized in **Chapter 6**. Additional information about the field study and about the vibrations measurements are provided in **Appendices**.

2 Literature review

2.1. Introduction

The literature review has the aim of providing basic knowledge about soil dynamics and vibrations in order to get a better understanding of the process of pile driving and generation and propagation of the vibrations. The chapter begins with a description of general dynamic theory, providing information about vibrations and wave propagation. The pile driving mechanism is studied, presenting both vibratory and impact driving techniques. The main differences between vibratory and impact hammers are discussed. The monitoring of ground vibration is briefly described. In addition, the prediction model for ground vibrations developed by Massarsch and Fellenius [15] is presented.

2.2. General dynamics of vibratory systems

In this section it is presented basic theory of dynamics for vibratory systems. In order to understand the ground vibrations due to pile driving, definitions of common terms in soil dynamics are introduced. The section continues with describing the vibratory motions and the general wave propagation.

2.2.1. Parameters

Some important parameters used in soil dynamics to describe vibratory motion are:

- Period (T) represents the time a particle or object needs for a full motion circle. The angular frequency, ω, is describing the rate of oscillation in radians per unit time.

$$T = \frac{2\pi}{\omega} \qquad [s] \tag{2.1}$$

- Frequency (f) is the number of vibrations or cycles occurring over a certain period of time.

$$f = \frac{1}{T} \qquad [Hz] \tag{2.2}$$

- Amplitude (A) is the displacement from the the equilibrium position. The displacement from the zero line is called single amplitude and the peak-to-peak displacement is referred to as double amplitude ($2A$). The magnitude of particle velocity an acceleration can be also defined by the amplitude expression.
- Wavelength (λ) represents the distance between successive crests of a wave. The wave length is defined by the ratio between the wave velocity divided by frequency.

$$\lambda = \frac{c}{f} \qquad [m] \tag{2.3}$$

- Wave velocity (c) is defined by the ratio of change in distance with respect to time.
- Particle velocity (v) is the ratio of the change in vibration displacement to the change in time.
- Phase angle (ϕ, measured in radians) measures the time in which the peaks are shifted relative to the peaks of a pure sinus function.

2.2.2. Vibratory motion

The simple vibratory motion has a vertical sinusoidal shape and it is described using a harmonic function in terms of displacement variation as a function of time, equation 2.4. The velocity is obtained by differentiating the equation of displacement, as shown in equation 2.5. The acceleration is the second order derivative of

the displacement equation, equation 2.6. The single amplitude A (see figure 2.1), the angular frequency (ω) and the phase angle (ϕ) are the parameters that define the harmonic vibratory motion.

$$u(t) = Asin(\omega t + \phi) \qquad [m] \tag{2.4}$$

$$\dot{u}(t) = \frac{du}{dt} = A\omega cos(\omega t + \phi) \qquad [m/s] \tag{2.5}$$

$$\ddot{u}(t) = \frac{d^2u}{dt^2} = -A\omega^2 sin(\omega t + \phi) \qquad [m/s^2] \tag{2.6}$$

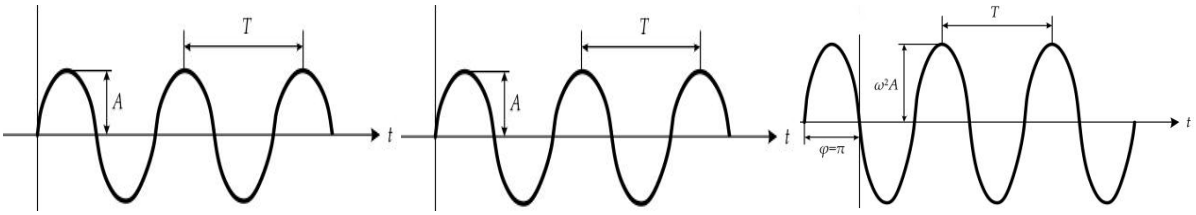

(a) Displacement, $u = Asin\omega t$ (b) Velocity, $\dot{u} = A\omega cos\omega t$ (c) Acceleration, $\ddot{u} = A\omega^2 sin\omega t$

Figure 2.1: Parameters describing vibratory motion (from [6])

In reality, the vibratory motion is more complex and the motion is defined by the source of vibrations. The vibratory motion can be periodic, transient or random. The periodic motion is repeated after a period T, figure 2.2a. The transient motion starts at high intensity and it decreases gradually, as shown in figure 2.2b. For random motions the pattern does not repeat, figure 2.2c.

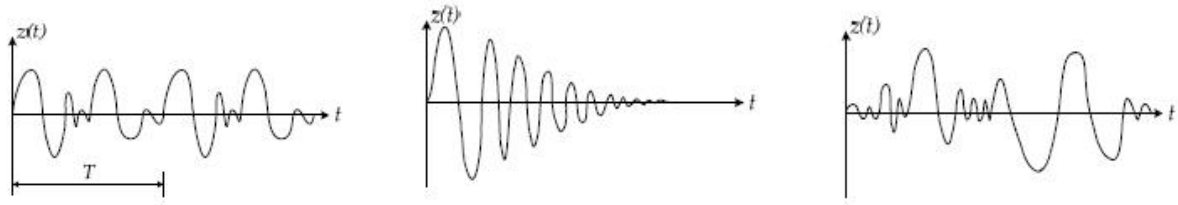

(a) Periodic motion (b) Transient motion (c) Random motion

Figure 2.2: Types of vibratory motion (from [6])

In the orthogonal coordinate system, the motion is measured in two horizontal perpendicular directions (a longitudinal and a transverse direction) and one vertical direction.

2.2.3. Soil dynamic parameters

The factors that define the dynamic loading are related to the speed of loading and number of loading cycles. The situations for which the load is applied for less than tens of a second define the dynamic problems. For such cases the load is applied repetitively, with a certain frequency. The soil susceptibility to deformations depends on the degree of the shear strains magnitude to which the soil is subjected. For shear strains lower than 10^{-5} (0.001%) the soil behaves purely elastic. These small strains are related to the propagation of vibrations. For the range of strains 10^{-4} to 10^{-2} the soil behaves elasto-plastic and irreversible deformations occur. The loading speed has no influence when the stains are lower than 10^{-3} [8].

The response of soil to vibrations is determined by the shear modulus G, the Poisson ratio ν and the soil density ρ. The value of the shear modulus is related to the elasticity modulus and Poisson's ratio and can be calculated according to elastic theory, according to equation 2.7. Poisson's ratio is defined by the strain changes in transversal and axial directions during compression or tension loading. The soil density represents the soil mass per unit volume.

$$G = \frac{E}{2(1+\nu)} \qquad [kPa] \tag{2.7}$$

The soil density and the Poisson ratio have a rather limited range of values. The relative density varies from 1600 kg/m^3 for dry soil to about 2000 kg/m^3 for saturated soil. The Poisson ratio varies from 0.3 for sands to 0.5 for clays. The shear modulus is the most important parameter and its magnitude is influenced by the level of shear strains [29].

2.2.4. The propagation of waves

Waves are caused by forced motions of a deformable medium. With the deformation of the elements of the medium, the disturbance or wave is transmitted from point to point and propagate through the medium. The propagation of waves in soils can be modeled as a simplified phenomenon based on the theory of elasticity and considering the soil an infinite, isotropic homogeneous, elastic solid. In reality, the soil characteristics and their influence on wave propagation differs from those considered for ideal solids.
The waves propagating through a medium are classified as body waves and surface waves. The body waves are waves at depth, traveling inside the medium. The surface waves occur when the body waves reach the surface. The wave carries along energy because the wave motion is passed on from a particle to another and not by the motion of the entire medium. The mechanical energy in the system contains kinetic energy from vibrations of wave particles and potential energy from strain energy in elastic deformations.

2.2.4.1. Body waves

Body waves originate from deep vibration sources such as earthquakes, pile driving, soil compaction or blasting in mining industries [26]. Body waves are classified as compression waves or shear waves, depending on the direction of propagation, as illustrated in figure 2.3.

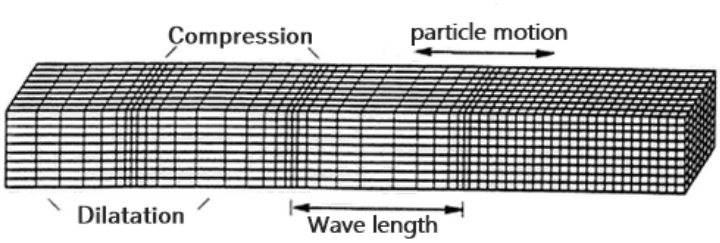

(a) Compression (P-) wave

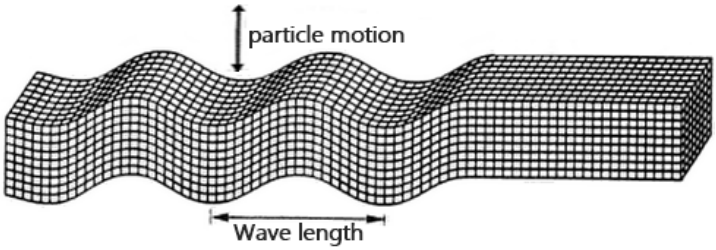

(b) Shear (S-) wave

Figure 2.3: Body waves (modified after [32])

Compression waves

Compression waves are associated to changes in volume from successive compression and dilatation. Compression and expansion waves can be referred to as longitudinal waves, because the particle displacements are parallel to the direction of propagation [4]. Compression waves or longitudinal waves are also known as dilational waves, irrotational waves and primary waves, shortly P-waves [27]. For an infinite medium, the compression wave velocity is expressed as shown in equation 2.8.

$$c_p = \sqrt{\frac{2G(1-\nu)}{\rho(1-2\nu)}} = \sqrt{\frac{E(1-\nu)}{\rho(1-2\nu)(1+\nu)}} \qquad [m/s] \tag{2.8}$$

Compression waves travel through both solid and liquid materials. For saturated soils, water modifies the characteristics of the wave propagation. The water transmits the P-waves at higher velocity compared to the

soil [24]. The compression wave velocity in saturated soils can be considered the velocity of compression waves in water, which is assumed $1400 m/s$ [15] .

Shear waves

The propagation of shear waves induces only particle displacements that are perpendicular to the direction of wave propagation [4]. Therefore shear waves are called transverse waves. Shear waves can be called distortional waves, equivolumial waves and secondary waves (S-wave). [27]. Unlike the compression waves, the shear waves are associated with changes in shape of elements in the medium, but the volume does not change. The S-wave velocity can be calculated from equation 2.9.

$$c_s = \sqrt{\frac{G}{\rho}} = \sqrt{\frac{E}{2\rho(1-\nu)}} \qquad [m/s] \tag{2.9}$$

From equations 2.8 and 2.9 it can be concluded that the propagation velocities of P-waves and S-waves depend only on the bulk density and on the elastic properties of the soil. The ration between wave velocities given in equation 2.10 is always greater than unity, because Poisson's ratio is smaller than 0.5. Therefore the compression (P-) waves propagate with a higher velocity than shear (S-) waves and the difference is proportional to the Poisson's ratio value.

$$\frac{c_p}{c_s} = \sqrt{\frac{2(1-\nu)}{1-2\nu}} < 1 \tag{2.10}$$

Because of the difference between the values of Poisson's ratios for different soils, the P-wave velocity is higher in clayey soils than in sandy soils [4]. The shear wave velocity is reduced after a certain level of strain is reached. This reduction of c_s is more pronounced in soils with low plasticity because soil softening depends on the plasticity [16]. Table 2.1 gives a range of approximate values for compression and shear wave velocities.

Table 2.1: Compression (P-) and shear (S-) wave velocities at small strains for different types of soils, from [15]

Soil type	P-wave velocity $[m/s]$	S-wave velocity $[m/s]$
Dry gravel	500 - 1000	250 - 400
Saturated gravel	1450	300 - 400
Dry sand	300 - 600	150 - 200
Saturated sand	1450	150 - 250
Silts and stiff clays	1450	100 - 200
Plastic clay	1450	50 - 100
Organic soils	1450	30 - 50
Water	1450	0

2.2.4.2. Surface waves

Surface waves occur when the body waves reach the surface. The two types of surface waves are Rayleigh (R-) waves and Love (L-) waves . R-waves are generated by the interaction of the P-waves and the vertical component of the S-waves with the surface. The particle motion has both vertical and horizontal components. L-waves occur as a result of the interaction between P-waves and the horizontal component of the S-waves with a softer layer. The particle motion has only the horizontal component. It is considered that R-waves become the predominant type of waves at increasing distance from the vibrations source because they have a smaller attenuation ratio and they convey a high percentage of the vibration energy. However, there is evidence that the amount of energy carried by the body waves an R-waves depends on the frequency of vibrations [2].

2.2.4.3. Waves propagation attenuation

The decrease of vibration amplitude in time is called damping. The wave propagation is attenuated by the extension of the wave front with the increase in distance from the source (geometric damping) and by the

soil internal damping of the energy (material damping). The geometric damping is described by the equation 2.11. The coefficient n depends on the wave type.

$$A_2 = A_1 \left(\frac{r_1}{r_2} \right)^n \qquad [m] \tag{2.11}$$

Where:

- A_1 = amplitude of motion at distance r_1 from the source [m]
- A_2 = amplitude of motion at distance r_2 from the source [m]
- n = 1/2 for R-waves, 1 for body waves and 2 for body waves at surface [-]

The material damping is usually described by the damping ratio, D. The damping ratio is frequency and vibration amplitude dependent. The material damping is described by equation 2.12.

$$A_2 = A_1 e^{-\alpha(r_2 - r_1)} \qquad [m] \tag{2.12}$$

Where:

- α = absorption coefficient [m^{-1}]

The absorption (attenuation) coefficient can be estimated from the material damping, vibration frequency and from the wave propagation velocity. The absorption coefficient is positively correlated to the vibration frequency and negatively correlated to the wave velocity. This means that for waves with low frequency the damping is less than for waves with high frequency. The absorption coefficient varies also with the properties of the materials and it has lower values for harder materials than for softer materials (sand will have less damping that clay). Equation 2.13 describes the combined effects of geometrical and material damping. The equation is valid for homogeneous conditions at a great distance from a deeper firm layer.

$$A_2 = A_1 \sqrt{\frac{r_1}{r_2}} e^{-\alpha(r_2 - r_1)} \qquad [m] \tag{2.13}$$

The equation describing waves propagation attenuation can be used to calculate the amplitude at a certain point, only when the amplitude of vibrations is known at a smaller distance from the source. The fact that the amplitude of vibrations has to be know at a certain distance from the source represents a limitation of the equation 2.13. When considering a pure elastic medium there will be no energy absorption and the coefficient of absorption will be zero. As a consequence, the coefficient α is a soil constant that determines the deviation of the soil properties from the properties of an pure elastic medium.

2.2.5. Energy transmission in elastic medium

The total energy density contained in a wave length is calculated according to equation 2.14 [7]. From this equation, the maximum vibration energy can be determined for different types of waves. The difference is made by the wave front area. Shear waves propagating from the pile shaft have a cylindrical wave front, calculated as shown in equation 2.15. The height of the cylinder is determined by the length of the stress wave propagating through the pile, L_w. The P-waves emitted at the pile toe have a spherical wave front, given in equation 2.16. The cylindrical waves propagation and wave front can be visualized in figure 2.4 and the spherical waves in figure 2.5. The last step is to determine the particle velocity of the different waves at a certain distance from the source.

$$W = \frac{1}{2} \rho v_0^2 A \lambda \quad [J] \tag{2.14}$$

$$A_{S-wave} = 2\pi L_w r \quad [m^2] \tag{2.15}$$

$$A_{P-wave} = 4\pi r^2 \quad [m^2] \tag{2.16}$$

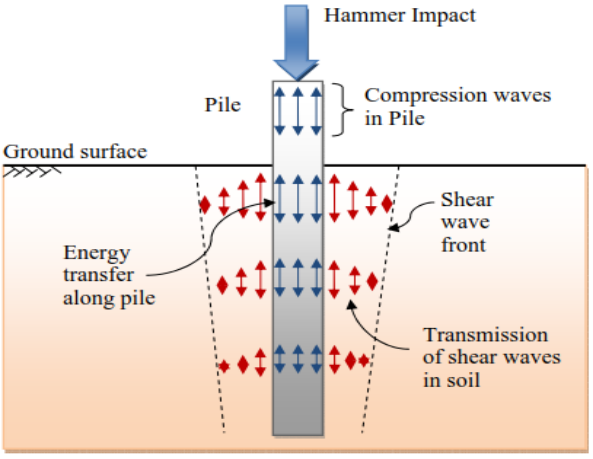

Figure 2.4: Generation of cylindrical waves along the pile shaft, from [25]

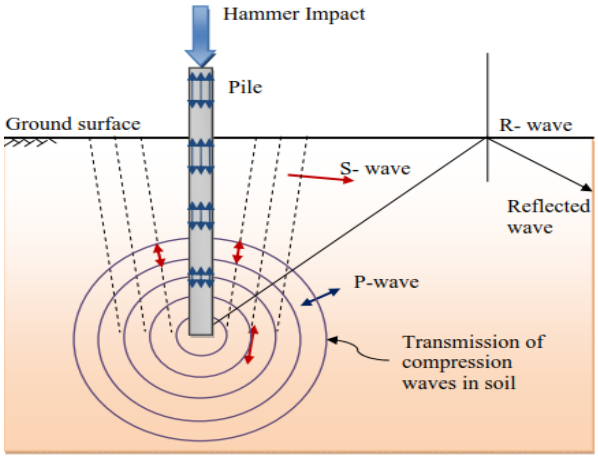

Figure 2.5: Spherical waves emitted at the pile toe, from [25]

The energy density at a distance r from the pile, W_r, equals the energy at the source, considered W_0 [15]. This is expressed in equation 2.17.

$$W_0 = W_r = \frac{1}{2}\rho v^2 \lambda A \tag{2.17}$$

2.2.5.1. Cylindrical waves

The vertical component of the cylindrical waves velocity is obtained by substituting equation 2.15 in equation 2.17. This is given in equation 2.18.

$$W_0 = \frac{1}{2}\rho v^2 \lambda (2\pi L_w r)$$

$$v_c = \sqrt{\frac{W_0}{\rho\lambda\pi L_w r}} = \frac{1}{\sqrt{\rho\lambda\pi L_w}}\sqrt{\frac{W_0}{r}} = k_c\sqrt{\frac{W_0}{r}} \quad [mm/s] \tag{2.18}$$

2.2.5.2. Spherical waves

The same principle as for cylindrical waves is applied in order to obtain the velocity of spherical waves. The result is given in equation 2.19.

$$W_0 = \frac{1}{2}\rho v^2 \lambda (4\pi r^2)$$

$$v_s = \sqrt{\frac{W_0}{\rho\lambda 2\pi r^2}} = \frac{1}{\sqrt{2\pi\rho\lambda}}\frac{\sqrt{W_0}}{r} = k_c\frac{\sqrt{W_0}}{r} \quad [mm/s] \tag{2.19}$$

2.2.6. Ground conditions influence on vibrations propagation

The velocity of waves propagation is influenced by the characteristics of the material the waves travel through and by the type of wave. The following factors have an influence on the ground waves propagation velocities: effective stress, void ratio, Poisson's ratio, stratification moisture content, temperature. The P-waves and S-waves velocities depend on the density and of the stiffness of the material. The soil has higher stiffness in compression than in shear so P-waves have a higher velocity than S-waves. During pile driving in coarse-grained soils, when compression occurs at the pile tip level, the propagation velocity of P-waves increase; but it can decrease in saturated fine-grained soils due to increase of pore water pressures. The void ratio influences the propagation velocity of S-waves. The increase of void ratio means a decrease in density which is associated with the increase of the rate of strain accumulation.

The ground water conditions influence the propagation of compression waves only since the water does not have shear stiffness. For P-waves, the propagation velocity through loose soils depends on the degree of saturation. S-waves and R-waves are not influenced by the ground water. The propagation velocity of shear waves depends on the strain level since the shear modulus is one of the parameters determining the shear wave velocity.

2.3. Pile driving

The vibratory and impact pile driving methods are presented in this section. For both driving techniques the principles of operation and the interaction between hammers and piles are discussed. The section includes a summary of the differences between vibratory hammers and impact hammers.

2.3.1. Vibratory pile driving

A typical vibratory hammer mechanical configuration and the main components of the hammer are shown in figure 2.6. Vibratory hammers were first developed to function on electric power [11]. Nowadays, vibratory hammers are available as driven by both electric power and hydraulic power, the last ones being more common because they are equipped with a smaller and lighter engine. The equipment is used for driving and extracting sheet piled walls, piles or pipes by vertical vibrations. For piles there is less common to use this technique because it is difficult to control and achieve the bearing capacity [6].

2.3.1.1. Principle of operation

The eccentric masses incorporated in the oscillator block are rotating in opposite directions, such that the horizontal components of the generated centrifugal forces have always opposite signs. Only the vertical components are added, generating vertical vibrations. The basics of this principle are shown in figure 2.7b. The amplitude of the generated vibrations is a function of the eccentric moment and of the total dynamic mass [11].

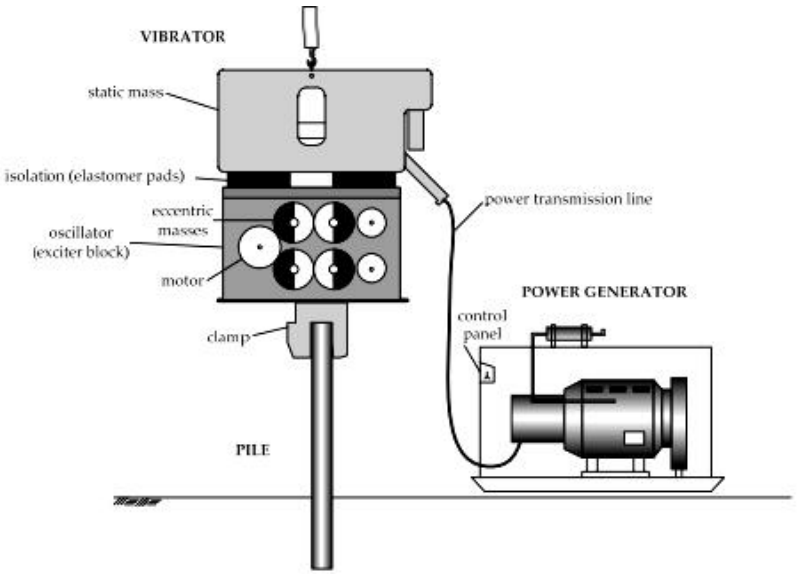

Figure 2.6: Free hanging vibratory hammer equipment (from [6])

The static moment represents the product of the mass of the eccentric masses, G_{ecc}, and the distance between the rotation axis and the center of gravity of the eccentric masses, r.

$$M_{ecc} = G_{ecc} r \qquad [kNm] \tag{2.20}$$

The maximum centrifugal force,F , is calculated from the static moment and the circular frequency of the eccentric masses, ω, and is acting only in the vertical direction. The circular frequency is correlated to the vibration frequency and so the centrifugal force is a function of the vibratory frequency. The principle of operation is shown in figure 2.7a.

$$F = M_{ecc}\omega^2 \qquad [kN] \tag{2.21}$$

The mass of the oscillating parts (vibrator, clamp and pile – the components that move in longitudinal direction) is called the total dynamic mass, G_{dyn}, equation 2.22.

$$G_{dyn} = G_v + G_c + G_p \qquad [kN] \tag{2.22}$$

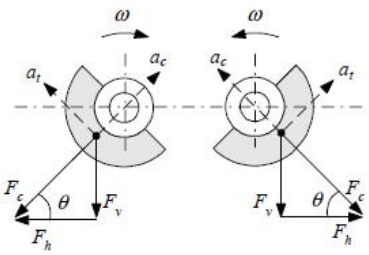

(a) Centrifugal forces (from [30])

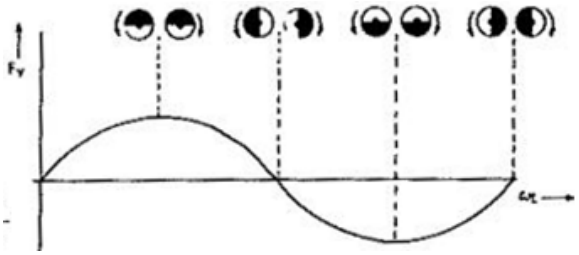

(b) Sinusoidal motion (from [11])

Figure 2.7: Principle of operation for a vibratory hammer

The displacement amplitude, A_d, is defined by the ratio between the static moment and the total dynamic mass for the case of free hanging. Thus, the displacement amplitude is not depending on the driving force frequency. When the pile is inserted in the ground, the displacement amplitude represents the difference between the amplitude of ground vibrations and the amplitude of the pile. The resonance phenomenon occurs thus when the pile and the soil surrounding the pile oscillate in the same phase and the relative displacement amplitude has a small value. The vibrations will be then efficiently transmitted into the ground [17].

$$A_d = 2\frac{M_{ecc}}{G_{dyn}} \qquad [m] \tag{2.23}$$

Modern vibrators are able to operate with variable frequencies and variable static eccentric moments, function of the rotating masses arrangements and their relative positions [17].

2.3.1.2. Forces acting on the pile during vibratory piling

the following forces act on a pile during vibratory driving process (from [19], [6]):

- The weight of the pile, G_p;
- The weight of the vibrator (including the static mass, the weight of the clamps and the weight of the vibrator), G_v;
- The centrifugal (dynamic) force from the vibrator, F_{dyn};
- The pile tip resistance, R_{typ};
- The friction resistance along the pile shaft, $R_s = R_{si} + R_{se}$;
- The inertia force of the pile, $F(t)$.

The dynamic force, F_{dyn}, has a sinusoidal shape and it is a function of time and of the driving frequency. The penetration process contains both downward and upward movements. This leads to a variation of the shaft resistance, R_s, from positive to negative values. The inertia force (net force) is induced by the movement of the pile mass and of the vibrator. This force is a function of time and it has the following expressions:

- Downward movement:

$$F(t) = ma = G_p + G_v + F_{dyn} - R_{tip} - R_s \qquad [kN] \tag{2.24}$$

- Upward movement:

$$F(t) = ma = G_p + G_v - F_{dyn} + R_s \qquad [kN] \tag{2.25}$$

2.3.1.3. Vibrations in piles

The harmonic function in time of the centrifugal force, equation 2.21, has a sinusoidal shape and it is described by equation 2.26.

$$F(t) = M_{ecc}\omega^2 \sin(\omega t) \qquad [kN] \tag{2.26}$$

The system vibratory hammer-pile can be considered a rigid body. The system movement is described by equation 2.26 and the components have the same displacement amplitude and acceleration. A pile shorter than 10 m is considered to oscillate as a rigid body. Another rule of thumb for obtaining the rigid behaviour of the pile takes into account the period of the driving frequency and the time the vibrations travel through the pile [11], equation 2.27.

$$\frac{T}{4} \geq t\left(t = \frac{4L_p}{c_p}\right) \tag{2.27}$$

2.3.2. Impact pile driving

A basic configuration of an impact hammer consists of a base machine which has attached a stabilizer for holding the steering of the hammer. Impact hammers include different types of hammers such as drop hammer, diesel hammer, pneumatic hammer and hydraulic hammer.
For drop hammers, a weight (ram) is lifted up to a certain height and released onto the pile. For diesel hammers, a free piston inside a cylinder is lifted by an explosion. The last two function in the same way as the drop hammer, but the ram lifting and downward acceleration is helped by cylinders and pistons (pneumatic hammer) and by hydraulic devices (hydraulic hammer).
The pile driving is realized as the hammer strikes the pile head with a certain impact velocity. The vibrations produced by one blow are not regular and generally they die away before the next blow. For some types of hammers, the vibrations are not completely dissipated before the next blow [6].

2.3.2.1. Energy transfer

When the hammer hits the pile head, the energy is transfered to the pile and a compression wave is generated within the pile. The wave travels to the pile toe where part of it is reflected and the rest is transmitted to the surrounding soil [15]. A stress wave is the result of the difference in stresses at pile-soil interface. Particle motions are generated for creating equilibrium between stresses and inertia forces [23].
A theoretical approach to describe the dynamic soil-pile interaction is developed by Massarsch and Fellenius in [15]. The authors considered a simplified model, assuming that no energy is lost during the falling phase of the ram. Another simplification is related to the vibratory motion, considering velocities as rectangular waves.
The propagation of the stress wave in the pile is described in figure 2.8. The particle velocity of dropping ram, v_0, is estimated from the height of fall, h, and the gravitational acceleration, as shown in equation 2.28.

$$v_0 = \sqrt{2gh} \quad [m/s] \tag{2.28}$$

For pile driving, the transfer and propagation of vibrations in the pile are governed by the pile impedance.

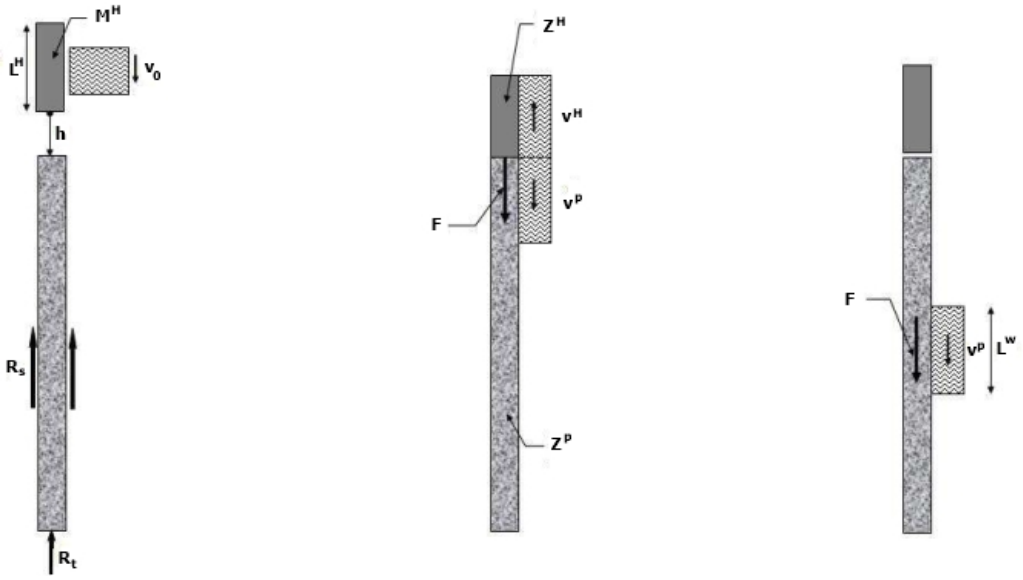

(a) Before the impact (b) At impact (c) After impact

Figure 2.8: Stress wave generation and propagation in the pile during impact driving (from [15])

The impedance represents the ratio between normal force and the particle velocity, $Z = F/v_p$, and it is determined by the product of cross-section area, particle velocity and material density, 2.29.

$$Z^P = A^P c^P \rho^P \quad [Ns/m] \tag{2.29}$$

Where:

- Z^P = impedance of the pile $[Ns/m]$

- A^P = pile cross section area $[m^2]$
- c^P = stress wave velocity in the pile $[m/s]$
- ρ^P = pile material density $[kg/m^3]$

The axial force transmitted to the pile is calculated as the product between the pile impedance and the particle velocity of the pile, equation 2.30.

$$F = Z^P v^P \quad [N] \tag{2.30}$$

The particle velocity of the pile, v^P can be calculated from the equilibrium of forces. At the impact, figure 2.8b, the force in the pile and the hammer are equal. This relation is given in equation 2.31, where the force in the hammer is calculated in the same way as the force in the pile, equation 2.30. Furthermore, at the contact surface, the the pile head velocity increases, while the hammer velocity decreases and is directed upward, as indicated in figure 2.8b. The decrease is given by the particle velocity of the stress wave which is reflected back in the hammer. Applying the same concept as for the forces, the reduced hammer particle velocity will be equal with the pile head particle velocity, equation 2.32.

$$Z^H v^H = Z^P v^P \tag{2.31}$$

$$v_0 - v^H = v^P \tag{2.32}$$

Combining equations 2.31 and 2.32, the particle velocity in pile can be calculated in terms of hammer velocity at impact, the pile impedance and the hammer impedance. This result is given in equation 2.33.

$$v^P = \frac{v_0}{1 + \frac{Z^P}{Z^H}} \quad [m/s] \tag{2.33}$$

From equations 2.30 and 2.33, the peak force imparted to pile can be now calculated as a function of the velocity of the hammer at impact and impedance relationship, equation 2.34. This equation is valid for the wave traveling downward in the pile and it holds until the wave reflected at pile toe arrives at the pile head [22]. The same derivation of the force in pile is shown in reference [5].

$$F = \frac{Z^P Z^H}{Z^H + Z^P} v_0 \quad [N] \tag{2.34}$$

The duration of contact between hammer and pile represents the time the stress wave travels upwards in the hammer and returns, equation 2.35. The hammer end is considered in contact with a material with the cross section and the impedance equal to zero. In this case, the return wave will have the speed equal to the speed of the compressing wave traveling upward, but it has opposite sign (tension wave), [7]. Thus, duration of impact is mainly influenced by the length of the hammer.

$$t = \frac{2L^H}{c^H} \quad [s] \tag{2.35}$$

Where:

- L^H = length of the hammer $[m]$
- c^H = stress wave velocity in the hammer $[m/s]$

The length of the stress wave in the pile is determined by the speed of stress wave in pile and by the impact duration, equation 2.36. The result is of importance because the length of the stress wave equivalent to the length of the pile over which the vibrations are transmitted to the surrounding soil.

$$L^W = t c^P = 2L^H \frac{c^P}{c^H} \quad [m] \tag{2.36}$$

Where:

- L^W = length of the stress wave in pile $[m]$
- t = duration of impact $[s]$

2.3.3. Differences between impact pile driving and vibratory pile driving

Differences between the two driving methods are related to the frequency of operation, to the connection between hammer-pile and to the way the energy is transmitted into the soil [11]. Frequency of excitation for vibratory hammers is lower than for impact hammers, reaching values up to 50 Hz. Impact hammers can reach driving frequencies up to 300 Hz [6]. The connection between pile and vibratory hammer is rigid, the pile becoming part of the vibratory exciter. For this case, energy is transfered to soil permanently and over the length of the pile. For the impact driving, the pile does not have a tension connection with the hammer and the energy supplied to soil is intermittent. The vibrations generated during vibratory driving are continuous, while the vibrations generated during impact driving are transient.
Another difference between the two pile driving methods is related to the penetration resistance. During the impact driving the soil resistance acts only on the positive direction, considered downwards. For the vibratory driving, the shaft resistance varies from positive to negative and the soil resistance at pile tip is either positive or zero, as a consequence of rigid connection between the vibratory hammer and the pile.
After extensive field tests, Massarsch and Westerberg concluded in [18] that the transmission of ground vibrations in the surrounding soil is influenced by the type of vibrator, type of pile and by the dynamic properties of the soil. In some cases, vibratory driven piles are restriked with an impact hammer due to uncertainties in estimating the bearing capacity. With the impact driving, the pile can reach the design bearing capacity [31].

2.3.4. Interaction between pile and soil during pile driving

The vibratory pile driving method is known to perform best in loose non-cohesive soils because the dynamic soil resistance has a higher decrease during pile installation than in moderately stiff saturated clays or in dense sands or gravel . When soil is subjected to vibrations, it temporarily changes/reduces the resistance. In non-cohesive soils, the driveability is influenced by the factors contributing to the reduction of soil resistance. These factors are: the induced cyclic loading on soil grains, the initial relative density, local liquefaction, the higher density of dense soil layers. Other factors that have lower influence on the driveability are the angle of internal friction, the grain size and the content of fine grains [30].
The relative acceleration amplitude is correlated to the void ratio which relates to the densification occurring during pile driving. Barkan, [4], performed experiments to show that a certain relative acceleration level in loose soils lead to densification to a corresponding void ratio. Local sand liquefaction due to vibratory driving is related to the excess pore pressure occurring during pile installation. Hence, the presence of water in non-cohesive soils is a positive influence on pile driveability.

2.3.4.1. Dynamic soil resistance

The pile driving process generates dynamic soil resistance along the pile shaft and at the pile toe during the propagation of the stress wave. The dynamic resistance is influenced by the soil impedance and it has an important role in vibrations emission [15].

Dynamic soil resistance along pile shaft

The dynamic soil resistance generated along the pile shaft is the source of cylindrical waves which propagate around the shaft. Dynamic shaft resistance is calculated from the specific soil impedance, contact area between pile shaft and soil and the particle velocity of the pile [15], equation 2.37.

$$R_S = z_S v^P A_{contact} \tag{2.37}$$

Where:

- R_S = dynamic soil resistance along the shaft $[N]$
- z_S = specific soil impedance $[Ns/m^3]$
- v^P = particle velocity in the pile $[m/s]$
- $A_{contact}$ = contact area between pile shaft and soil $[m^2]$

Dynamic soil resistance at pile toe

The dynamic soil resistance at the pile toe is the source of emission of spherical waves. According to [15], the dynamic toe resistance can be calculated from the soil impedance for P-waves at pile toe and from the pile particle velocity, as indicated in equation 2.38.This equation is derived from the Case method. The method assumes proportionality between dynamic soil resistance at pile toe and pile particle velocity [7], as shown in equation 2.39.

$$R_T = 2 Z_{S,P} v^P \tag{2.38}$$

Where:

- R_T = dynamic soil resistance at pile toe $[N]$
- $Z_{S,P}$ = soil impedance for P-waves $[Ns/m]$

$$R_T = J_c Z^P v^p \tag{2.39}$$

Where:

- Z^P = pile impedance $[Ns/m]$
- J_c = damping factor $[-]$
- v^P = particle velocity in the pile $[m/s]$

Iwanowski and Bodare [10] studied the dynamic interaction between pile toe and soil and concluded that the dimensionless damping factor is the ratio between the soil impedance to P-waves and pile impedance, equation 2.40. They considered that the soil impedance to P-waves is sufficient for characterizing the soil dynamic behaviour at the interface between pile toe and soil. As the damping factor depends on the material of the pile and its cross-section, the geometry pf the pile cross section plays an important role in determining the J_c factor. For tubular piles the ratio between the cross-section area and the area determined by the external perimeter of the cross-section has to be considered.

$$J_c = 2\frac{Z_{S,P}}{Z^P} \tag{2.40}$$

Where:

- $Z_{S,P}$ = soil impedance for P-waves $[Ns/m]$
- Z^P = pile impedance $[Ns/m]$

2.3.4.2. Soil relative density

The soil density is one of the main factors that govern the sand behaviour during cyclic loading. Loose sand tend to densify and dense sands dilate when subjected to repeated cycles of loading. Sand densification is related to compaction and settlements. Densification may be beneficial when compacting sandy soils using vibratory compactors, but settlements are related in most of the cases to negative effects such as damaging the nearby structures. Liquefaction is defined by a decrease of the effective stresses and an increase of pore pressure and the soil behaves as a liquid.
The relative density refers to the in situ soil dry density, which is defined by the minimum density and maximum density. These densities are obtained from laboratory tests. The relative density can be related to the void ratio and porosity [28]. In absence of laboratory tests, the cone resistance from cone penetration tests can be used to determine the relative density. Such correlations between relative density and cone resistance are given by Baldi [3] and Lunne and Christoffersen [13]. The relation of Baldi, shown in equation 2.41, is valid for freshly deposited sands. The relation of Lunne and Christoffersen, equation 2.42, applies for normally consolidated and overconsolidated sands.

$$R_D = \frac{1}{2.41}\ln\left(\frac{q_c}{157{\sigma_v}^{0.55}}\right) \tag{2.41}$$

$$R_D = \frac{1}{2.91}\ln\left(\frac{q_c}{61{\sigma_v}^{0.71}}\right) \tag{2.42}$$

2.3.4.3. Soil plug

During the installation process of open-ended piles, two penetration modes can be encountered: coring and plugging. The coring mode occurs when the soil enters inside the pile as the penetration progresses. If frictional resistance is developed by the core along the inner wall, the soil intrusion will stop and the piles becomes plugged [9]. In case of plugging, the plug will contribute to the base capacity of the pile, together with the annulus [21]. The plug formation has an indirect contribution to the shaft resistance development, due to the fact that in plugged mode more soil is displaced, increasing the effective stresses in the vicinity of the pile. Not only the static soil resistances, but also the dynamic behaviour of the piles is influenced by plugging [9]. The open ended pipe piles with large diameter tend to be driven in a fully coring mode when installed in sand [21].

2.4. Vibration monitoring

Vibration monitoring during pile driving may be required to ensure that vibrations do not cause damage to the surroundings. Ground vibration measurements are important for checking the levels of amplitude and compare them to the predicted values. The data can be used to verify or improve empirical prediction models. Measurement instrumentation consists of transducers and data acquisition systems.

2.4.1. Transducers

Transducers produce a voltage output. Transducers have different response curves that determine the voltage output for a given particle motion. Hence, the selected transducers for a certain monitoring program should have a frequency range that cover the expected particle motion. Transducers measure vibrations in one or two orthogonal directions. For measurements of velocity in all the three directions, three transducers are assembled in a case (orthogonal arrangement) [14].The output for geophones is proportional to the particle velocity and for accelerometers it is proportional to particle acceleration.

2.4.1.1. Geophones

A geophone consists of a magnet suspended from springs and surrounded by a coil of copper fine wire. The mechanism is placed into a tubular metal casing. Principle of operation: the casing and the coil move when ground disturbances occur, while the magnet stays steady. As a result, it is produced a voltage proportional to the movement of the coil [26]. The results in terms of velocity are obtained from dividing the recorded voltage by the sensitivity constant of the geophone, measured in $V \cdot m/s$. A geophone can record frequencies higher than its resonant frequency.

2.4.1.2. Accelerometers

The most common transduction principle of the accelerometers is based on the piezoelectric properties of certain crystals. When the crystal is subjected to compression or shear, it produces a current which is proportional to the applied pressure or shear force. The current is transmitted to a conductor which is attached on the crystal, on opposite sides.
Accelerometers are acceleration transducers and can measure frequencies greater than 500 Hz and vibration amplitudes higher than 250 mm/s, which are higher than what geophones can record [32]. Accelerometers are able to operate in the near field of high energy vibrations, but are not recommended for low frequency measurements and are more sensitive to background noise [26].

2.4.2. Data acquisition systems

Automatic systems can be used to collect automatically the date from transducers. Such a system consists of a computer, a signal converter from analog to digital and a data acquisition software [9]. Data loggers are less sophisticated instruments for data acquisition and they are chosen for practical reasons, when it is not convenient to have a computer on the site, but they are limited in terms of storage capacity [12].

2.5. Prediction of ground vibrations from impact driving

The following prediction model is developed by Massarsch and Fellenius and can be found in reference [15]. This section includes a description of the model in order to make it easier for the reader to understand the results of of the current research.

2.5.1. Method

From the energy transmitted in the elastic medium, the vertical component was calculated as a function of the coefficient k_c, the energy at the source of vibrations and as a function of the distance from the source, equation 2.18. The prediction model proposed by Massarsch and Fellenius has included two additional factors in equation 2.18 in order to predict the vibrations from impact driving. The first factor is the hammer efficiency factor F^H, which represents the loss in impact energy. The second factor is the vibrations transmission efficacy, a quantitative measure of the potential driving energy transfered to the surrounding soil. The transfered energy is limited by the maximum force applied to the pile head and by the dynamic soil resistance.

2.5.2. Vibrations transmission efficacy

The vibrations transmission efficacy is defined as the ratio between dynamic soil resistance and the force in the pile. Since the dynamic soil resistance determines the maximum force that can be transmitted in the

soil, the vibration transmission efficacy cannot be larger than unity. The vibrations transmission efficacy is calculated for vibrations transmitted along the pile shaft and for vibrations emitted at the pile toe.

2.5.2.1. Vibrations transmission efficacy along the pile shaft

The ratio between the dynamic soil resistance and the force applied to the pile head determines the vibrations transmission efficacy along the pile shaft, E_s. The soil dynamic resistance along the shaft is given in equation 2.37 and the force in the pile is given in equation 2.30.
Regarding the dynamic soil resistance, reduction factors are applied to account for the decrease in soil stiffness. One factor is related to the reduction of shear wave speed at small strains and the other reduction factor represents the disturbance and remolding effects. Including the reduction factors the soil dynamic resistance is calculated as shown in equation 2.43.

$$R_S = R_c r z_S v^P A_{contact} \tag{2.43}$$

The force in the pile is defined by the product between the pile impedance and the particle velocity in the pile. The particle velocity v^P is present in the equations for both soil dynamic resistance and force and since the vibrations transmission efficacy is defined by the ratio of these two terms, the equation for E_S can be then simplified and calculated as shown in equation 2.44.

$$E_S = \frac{R_S}{F} = \frac{R_c R_r z_S v^P A_{contact}}{Z^P v^P} = R_c R_r \frac{z_S A_{contact}}{Z^P} \tag{2.44}$$

Where:

- E_s = vibration transmission efficacy along the pile shaft [−]

2.5.2.2. Vibrations transmission efficacy at the pile toe

The vibrations transmission efficacy at the pile is determined by the dynamic soil resistance at the pile toe and by the force in the pile. In order to account for disturbance and soil compaction at the pile toe, an empirical factor r is included in the calculation of the soil dynamic resistance. It is mentioned in [15] that a conservative value of $R_r = 2$ should be assumed for loose to dense coarse-grained soils.
For open-ended piles, with no soil plugging considered, the damping factor J_c needs to be corrected by applying a reduction factor determined by ratio between the pile cross-section A^P divided by the area delimited by the pile diameter. Including this ratio, J_c is calculated for open-ended piles as shown in equation 2.45.

$$J_c = 2 \frac{Z_{S,P}}{Z^P} \frac{A^P}{A^P_{ext}} \tag{2.45}$$

The new formulation for vibrations transmission efficacy, inserting the reduction factor r and equation 2.45, is shown in equation 2.46.

$$E_T = \frac{R_T}{F} = \frac{2 R_r Z_{S,P}}{Z^P v^P} = 2 R_r \frac{Z_{S,P}}{Z^p} \frac{A^P}{A^P_{ext}} \tag{2.46}$$

Where:

- E_T = vibration transmission efficacy at the pile toe [−]

2.5.3. Vertical component of waves velocity

The amplitudes of vertical component of cylindrical and spherical waves velocity are calculated as a function of the energy released by the impact hammer. The principle of operation of impact hammer was presented in section 2.3.2 and the energy concept in section 2.2.5. Massarsch and Fellenius [15] introduce the transmission efficacy factors and the hammer efficiency factor, proposing the calculation of cylindrical and spherical wave amplitudes as shown below.

2.5.3.1. Vertical component of cylindrical waves velocity

Shear waves are emitted along the pile shaft and are propagating on a cylindrical wave front. The height of the cylinder is given by the the length of the shaft along which the stress wave is propagating in the pile. The vertical component of the the cylindrical waves velocity is determined from equation 2.47.

$$v_c = k_c E_S \sqrt{\frac{F^H W_0}{r}} \quad [mm/s] \tag{2.47}$$

The decrease in amplitude of the cylindrical wave velocity over the horizontal distance from the pile is given by $\frac{1}{\sqrt{r}}$, where r is the horizontal distance between the pile shaft and the point of interest. The material factor k_c is calculated as shown in equation 2.48. It is defined by the soil density, wave length and by the height of the cylinder representing the wave front.

$$k_c = \frac{1}{\sqrt{\rho \lambda \pi L_w}} \quad [\sqrt{m/kg}] \tag{2.48}$$

2.5.3.2. Vertical component of spherical waves velocity

The spherical waves emitted at the pile toe contain both shear and compression waves. For simplification, in the prediction model only the compression waves are taken into account. The vertical component of the spherical waves can be calculated according to equation 2.49. This equation takes into account the decrease in amplitude of the spherical wave velocity over the horizontal distance from the pile given by $\frac{1}{r_s}$, where r_s represents the radial distance to the pile toe. The material factor for spherical waves, k_s, is determined according to equation 2.50.

$$v_s = k_s E_T \frac{\sqrt{F^H W_0}}{r} \quad [mm/s] \tag{2.49}$$

$$k_s = \frac{1}{\sqrt{2\pi\rho\lambda}} \quad [\sqrt{m^2/kg}] \tag{2.50}$$

3
Field study

3.1. Introduction

The current field study is part of the project for expansion and modernization of the mooring places for the oil tankers in the port of Rotterdam. Dolphin configurations and buoy berths were replaced and extended. The main stakeholders of the research are the Engineering Department of Rotterdam City Development and the Port of Rotterdam.
The installation of these piles was extensively monitored for the changes in water pressures and in accelerations in order to prevent the slope instability. From experience and based on past measurements no problems were expected regarding the slope stability. The monitoring plan was developed create the possibility to intervene during the execution in case the measurements exceed the required values. The objectives of the extra monitoring are: verification of initial calculations, of the existing models and experience, contribution to increase of knowledge about soil behaviour during pile driving and improving monitoring techniques for better assessment of slope instability.
In this chapter, a description of the project is presented, including information about the monitoring plan and about the soil profile at the locations of pile 79B_T02 and pile 82_T07.

3.2. Project description

In figure A.1 from appendix A, the different mooring places available in Caland Canal are shown. The locations of interest for this research are dolphin configurations 79B and 82.
Dolphin 79B is built as a new mooring place and it can accommodate vessels with lengths between 70 and 160 meters [1]. This dolphin configuration consists of 4 pile supported dolphins. Dolphin configuration 82 was created by replacing the existing buoys with 10 dolphins. This mooring place can accommodate large ships with length 225 up to 360 meters [1].
A typical cross-section of the construction is shown in appendix A, figure A.2.
Information about the schedule of the piles installation is given in table 3.1. The driving process of pile 79B_T02 took place in two consecutive days, while pile 82_T07 was installed in one day.

Table 3.1: Schedule pile driving

Dolphin configuration	Pile	Date	Driving method
79B	79B_T02	12.05.2015	Vibratory driving
		13.05.2015	Impact driving
82	82_T07	25.06.2015	Vibratory and impact driving

3.2.1. Geometry of the dolphin piles

The open-ended steel tubular piles supporting the dolphins have a diameter of 2.5 m and the lengths of the piles is 44.50 m. The thickness of the pile wall varies along the length of the pile. The piles were manufactured by welding together different parts with various wall thicknesses and the height 3.50 m. Figure A.3 from appendix A shows the pile geometry and the variation of the cross-section along the pile length.

3.2.2. Driving equipment

The vibratory driving of pile 79B_02 was performed using the vibratory hammer ICE 36RF and vibratory hammer IHC 105M for pile 82_T07. For both piles, the final installation depth was reached using the impact hammer IHC S280.

3.3. Vibration monitoring

Monitoring of ground vibrations at the field study in Caland Canal was carried out using geophones and pore-pressure transducers. The signals from the transducers were captured by the data acquisition system, which can sample up to 64 channels. The maximum sampling frequency is 1 kHz, the system being able to record frequencies up to 500 Hz.
The 3D geophones are built as three geophones fixed in a steel case, each geophone measuring vibrations in one of the three orthogonal directions. The sensors were installed in the ground by attaching the metal tubular case containing the geophones to cone penetration rods. After reaching the required depth, the rod was retracted. Due to this installation method, there are some uncertainties regarding the orientation of the two geophones recording horizontal vibrations. The measurement of ground vibrations induced by pile driving were recorded in terms of particle velocity.
During pile driving the pore-pressure transducers monitor the generation of pore water pressure. The water pressure sensors measured the absolute and the relative water pressures. Sensors were installed also outside the area of pilling influence for measuring barometric pressure and tidal variations. At each berth there is a sensor measuring continuously the tide. The measured value of the water pressures is therefore reported using the tide and placement depth corrections. The water pressures are measured in kPa.

3.3.1. Field data processing

A total amount of 77 GB of data was recorded from the field study in Caland Canal. Data was available for post-processing in large size files. Data was sampled for 64 channels, meaning that the system could record simultaneously signals from 16 sensors, with 4 channels each: 3 channels corresponding to the 3 geophones measuring vibrations in the orthogonal directions and one channel for the vector of directions.
Due to the large size of the files with the measurement data, the velocities corresponding to each sensor had to be extracted and saved in individual files for both vibratory and impact driving. Only 1% of the total amount of data, corresponding to vibration velocities from driving both pile 79B_T02 and pile 82_T07, has been analyzed in the current research and the results of the post processing are presented in chapter 4.
The first outputs of the analyses were unreliable which led to the discovery that the measurements were the velocity recordings and not the voltage output of the sensors. Another issue encountered during the measurements processing was the correct association of the data to the right sensor. In order to overcome any doubts, the arrival time of the impulse from the impact driving vibrations measurements has been analyzed: sensors further away are later excited.

3.3.2. Sensors location overview

The pile driving process has been extensively monitored at both dolphin configurations, 79B for gaining experience with the measurements calibration and 82 because of the increased risk of soil softening during pile driving. A total of 16 sensors were placed in the ground for pile driving monitoring purpose. 9 sensors were distributed around pile 79B_T02 and 6 around pile 82_T07. This section provides information about the location of the sensors in terms of depth and distance from the piles.

Table 3.2: Locations of sensors around pile 79B_T02

Sensor	Distance to pile 79B-T02 [m]	Depth [m]	Location
VP001	16.20	-11	Perpendicular to the riverbank
VP002	15.70	-17	
VP003	16.40	-22	
VP004	11.10	-17	
VP005	11.20	-22	
VP006	6.20 0	-17	
VP007	15.90	-17	Along the riverbank
VP008	15.50	-17	
VP009	6.40	-17	

3.3.2.1. Sensors at dolphin configuration 79B

Nine sensors were placed around pile 79B_T02 at three different depths: at NAP -11 m, at NAP -17 m and at NAP -22 m. Six sensors were placed perpendicular to the riverbank and three sensors were placed along

the riverbank. The information about the sensor locations is summarized in table 3.2, which includes the distance from the pile to the sensors and the depth of sensors placement.

Figure 3.1 shows the location of the sensors in the cross section of the riverbank. Figure 3.2 shows a top view of the sensors.

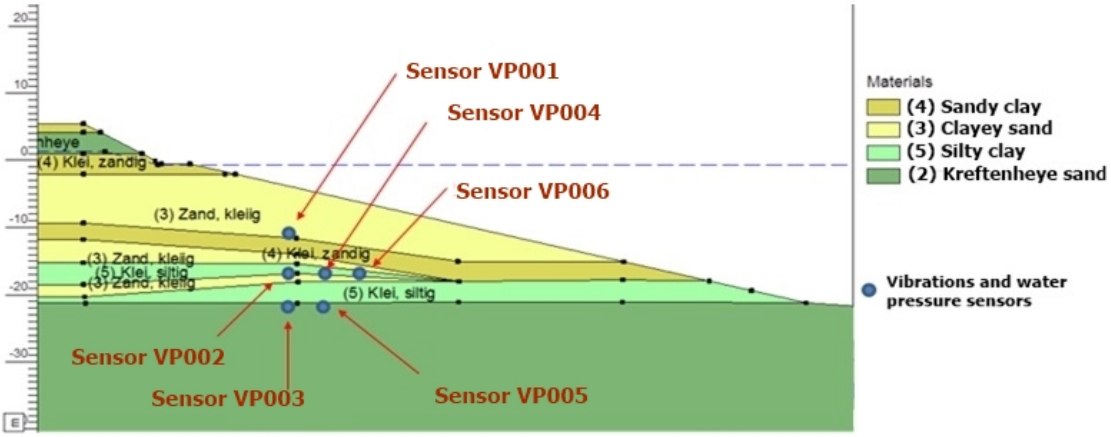

Figure 3.1: Riverbank cross section, pile 79B_T02

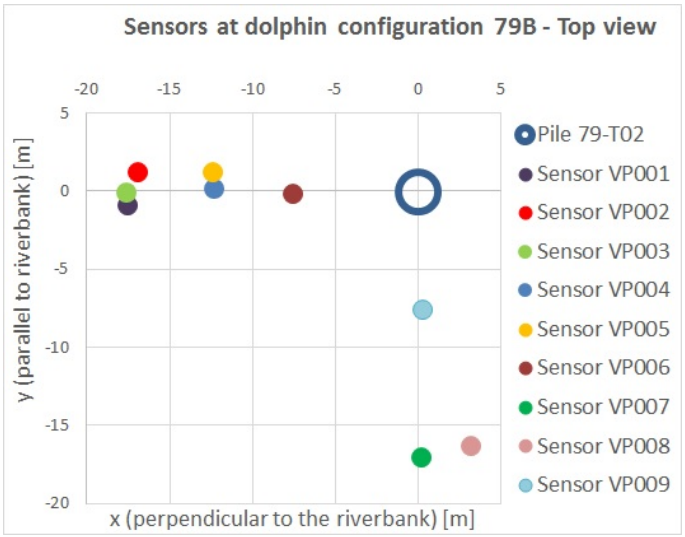

Figure 3.2: Top view of sensors, pile 79B_T02

Table 3.3: Locations of sensors around pile 79B_T02

Sensor	Distance to pile [m]	Depth [m]	Location
VP011	17.20		Perpendicular to the riverbank
VP012	12.50	-18.50	
VP013	7.10		
VP014	7.90		Along the riverbank
VP015	12.40	-18.50	
VP016	17.60		

3.3.2.2. Sensors at dolphin configuration 82

At this location, six sensors were installed around pile 82_T07. The sensors are all located at the same depth, NAP -18.50 m. Three sensors were placed perpendicular to the riverbank and other three sensors were installed along the riverbank. The sensor location is summarized in table 3.3.Vibrations measurements data

is available for two piles. Both piles were driven along the riverbank, at 28 m distance from each other. Table 3.3 includes the distances from the sensors to pile. Figure 3.3 shows the positions of the sensors in the cross-section of the riverbank. The arrangement of the sensors in the horizontal plan is shown in figure 3.4.

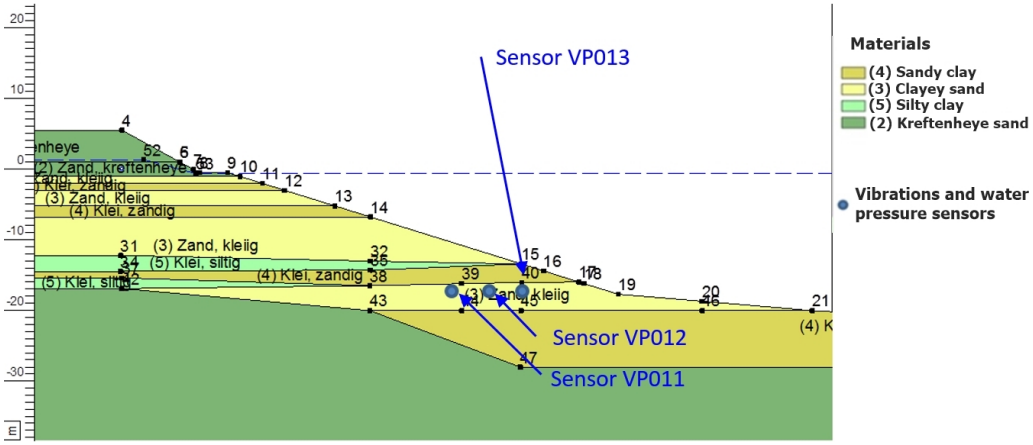

Figure 3.3: Riverbank cross section, pile 82_T07

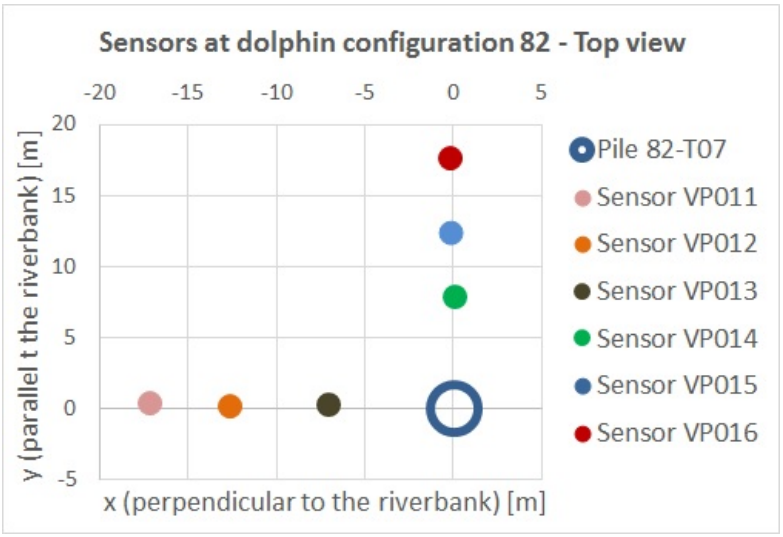

Figure 3.4: Top view of sensors, pile 82_T07

3.4. Execution

The installation process took place in two parts: first the piles were driven by a vibratory block and from the depth of the sand layer the piles were driven by an impact hammer. The soil conditions were found to be most sensitive at dolphin 82 and less critical at location 79B. The pile installation process was monitored using threshold levels for extra attention, S-values, and for intervention, I-values, in order to ensure the stability of the slope.

The expected values of water surcharge are managed as S-values, used for stability calculations. For safety reasons, the I-values of the water pressure are set at 1.2 times S-values. For the achievement of the I-value of the water pressures, the vibratory or impact driving process will be stopped until the water pressure has fallen below 30% of the I-value.

S-values are used for accelerations expected value (50% probability of exceeding). The I-values are determined at 95% of the estimated accelerations (5% probability of exceeding). When I-values are exceeded for at least 5 seconds, the vibratory driving is stopped and switched to impact driving. This time length of 5 seconds was chosen for avoiding the situation where the vibratory driving process would be interrupted when the first peak value is measured. The I-values are reached during impact driving.

3.4.1. Dolphin configuration 79B (pile 79B_T02)

At this location, the existing sheet pile wall along the riverbank was pulled, the piles were driven and in the end two sheet pile walls are installed for controlling the slope stability in the riverbank.

3.4.1.1. Observations during execution

During pile driving no significant deviations of the water pressures occurred. In the measurements no difference was found between the moment of starting and of stopping the impact driving. The maximum increase in the water pressure during vibratory driving is just 0.2 kPa The effect of the vibrations on the water surcharge is therefore negligible.
The measured accelerations followed the soil resistance at the pile tip level. When the pile tip reached the sand layer at NAP -21.0 m, the vibrations were transmitted in the surrounding soil and the progress of the driving process decreased.
The measurements and the driving progress as a function of depth show that the ICE 36RF vibrator block was suitable for the project, but it does not have enough strength to reach the designed foundation depth of the piles. In order to decrease the vibrations propagation in the surrounding soil and to avoid the damaging of the piles, at the sand layer depth, approximately NAP -21.0 m, the vibratory driving is switched to impact driving.

3.4.2. Dolphin configuration 82 (pile 82_T07)

For the impact driving the S280 block was used with an impact rate of less than one blow per second. This will gave time for the water pressures to dissipate. The vibratory hammer IHC 105M was used for driving the piles at this dolphin configuration.

3.4.2.1. Observations during execution

No increase was observed for water pressure values. The acceleration measurements are similar to the ones in other locations, but for the sand layer the vibrations exceeded the threshold values.

3.5. Soil profile

In this section the soil profile at the site location is presented. A total of 32 cone penetration tests have been conducted during the field study in order to study the pile driving effects on the surrounding soil. For both dolphin configurations 79B and 82 extensive CPT data is collected before and after the piles were driven. At both locations, 8 CPTs were performed before and 8 CPTs after pile installation.

3.5.1. Cone penetration tests

The locations of the CPTs are given in figure 3.5 dolphin configurations 79B and figure 3.6 dolphin configurations 82. The same figures are given in appendix A, including the location of the sensors. All the CPTs can be found in annex E.

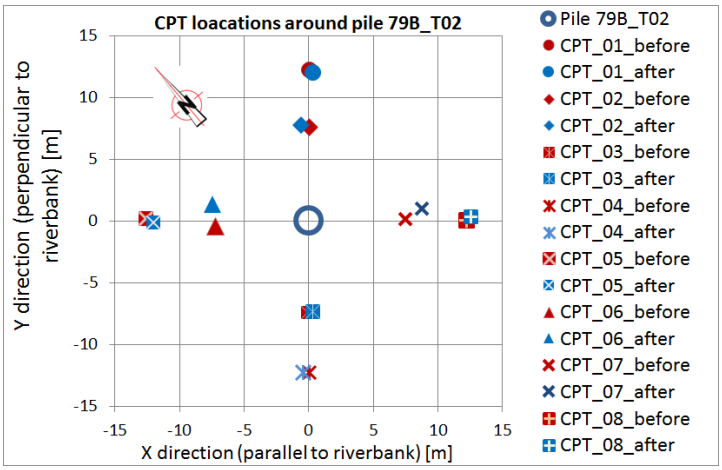

Figure 3.5: CPTs from before and after pile driving

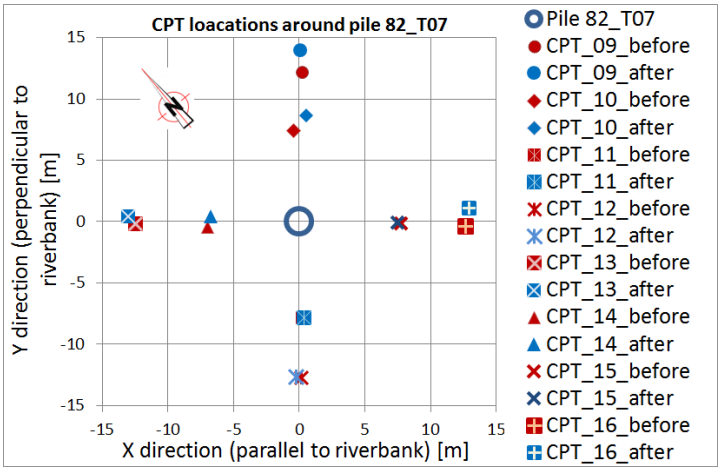

Figure 3.6: CPTs from before and after pile driving

At dolphin configuration 79B, the CPTs located at 5 m distance from pile 79B_T02 are: CPT 2, CPT 3, CPT 6, CPT 7. The CPTs located at 10 m distance are: CPt 1, CPT 4, CPT 5, CPT 8. The cone resistance from CPTs 1, 2, 6, 7 and 8 showed no significant increase or decrease. CPT 3 showed a 50% decrease above NAP -30 m and no change below this level. CPTs 4 and 5 showed a decrease in cone resistance of 25-50%.
At dolphin configuration 82 the CPTs located at 5 m distance from pile 82_T07are: CPT 10, CPT 11, CPT 14, CPT 15. The CPTs located at 10 m distance are: CPT 9, CPT 12, CPT 13, CPT 16. The locations of these CPTs are shown in figure 3.6. CPTs 11, 14 and 15 present a decreased cone resistance by 50% above NAP -30 m. CPTs 12 and 13 have a slight decrease and for CPTs 9, 10 and 16 the differences are negligible.
The overall results of the CPTs show a decrease in the cone resistance and there is no clear effect of the pile distance. The same values are found at both distances, 5 m and 10 m, from pile 79B_T02. For the CPTs surrounding pile 82_T07 the decrease of the cone resistance is greater at 5 m than at 10 m. However, the decrease is smaller for the CPTs taken in the upper part of the slope, above the pile location; for the CPTs taken below the pile location the decrease of the cone resistance is larger, mostly for the piles at 10 m distance.

3.5.2. Average CPT profile at the piles locations

CPT profiles at the locations both piles are obtained by averaging the cone resistance from the CPTs closer to the pile. As a result, the CPT profile shown in figure 3.7 is obtained at the location of pile 79B_T02, calculated from CPT 2, CPT 3, CPT 6 and CPT 7 (before pile driving). Figure 3.8 shows the assumed CPT profile at the location of pile 82_T07, obtain from CPT 10, CPT 11, CPT 14 and CPT 15.
The properties of the soil layers at the depths where sensors were placed are summarized in table 3.4. The soil parameters are determined from the CPT profiles shown in figure 3.7 and figure 3.8 based on Table 1 from NEN 6740 [20]. The the soil layers of interest at the location of pile 79B_T02 are the sandy clay layer from NAP -17 m to NAP -19 m and the sand layer from NAP -22 m to NAP -26 m. At the location of pile 82_T07, the soil parameters are given for the clay layer, from depth NAP -16.20 m to NAP -20 m.

Table 3.4: Soil parameters from NEN 6740 [20]

Location	Layer	from NAP $[m]$	to NAP $[m]$	thickness $[m]$	γ_{dry} $[kN/m^3]$	γ_{sat} $[kN/m^3]$	E $[MPa]$	ν $[-]$
Pile 79B_T02	sandy clay	-17	-19	2	18	18	4	0.24
	sand	-22	-26	4	20	22	50	0.3
Pile 82_T07	clay	-16.20	-20	3.8	17	20	7	0.45

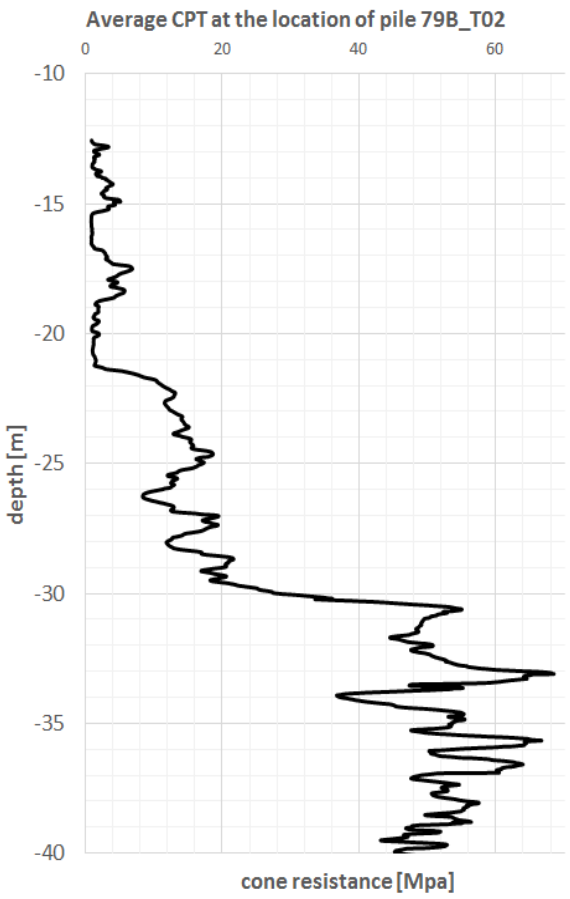

Figure 3.7: Assumed CPT profile at the location of pile 79B_02

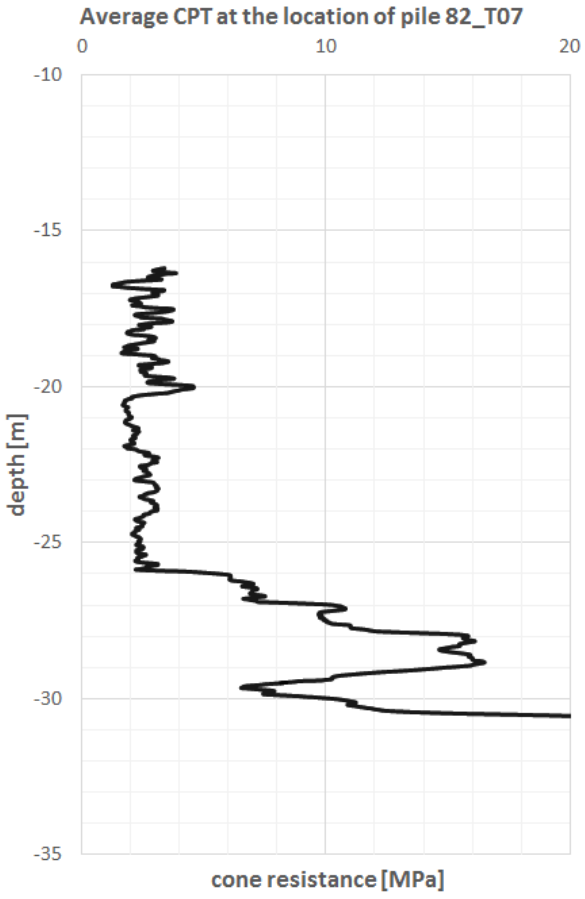

Figure 3.8: Assumed CPT profile at the location of pile 82_07

3.5.3. Influence of pile driving on relative density

The correlations given in equation 2.41 and equation 2.42 are used for determining the relative density of the Pleistocene sand from the results of the cone penetration tests performed before and after the installation of the dolphin piles. Comparing the relative densities calculated for CPT profiles before and after pile installation, the influence of pile driving on on the surrounding soil can be assessed. The decrease in relative density as a result of ground vibrations induced by pile driving is related to a looser soil state, while the increase of soil density is related to densification.

According to the plots of the calculated relative density from appendix F, the relative densities obtained from the method of Baldi, equation 2.41, are larger than the relative densities calculated from equation 2.42. For all the cases, the relative density calculated for the sand below NAP -30 m is higher than unity, which is not a realistic result. Decreases in relative density are mostly visible above NAP -30m.

After the pile installation, the relative densities calculated from the CPTs around pile 79B_02 show clear decreases for CPT 3, CPt 4 and CPT 5. At the location of pile 82_07, only CPT 10 and CPT 13 show a reduction of relative density. For CPT 10, the decrease on relative density is encountered below NAP -30 m, while for CPT 13 the relative density decreases above NAP -30 m.

The changes in relative density after the pile installation cannot be related with the effect of either vibratory driving or impact driving because the second set of CPT data is recorded after the piles reached the designed depth, after both driving methods were used.

4 Results

4.1. Introduction

The results from the field measurements in Caland Canal are presented and analyzed in this section. The analysis starts with the measurements from the location of berth 79B, for which pile 79B_T02 was extensively monitored (9 sensors). The second location is berth 82, where 6 sensors were installed and the vibrations are recorded for the installation of pile 82_T07.
The purpose of the analysis is to provide a better understanding and insight to the behaviour of the ground vibrations due to pile driving. Results from both vibratory driving and impact driving are shown. A description of the sensor locations and information about data processing were presented in chapter 3. The measurements dataset was processed using MATLAB.

4.2. Particle velocity

The particle velocity can be used in different ways for describing the wave motion. The particle velocity refers to the velocity at which an individual particle oscillates about the initial position. A common way to visualize the vibrations is to plot the velocity against time. The attenuation of vibrations is presented by plotting the vibrations against the distance from the source. The vibrations can be related to the soil profile when they are plotted against the penetration depth and the CPT results. These results are presented in the following subsections.

4.2.1. Time domain

In the time domain the variation of of particle velocity over the duration of measurement can be visualized.

4.2.1.1. Vibratory pile driving

The time domain plots of velocities can be found in appendix B. From these plots it can be noticed that the increase of vibrations occur at the same time for all the sensors, mainly towards the end of the time interval. The increase in ground vibrations in the sand layer is the result of the driving technique not being suitable for this soil layer.

4.2.1.2. Impact pile driving

The impact driving process does not start from the surface level, but from the depth of the dense sand layer. Since the pile penetrates through a soil layer with almost the same properties over depth, the variation in vibrations amplitude is present as a small decrease in vertical vibrations amplitude with the increasing installation depth. The measurement for horizontal vibrations do not show a noticeable variation in amplitude.
The recordings show that the installation process was not continuous. The agenda of the monitoring program does not specify the cause. Possible explanations could be the changes of the driving energy until a suitable driving energy was found, the pile was not properly attached to the hammer or the hammer needed some inspection due to operational problems.
In order to find the influence of the vibrations emitted from the pile toe, the vertical vibrations recorded by sensors at different depths are compared. Sensor VP004 is placed at depth NAP -17 m and sensor VP005 at depth NAP -22 m. Both sensors are located at 11 m horizontal distance from the pile. The time history for vertical vibrations is plotted in figure 4.1 for senors VP004 and in figure 4.2 for sensor VP005. The vertical vibrations amplitude recorded by sensor VP004 stays around 8 mm/s, while for sensor VP005 the amplitude decreases from 12 mm/s to 8 mm/s. Sensor VP005 is placed at the same depth where the driving process is switched to impact driving and the decrease in amplitude shown in the measurements can be related to the influence of the vibrations emitted from the pile toe. As the distance between the sensor VP005 and the

pile toe increases, the amplitude decreases to 8 mm/s, the same vertical vibrations amplitude as for sensor VP004. This means that after a penetration depth, the vibrations are transmitted as cylindrical waves and the influence of spherical waves is not very significant.

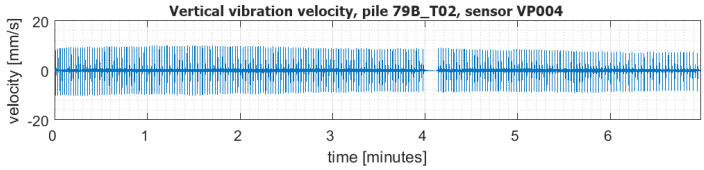

Figure 4.1: Vertical vibrations recorded by sensor VP004

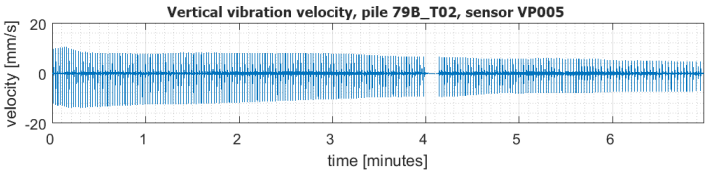

Figure 4.2: Vertical vibrations recorded by sensor VP005

The same conclusion regarding the mechanism of waves transmission can be reached when comparing sensors VP001, VP002 and VP003, which are placed at approximately the same horizontal distance from the pile, 16 m. Sensor VP001 is placed at depth NAP -11 m, sensor VP002 at NAP -17 m and sensor VP003 at NAP -22 m. The vertical velocities for sensor VP001 are shown in figure 4.3, for sensor VP002 in figure 4.4 and for sensor VP003 in figure 4.5. For sensor VP001, the amplitude does not vary and it is in a range of 4-5 mm/s. The absence of amplitude variation shows that vibrations are generated from cylindrical waves. For sensor VP002, the amplitude decreases from 6 mm/s to 4 mm/s. Compared to the vertical vibrations from sensor VP004, figure 4.5, the small change in amplitude suggests that at the same depth and higher horizontal distance from the pile, the source of vibrations is influenced by the combination of spherical and cylindrical waves. For sensor VP003 the decrease in amplitude is from 8 mm/s to 5 mm/s. As this sensor is closer to the pile toe, the influence of the of the spherical waves transmitted from the pile toe is more visible.

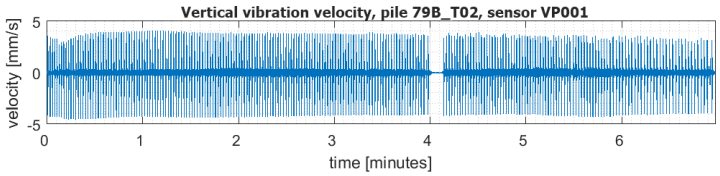

Figure 4.3: Vertical vibrations recorded by sensor VP001

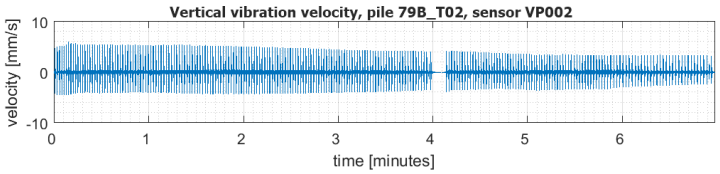

Figure 4.4: Vertical vibrations recorded by sensor VP002

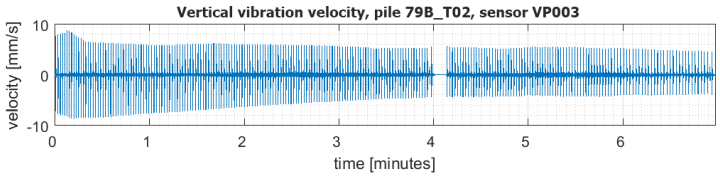

Figure 4.5: Vertical vibrations recorded by sensor VP003

A decrease in amplitude is visible also in the vertical vibration measurements from sensor VP006, figure 4.6, and from sensor VP009, figure 4.7. The sensors are both at the same depth, NAP -17 m, and about the same horizontal distance, 6 m. The only difference between the locations of there two sensors is that sensor 9 is placed along the riverbank and sensor 6 is placed perpendicular to the river bank. The amplitudes are in the same ranges for both sensors, which means that the presence of the overburden stress does not influence the resulting vertical vibrations due to impact pile driving. The gradual decrease in vertical vibrations amplitude can be an effect of the small horizontal distance from pile to sensors. Closer to the pile, the vibrations transmission mechanism might be more complex that at larger distance.

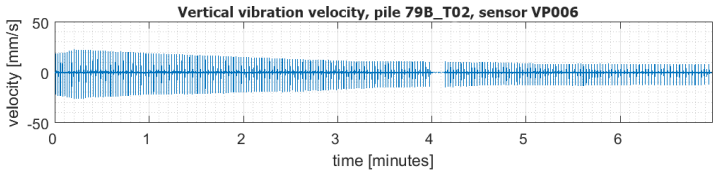

Figure 4.6: Vertical vibrations recorded by sensor VP006

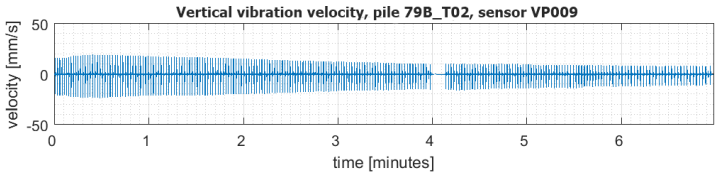

Figure 4.7: Vertical vibrations recorded by sensor VP009

For the second data set, time history shows a small interruption of the driving process, where the vibration energy is changed. The vibrations amplitude does not show clear variations. Small variations are visible for the first five minutes of the pile installations, where the blow rate is higher. The sensors at this location are all installed at the same depth, NAP -18.50 m, The ground level is at NAP - 16.20 m, resulting a minimum depth of 2.30 m for the six sensors. The driving process is switched to impact driving at NAP -27 m depth, meaning that the pile toe is 6.50 m below the depth of the sensors at the beginning of the pile installation. The pile driving is stopped when the pile reaches the depth NAP -38 m. The vertical distance between the sensors and the pile toe during impact driving increases from 6.50 m to 17.50 m. If no visible variation in amplitude with the increasing penetration distance is found, the vibrations are considered to be mainly generated by cylindrical waves.

4.2.2. Maximum vibration level

The maximum vibration level is described by the peak particle velocity for each direction of the sensors.

4.2.2.1. Vibratory pile driving

The peak particle velocities are shown in table for the sensors that recorded the vibrations resulting from driving pile 79B_T02. Table shows the peak velocities from driving pile 82_T07. The range of values is up to 12 mm/s and the highest values are recorded for vertical vibrations.

Table 4.1: Peak particle velocities from vibratory driving, pile 79B_T02 (in mm/s)

Direction	Sensors								
	VP001	VP002	VP003	VP004	VP005	VP006	VP00 7	VP008	VP009
Horizontal 1	2.99	2.75	1.74	3.37	–	3.43	3.01	3.93	4.56
Horizontal 2	1.53	2.95	4.36	1.80	1.44	5.52	2.07	3.31	6.36
Vertical	1.53	4.40	5.41	6.22	7.85	9.57	3.01	2.53	9.15

Table 4.2: Peak particle velocities from vibratory driving, pile 82_T07 (in mm/s)

Direction	Sensors					
	VP011	VP012	VP013	VP014	VP015	VP016
Horizontal 1	5.14	5.71	–	–	5.77	6.02
Horizontal 2	3.85	5.83	9.35	7.19	10.97	5.92
Vertical	4.19	4.96	11.84	7.00	5.94	5.67

4.2.2.2. Impact pile driving

The maximum vibrations from the sensors around pile 79B_T02 can be found in table 4.5 and from the sensors around pile 82_T07, in table 4.6.
For pile 79B_T02, the maximum horizontal vibrations are smaller than the vertical ones. For pile 82_T07, the maximum level of horizontal vibrations is higher than for the vertical vibrations. However, due to the unknown orientation of the horizontal sensors, it is difficult to draw conclusions from the interpretation of the horizontal vibration measurements.

When calculating the critical distance from the pile where wave reflections at the ground surface occur, the result indicated that the surface waves can be encountered at less than 1 m distance. This small distance is obtained because the critical angle depends on the ratio between S-waves velocity and P-waves velocity. At the location of the pile installation, the soil is saturated and the P-wave velocity is high compared to shear wave velocity. This leads to a small ratio c_s/c_p and a small critical angle and critical distance. This formulation does not make a difference between pile material and geometry. The surface waves are the result of the spherical waves refraction when they reach surface level, but in case of open-end tubular piles driven in unplugged mode, the waves emitted at the pile toe are much smaller than in case of closed-end piles.

Table 4.3: Peak particle velocities from impact driving, pile 79B_T02 (in mm/s)

Direction	Sensors								
	VP001	VP002	VP003	VP004	VP005	VP006	VP00 7	VP008	VP009
Horizontal 1	7.87	6.10	4.98	11.61	–	5.10	3.80	7.69	11.42
Horizontal 2	1.78	5.55	2.22	3.07	6.29	14.49	4.84	8.36	12.69
Vertical	4.56	6.03	8.86	10.23	13.84	26.31	3.97	10.79	23.65

Table 4.4: Peak particle velocities from impact driving, pile 82_T07 (in mm/s)

Direction	Sensors					
	VP011	VP012	VP013	VP014	VP015	VP016
Horizontal 1	8.47	23.06	–	1.42	1.69	9.97
Horizontal 2	5.55	21.66	25.99	11.45	20.55	13.78
Vertical	10.37	14.05	20.23	13.63	11.16	9.28

4.2.3. Vibrations attenuation

The vibrations attenuation is visualized by plotting the peak particle velocities versus the horizontal distance from the pile to the sensors.
For pile 79B_T02 the propagation of vibrations as a function of distance from the source can be analyzed for three cases, while for pile 82_T07 only for two cases. For pile 79B_T02, the three cases are:

- vibrations recorded by sensors VP006, VP004 and VP002, placed in the riverbank section at depth NAP -17 m (sensor VP006 is the closest to the pile)
- vibrations recorded by sensors VP005 and VP003, placed in the riverbank section at depth NAP -22 m
- vibrations recorded by sensors VP009 and VP007, placed along the riverbank, at depth NAP -17 m

For pile 82_T07, the two cases for visualizing the vibrations attenuation are the following:

- vibrations recorded by sensors VP013, VP012 and VP011, placed in the riverbank section at depth NAP -18.50 m (sensor VP013 is the closest to the pile)
- vibrations recorded by sensors VP014, VP015 and VP016, placed along the riverbank, at depth NAP -18.50 m

4.2.3.1. Vibratory pile driving

The vibrations recorded from the installation of pile 79B_T02 present a general trend of attenuation with increasing distance horizontal distance from the source, figure 4.8. Exceptions are the horizontal vibrations, from sensor VP006 to sensor VP004 in figure 4.8a and in figure 4.8b the horizontal vibrations from channel 2, transmitted at more than 11 m distance from the pile. For sensor VP001 to VP009, the vertical vibrations recorded by the sensors closer to the pile have about the same values. After 11 m distance, the vibrations attenuate less for the sensors in the section perpendicular to the riverbank, from sensor VP004 to VP002. The sensors VP003 and VP005, which were placed in the sand layer at NAP -22 m, show higher vertical vibrations than the other sensor placed at the same distances, but at lower depth.

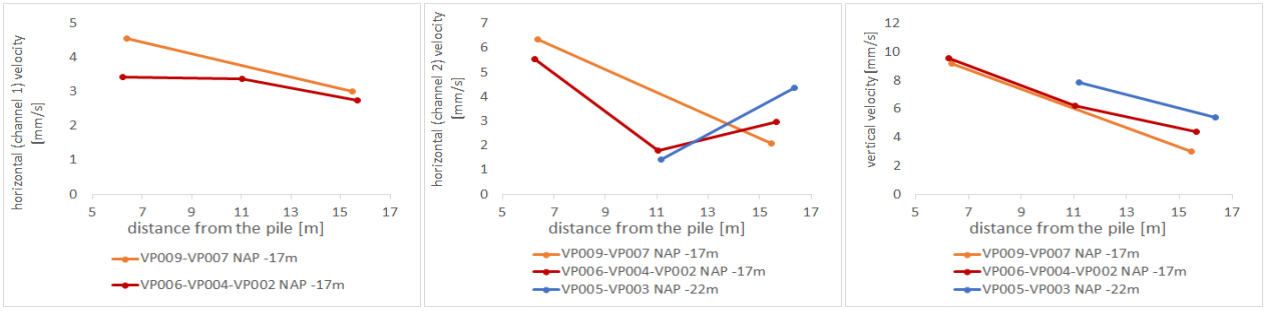

(a) Horizontal PPV (channel 1) (b) Horizontal PPV (channel 2) (c) Vertical PPV

Figure 4.8: Peak particle velocity propagation (PPV) from the source, pile 79B_T02

For the second case, the vibrations recorded from driving pile pile 82_T07 shown in figure 4.9, the horizontal vibrations are higher for the sensors placed along the riverbank, sensor VP014 to sensor VP016. The vertical vibrations measured closer to the pile are higher in the riverbank section, but they show a significant decrease in amplitude, from 11.84 mm/s to 4.19 mm/s, compared to the vertical vibrations transmitted along the riverbank. The vibrations recorded by sensor along the riverbank decreased in amplitude from 7 mm/s to 5.67 mm/s. This is visible in figure 4.9c.

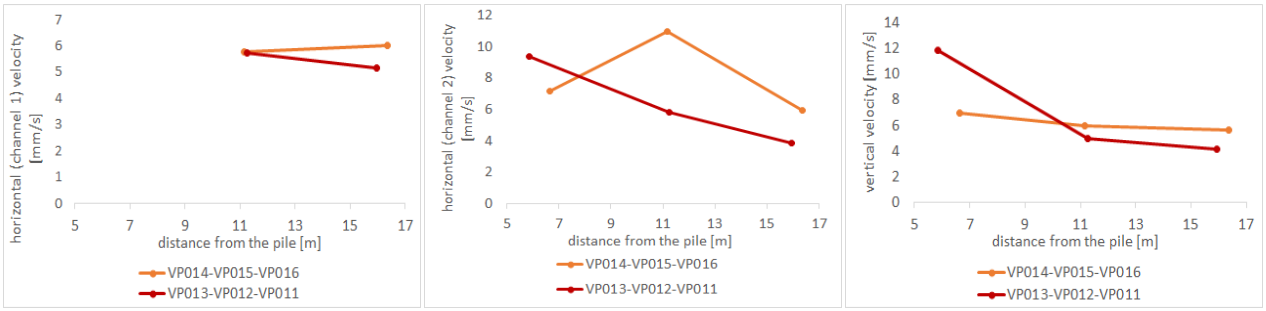

(a) Horizontal PPV (channel 1) (b) Horizontal PPV (channel 2) (c) Vertical PPV

Figure 4.9: Peak particle velocity (PPV) propagation from the source, pile 82_T07

4.2.3.2. Impact pile driving

Figure 4.10 and figure 4.11 show the vibrations attenuation from the impact driving of pile 79B_T02 and of pile 82_T07. The attenuation of vertical vibrations is clear for both cases, as it can be seen in figure 4.10 and figure 4.11. The difference in orientation of the sensors in the horizontal plane makes it difficult interpret the results from the horizontal vibrations. In addition, channel 1 from sensor VP005 and from sensor VP013 recorded only noise.

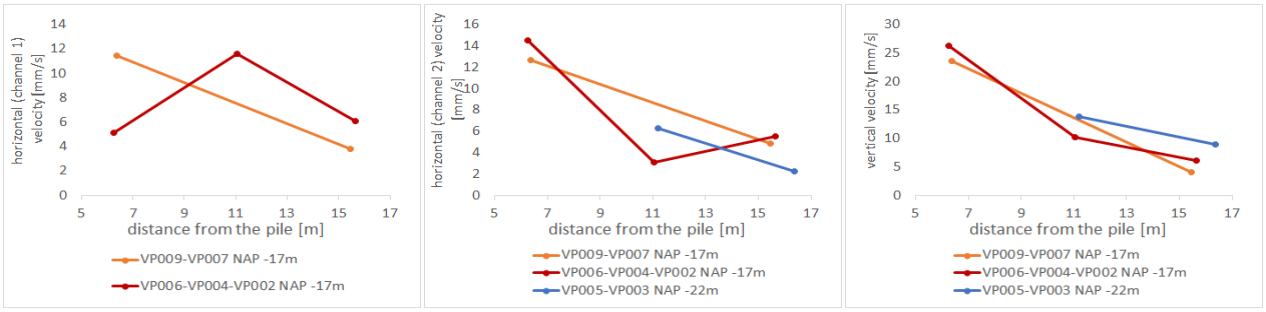

(a) Horizontal PPV (channel 1) (b) Horizontal PPV (channel 2) (c) Vertical PPV

Figure 4.10: Peak particle velocity propagation (PPV) from the source, pile 79B_T02

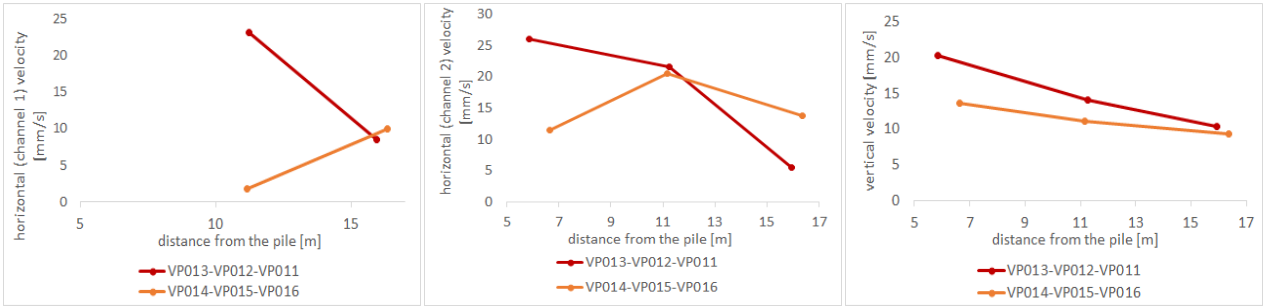

(a) Horizontal PPV (channel 1) (b) Horizontal PPV (channel 2) (c) Vertical PPV

Figure 4.11: Peak particle velocity (PPV) propagation from the source, pile 82_T07

4.3. Ground accelerations

The ground accelerations, obtained from the derivation with respect to time of the recorded vibrations, are presented in this section in terms of maximum acceleration levels. The attenuation of accelerations is presented as plots of peak accelerations versus the distance between pile and sensors. The plots of accelerations in the time domain can be found in appendix C.

4.3.1. Vibratory pile driving

The ground accelerations due to vibratory driving reach a peak value of 3.33 m/s^2 for sensor VP006, according to table 4.5. For the other set of data, given in table 4.6, the maximum acceleration level is 3.11 m/s^2. On average, the accelerations are higher during the installation of pile 82_T07 than the accelerations obtained for pile 79B_T02.

Table 4.5: Peak accelerations from vibratory driving, pile 79B_T02 (in m/s^2)

Direction	Sensors								
	VP001	VP002	VP003	VP004	VP005	VP006	VP00 7	VP008	VP009
Horizontal 1	0.61	0.74	0.57	1.08	–	1.13	0.78	1.06	1.20
Horizontal 2	0.47	0.76	1.08	0.73	0.35	2.29	0.66	0.76	1.65
Vertical	0.35	1.19	1.45	1.30	1.91	3.33	0.74	0.60	1.84

Table 4.6: Peak accelerations from vibratory driving, pile 82_T07 (in m/s^2)

Direction	Sensors					
	VP011	VP012	VP013	VP014	VP015	VP016
Horizontal 1	0.79	1.32	–	–	1.21	1.66
Horizontal 2	0.81	2.05	2.59	1.51	2.62	1.86
Vertical	0.77	2.44	3.11	2.83	1.99	1.81

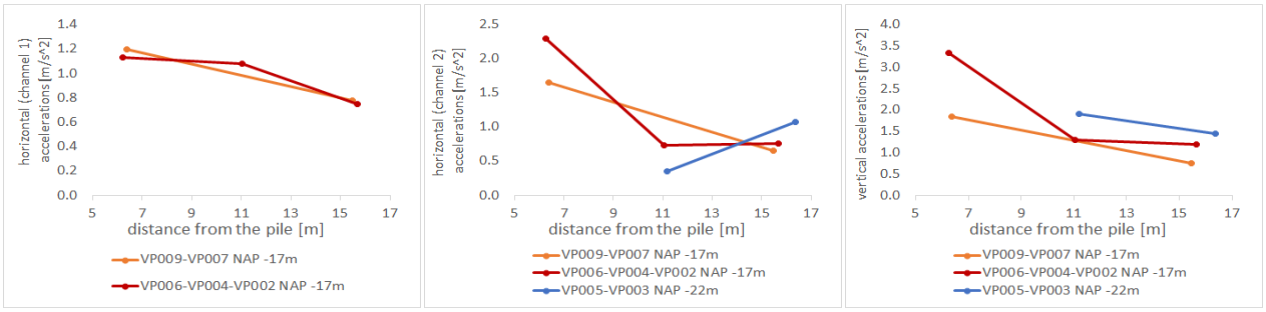

(a) Horizontal accelerations (channel 1) (b) Horizontal accelerations (channel 2) (c) Vertical accelerations

Figure 4.12: Accelerations attenuation from the source, pile 79B_T02

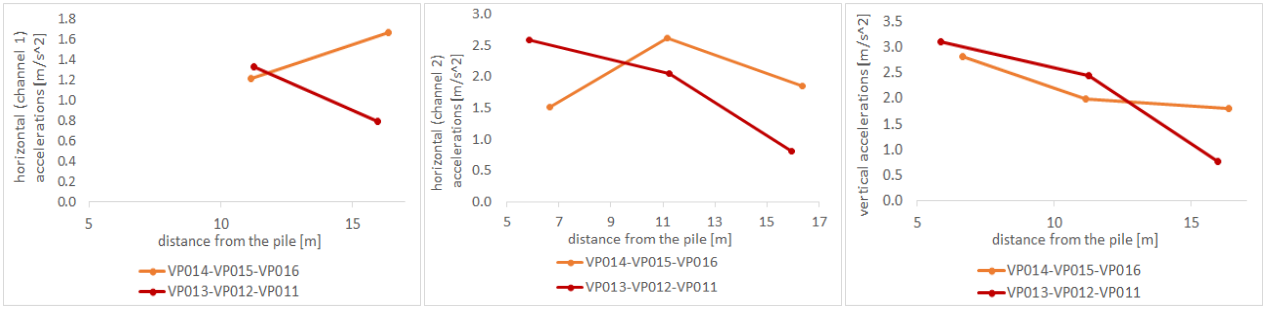

(a) Horizontal accelerations (channel 1) (b) Horizontal accelerations (channel 2) (c) Vertical accelerations

Figure 4.13: Accelerations attenuation from the source, pile 82_T07

4.3.2. Impact pile driving

The peak accelerations calculated for sensors VP001 to VP009 are given in table 4.7 and for sensors VP011 to VP016 in table 4.8. The ground accelerations from driving pile 79B_T02 show higher values for vertical accelerations, while for driving pile 82_T07, the resulting horizontal accelerations are higher than the vertical accelerations.

Table 4.7: Peak accelerations from impact driving, pile 79B_T02 (in m/s^2)

Direction	Sensors								
	VP001	VP002	VP003	VP004	VP005	VP006	VP00 7	VP008	VP009
Horizontal 1	7.75	1.82	1.49	3.95	–	3.39	3.90	6.23	7.55
Horizontal 2	2.20	1.15	0.73	1.86	2.13	5.68	4.90	5.75	5.77
Vertical	3.84	1.57	1.77	5.71	2.85	8.35	3.59	15.47	12.56

Table 4.8: Peak accelerations from impact driving, pile 82_T07 (in m/s^2)

Direction	Sensors					
	VP011	VP012	VP013	VP014	VP015	VP016
Horizontal 1	9.11	26.61	–	1.93	6.36	10.67
Horizontal 2	6.02	33.55	29.73	6.38	25.51	18.66
Vertical	14.40	15.18	19.50	15.78	8.12	10.10

The ground accelerations emitted during the installation of pile 79B_T02 are plotted in figure 4.14. The results show a general decrease with increasing horizontal distance from the source, except for the horizontal vibrations from channel 1, figure 4.14a. Comparing the acceleration levels from the sensors placed along the riverbank and from the sensors placed perpendicular to the riverbank, it can be noticed that for all the three directions, the accelerations are higher along the riverbank, from sensor VP009 to VP007. For the present

case, the increase in overburden stresses leads to a decrease in ground accelerations.This result regarding the influence of vertical effective stress was not visible from the vibration attenuation plots, figure 4.10.

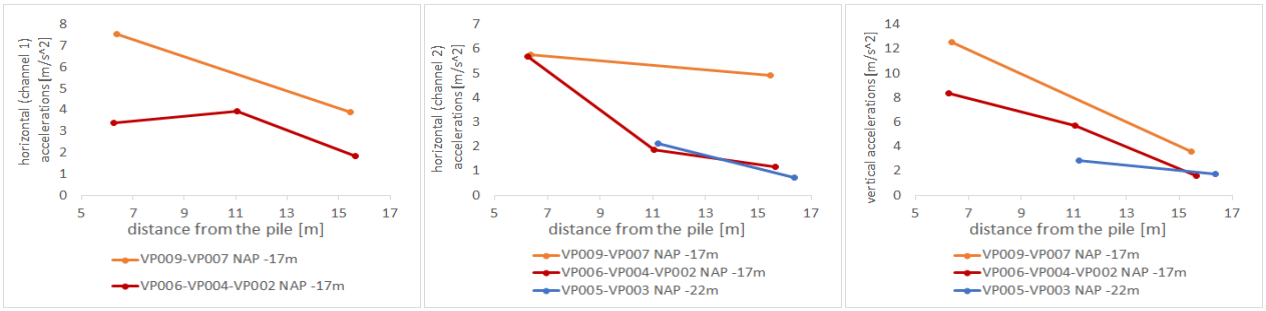

(a) Horizontal accelerations (channel 1) (b) Horizontal accelerations (channel 2) (c) Vertical accelerations

Figure 4.14: Accelerations attenuation from the source, pile 79B_T02

Figure 4.15 shows the peak accelerations recorded for the impact driving of pile 82_T07. Only vertical accelerations show a decrease over increasing horizontal distance from the pile, figure 4.15c. For this case, the vertical accelerations recorded along the riverbank are smaller than the vertical accelerations recorded by the sensors placed perpendicular to the riverbank. Compared to the results from installing pile 79B_T02, the vertical effective stress has the opposite influence, the ground accelerations decrease with the decreasing of effective stresses.

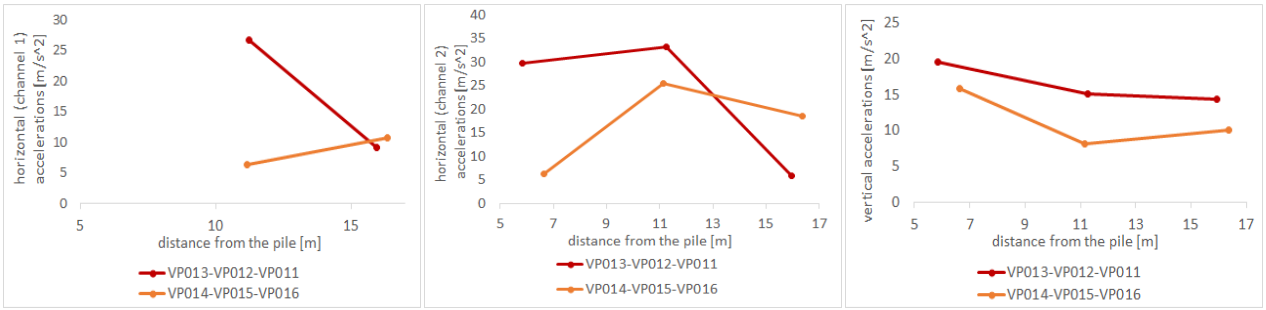

(a) Horizontal accelerations (channel 1) (b) Horizontal accelerations (channel 2) (c) Vertical accelerations

Figure 4.15: Accelerations attenuation from the source, pile 82_T07

4.4. Frequency domain

The vibratory motion consists of different frequencies occurring simultaneously. In the frequency spectrum the vibration signals are divided into individual components. The frequency content was estimated by performing a Fast Fourier Transform (FFT). The method changes the time domain to frequency domain. The frequency spectrum represents the frequency domain containing the the intensity of all frequencies. The maximum frequency in this spectrum is related to the measured samples per second. For the current field study, the geophones have a sampling rate of 1000 Hz, which means that the frequency spectrum reaches 500 Hz0. The fast Fourier transform is performed in MATLAB environment, using the built-in FFT facility.

4.4.0.1. Vibratory pile driving

For vibratory driving, hammer ICE36RF was used. The driving frequency of this type of hammer is 38.33 Hz (2300 rpm).
From the results shown in appendix D, it can be observed that the vibrations have the highest velocity at 35 Hz. The predominant frequency corresponds to the driving frequency. A sequence of harmonics occurs after 35 Hz. The peaks show up at an equal intervals, given by the driving frequency.

4.4.0.2. Impact pile driving

The frequency domain resulted from the measurements of velocities due to impact driving are shown in D. For impact driving, the frequencies do not show a clear dominant frequency as for vibratory driving.

5 Prediction model results

5.1. Introduction

The prediction model presented in section 2.5 is applied to the soil conditions in Caland Canal. The results will be compared with the field measurements. The following sections include information about the input data, the results of the velocities calculations and a comparison between predicted vibration velocities and measured velocities.

5.2. Input parameters

In the following subsections, information can be found about the data needed as input for the prediction model regarding the soil, the pile and the impact hammer.

5.2.1. Soil related parameters

Geotechnical related properties needed for calculating the velocity of the cylindrical waves are the shear modulus, the dry material density and the thickness of the soil layer at the depth where velocities are calculated. The shear modulus and the material density determine the shear wave velocity which is used in calculating the wave length. The wave length and the material density together with the thickness of the soil layer are used to calculate the material coefficient k_c.
For the calculation of the spherical waves velocity, the soil related parameters are the P-wave velocity and the total soil density. For soil layer under the ground water table, the compression wave speed is the same as for water and it is assumed to $1450 m/s$.

Table 5.1 summarizes the input parameters related to geotechnical characteristics of the two data sets. The values are chosen according to the soil profiles presented in appendix **??** and they are representative for the soil layers found at the depths where the vibrations are going to be calculated. At the location of pile 79B_T02, the depths of interest are at NAP -17 m, located in a 2 meters thick clay layer, and at NAP -22 m, which is in a sand layer of 4 meters thickness. At the location of pile 82_T07, the velocities will be calculated at the depth NAP -18.50 m, found in a sandy clay layer with a thickness of 3.80 meters.

Table 5.1: Geotechnical soil properties

Data set	Soil layer	Thickness [m]	G [MPa]	ρ_{dry} $[kg/m^3]$	ρ_{sat} $[kg/m^3]$	Shear wave velocity c_s $[m/s]$	P-wave velocity c_p $[m/s]$
Pile 79B_T02	Clay	2	2	1800	1800	30	1450
	Sand	4	19	2000	2200	98	1450
Pile 82_T07	Clay	3.8	2	1700	2000	38	1450

5.2.2. Pile parameters

Data related to the tubular pile includes geometrical properties, diameter and thickness, and material properties such as modulus of elasticity and material density. From these properties, the following terms are calculated: area of the cross-section, stress wave speed and impedance.
The piles installed at Caland Canal have different thicknesses along the length. Thus, an average thickness is chosen for calculating cylindrical waves and the thickness of the last pile segment is chosen for calculating

the spherical waves. Piles with the same characteristics were driven at both berthing locations. The pile data is summarized in table 5.2.

Table 5.2: Pile data

Pile diameter		2.5	$[m]$
Elasticity modulus		2.1e+11	$[N/m^2]$
Material density		7850	$[kg/m^3]$
Stress wave speed		5172	$[m/s]$
Pile thickness	$t^P_{average}$	0.052	$[m]$
	t^P_{toe}	0.023	$[m]$
Cross-section area	$A^P_{average}$	0.400	$[m^2]$
	A^P_{toe}	0.179	$[m^2]$
Pile impedance	$Z^P_{average}$	16237124	$[Ns/m]$
	Z^P_{toe}	7266883	$[Ns/m]$

5.2.3. Hammer parameters

The properties of the hydraulic hammer IHC S-280 are given in table 5.3. The input of the driving energy is taken as the maximum energy delivered by the hammer. The ratio between the actual energy delivered by the hammer divided by the hammer potential energy represent the hammer efficiency [9]. The efficiency can be determined from field tests. For the following calculations, the efficiency factor $F^H = 0.9$ was chosen as a conservative upper value for hydraulic hammers.
Other hammer related parameters are the frequency of vibrations, the length of the hammer and material properties. The elasticity modulus and the material density are used to calculate the speed of the wave stress which is further used together with the pile length to calculate the impact time, according to equation 2.35.

Table 5.3: Data for IHC S-280 hydraulic hammer

Potential energy	280000	$[Nm]$
Hammer efficiency factor	0.9	$[-]$
Frequency of vibrations	15	$[Hz]$
Length	7.45	$[m]$
Elastic modulus	2.1e+11	$[N/m^2]$
Material density	7850	$[kg/m^3]$

5.3. Results

In this section the results of applying the prediction model developed by Massarsch and Fellenius to the soil conditions at Caland Canal are presented. The input parameters for the calculations are given in the previous section. The calculations are performed for depths NAP -17 m and NAP -22 m at the location of pile 79B_T02 and for depth NAP -18.50 m at the location of pile 82_T07.
The velocities will be calculated for the first pile at 6.25 m, 11.05 m and 15.65 m horizontal distance from the pile for depth NAP -17 m. At NAP -22 m, the velocities are calculated at 11.15 m and 16.35 m distance. For the second pile, vibrations are calculated at 5.85 m, 11.25 m and 15.95 m horizontal distance. These values are chosen in order to compare the results of the prediction model with the measurements from the sensors placed at the mentioned depths and distances.

5.3.1. Calculations cylindrical waves velocity

The vertical component of the cylindrical waves velocity is calculated according to equation 2.47. The height of the cylinder representing the wave front of the shear waves emitted from the pile shaft is determined by the length of the stress wave in the pile. The value of the length of the stress wave is given in equation 5.1.

According to this results, the stress wave travels over the length of the pile for 14.90 m.

$$L_w = 2L^H \frac{c^P}{c^H} = 14.90 \quad [m] \tag{5.1}$$

The stress wave is the result of the difference in stresses at the pile-soil contact surface [23], meaning that the stress wave is considered to start from the ground level which is at NAP -12.50 m at the location of pile 79B_T02 and at NAP -16 m at the location of pile 82_T07. For pile 79B_T02, the stress wave will reach NAP -27.40 m and for pile 82_T07, it reaches NAP -30.90 m. For both cases, the length of the stress wave covers the depths at which the cylindrical wave velocities are calculated. This means that the length of the stress wave is substituted by the thickness of the soil layer at the depth where the velocities are calculated.
The contact area between the pile and the different soil layers, $A_{contact}$, is defined by the thickness of the soil layer, h_c, and the external pile diameter. The wave length of cylindrical waves is determined by the frequency of vibrations, given in table 5.3, and the speed of the shear waves in the soil, c_s. The shear wave velocity is a soil characteristic, given in table 5.1.
The reduction factor for strain-softening, R_c, is chosen 0.30. The other reduction factor related to the dynamic soil resistance along the pile shaft, R_r, is considered 1. This factor depends on the pile material and for a steel pile, a rather conservative approach is chosen, considering no dynamic soil resistance reduction due to remolding and disturbance along the pile shaft. In the article by Massarsch and Fellenius [15], the R_r reduction factor is 0.5 for concrete piles. Not much information is given about the reduction factors and for the current calculations, they are chosen based on assumptions made from the examples presented by Massarsch and Fellenius [15].
The vibrations transmission efficacy, E_s, is calculated according to equation 2.44. The calculations of the cylindrical waves velocity are summarized in table 5.4 for pile 79B_T02 and in table 5.5 for pile 82_T07.

Table 5.4: Calculations vertical component of cylindrical wave velocity for pile 79B_T02

Soil layer	Calc. depth	Emb. depth	h_c	$A_{contact}$	λ_c	k_c	R_c	R_r	E_s	r	v_c
	$[m]$	$[m]$	$[m]$	$[m^2]$	$[m]$	$\left[\sqrt{\frac{m}{kg}}\right]$	$[-]$	$[-]$	$[-]$	$[m]$	$[mm/s]$
Clay	-17	4.50	2	15.71	2	0.0067	0.30	1	0.02	6.25	20.90
										11.05	15.72
										15.65	13.21
Sand	-22	9.50	4	31.42	6.54	0.0025	0.30	1	0.11	11.15	42.22
										16.35	34.87

Table 5.5: Calculations vertical component of cylindrical wave velocity for pile 82_T07

Soil layer	Calc. depth	Emb. depth	h_c	$A_{contact}$	λ_c	k_c	R_c	r	E_s	r	v_c
	$[m]$	$[m]$	$[m]$	$[m^2]$	$[m]$	$\left[\sqrt{\frac{m}{kg}}\right]$	$[-]$	$[-]$	$[-]$	$[m]$	$[mm/s]$
Sandy clay	-18.50	2.5	3.8	18.65	2.51	0.0041	0.30	1	0.02	5.85	18.71
										11.25	13.49
										15.95	11.33

5.3.2. Calculations spherical waves velocity

The vertical component of the spherical waves is calculated for two cases. The first case is considered for the start of the impact driving, when the distance between the depth of interest for calculations and the depth reached by the pile toe is the smallest. In the second case, calculations are performed considering a higher depth for the pile toe, closer to the end of the driving process. The impact driving starts when the pile has reached depth NAP -22 m at the location of pile 79B_T02. The spherical wave velocities are calculated for when the pile toe is at NAP -23 m for the first case and for when the pile reaches NAP -30 m for the second case. For pile 82_T07, the impact driving starts at depth NAP -27 m and the two depths of interest are NAP

-28 m and NAP -38 m.
The plugging effect is not taken into account, which means that the soil resistance at the pile toe is calculated only at the contact surface between pile and soil. Since the soil resistance at pile toe is the source of spherical waves, their velocity is reduced in case of open-ended piles. The soil resistance at the pile toe was discussed in section 2.3.4.1. The empirical factor that takes into account the soil compaction at the pile toe is chosen $R_R = 2$ for sand. This value is suggested by the authors of the prediction model as a preliminary indication.
The length of the spherical waves is determined from the frequency of vibrations, given in table 5.3, and from the S-waves speed, given in table 5.1. The vibrations transmission efficacy is calculated from equation 2.46 and the vibrations velocity is determined using equation 2.49.
The distance between the source of vibrations and the location where the velocities are calculated is given by r_s, which is calculated from the horizontal distance r from the pile to the point of interest and the depth of the pile toe.
Table 5.6 and table 5.7 contain the velocity calculations from pile 79B_T02, for the two considered depths af the pile toe: NAP -23 m and NAP -30 m. Calculations for vertical component of spherical waves velocity from the installation of pile 82_T07 are presented in table 5.8, for pile toe depth NAP -27m, and in table 5.9, for pile toe depth NAP -38 m.

Table 5.6: Calculations vertical component of spherical wave velocity for pile 79B_T02, pile toe at -23 m depth

Soil layer	Calc. depth	Pile toe depth	λ_s	k_s	r	E_t	r	β	r_s	v_s
	$[m]$	$[m]$	$[m]$	$[\sqrt{\frac{m^2}{kg}}]$	$[-]$	$[-]$	$[m]$	$[°]$	$[m]$	$[mm/s]$
Clay	-17	-23	96.67	0.0010	2	0.023	6.25	46	8.66	0.90
							11.05	61	12.57	0.43
							15.65	69	16.76	0.24
Sand	-22		96.67	0.0009	2	0.029	11.15	85	11.19	0.47
							11.15	87	16.38	0.25

Table 5.7: Calculations vertical component of spherical wave velocity for pile 79B_T02, pile toe at -30 m depth

Soil layer	Calc. depth	Pile toe depth	λ_s	k_s	r	E_t	r	β	r_s	v_s
	$[m]$	$[m]$	$[m]$	$[\sqrt{\frac{m^2}{kg}}]$	$[-]$	$[-]$	$[m]$	$[°]$	$[m]$	$[mm/s]$
Clay	-17	-30	96.67	0.0010	2	0.023	6.25	26	14.42	0.70
							11.05	40	17.06	0.50
							15.65	50	20.35	0.35
Sand	-22		96.67	0.0009	2	0.029	11.15	54	13.72	0.55
							11.15	64	18.20	0.37

Table 5.8: Calculations vertical component of spherical wave velocity for pile 82_T07, pile toe at -27 m depth

Soil layer	Calc. depth	Pile toe depth	λ_s	k_s	r	E_t	r	β	r_s	v_s
	$[m]$	$[m]$	$[m]$	$[\sqrt{\frac{m^2}{kg}}]$	$[-]$	$[-]$	$[m]$	$[°]$	$[m]$	$[mm/s]$
Sandy clay	-18.50	-27	96.67	0.0009	2	0.058	7.10	37	18.86	0.82
							12.50	53	15.70	0.45
							17.20	61	19.65	0.28

Table 5.9: Calculations vertical component of spherical wave velocity for pile 82_T07, pile toe at -38 m depth

Soil layer	Calc. depth	Pile toe depth	λ_s	k_s	r	E_t	r	β	r_r	v_s
	$[m]$	$[m]$	$[m]$	$\left[\sqrt{\frac{m^2}{kg}}\right]$	$[-]$	$[-]$	$[m]$	$[°]$	$[m]$	$[mm/s]$
Sandy clay	-18.50	-38	96.67	0.0009	2	0.058	7.10	20	20.75	0.54
							12.50	33	23.16	0.44
							17.20	41	26.00	0.35

The results of the calculations show for the spherical waves velocities very small values compared to the velocities of cylindrical waves. A decrease in velocity should be visible with the increase of the distance between the pile toe and the point where the vibrations are calculated. Since the values are smaller than 1, these decreases are not considerable and the contribution of the spherical waves will be considered not to have a noticeable influence.

5.4. Comparison with field measurements

The vibration velocities determined in the the previous section will be compared with the measurements of vertical peak particle velocities. The results of the measurements in terms of peak particle velocity are given in section 4.2.2.
For the calculations of vertical component of cylindrical waves velocity it is not taken into account the difference between the vibrations propagating along the riverbank and perpendicular to the riverbank. However, the following plots include the comparison between the measured data and calculations the vibrations measured in both directions relative to the riverbank.

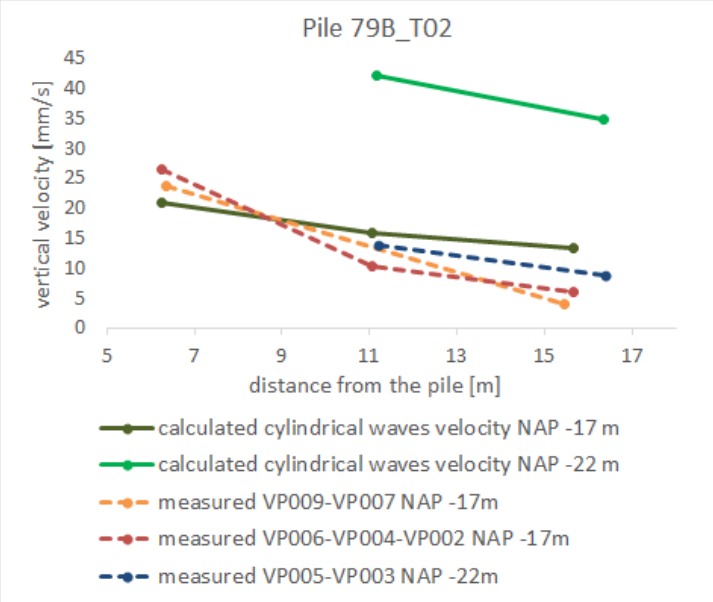

Figure 5.1: Comparison between measured vertical vibrations velocities and calculated velocities, pile 79B_T02

Figure 5.1 shows the comparison between calculated velocities and the measured peak particle velocities of vertical vibrations from the impact driving of pile 79B_T02. The calculated velocities at NAP -17 m are slightly smaller than the measured ones closer to the pile. As the distance between the pile and the sensors increases, the calculated velocities are higher than the measured ones. The prediction model does not show similar attenuation of vibrations as measured in the field. Regarding the vibrations velocities at NAP -22 m, the calculated values are about two times higher than the measured ones.

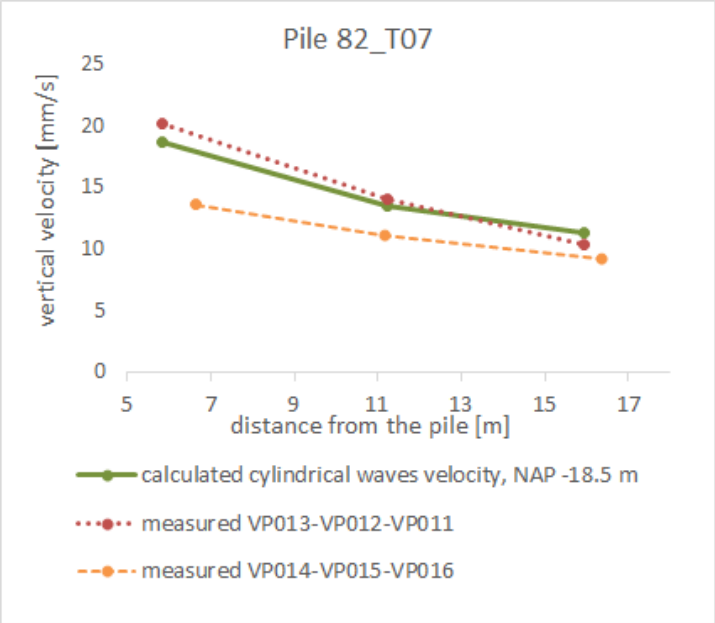

Figure 5.2: Comparison between measured vertical vibrations velocities and calculated velocities, pile 82_T07

In figure 5.2, the results of the measurements and of the calculations show a better fit for pile 82_T07 compared to pile 79B_T02. The calculated velocities very closely match the vibration velocities recorded by the sensors VP013-VP012-VP011, placed perpendicular to the riverbank.

5.5. Discussion

The calculations of the vertical component of the spherical waves are mainly influenced by the thickness of the toe for open ended tubular piles. This thickness determines the dynamic soil resistance at the pile toe by applying the reduction factor that takes into account the area of the pile cross-section divided by the area delimited by the external diameter of the pile. However, the results for spherical wave velocities are compatible with the assumption made when presenting the results in terms of vertical vibrations measurements. In section 4.2.2 it was considered that the absence of any visible variation of the vibrations amplitude during pile driving was due to the reduced influence of the spherical waves. For cylindrical waves, the amplitude of vibrations is not influenced by the penetration depth of the pile toe during pile driving.

Initially, it was considered that the thickness of the soil layer at the depth where the vibrations are calculated has the most impact on the predicted vibrations. At the location of pile 79B_T02, the thickness of the clay layer is 2 m and the thickness of the sand layer is 4 m. The thickness of the sandy clay layer surrounding pile 82_T07 from NAP -16 m to NAP -19.80 m is 3.80 m. For the clay layer the results of the prediction model show better results than the results for the sand layer, which is 4 m thick. For the sandy clay layer, the layer thickness is comparable to the one of the sand layer, but the calculated velocities fit the measured velocities.

The shear wave velocity has a considerable influence on calculating the vertical component of cylindrical wave velocity. For this reason, further research can be conducted in finding a correlation between the shear modulus of the soil and the reduction factor used when calculating the dynamic soil resistance along the pile shaft, further used in calculating the vibrations transmission efficacy. Using a different reduction factor related to the soil properties for the sand layer given in table 5.1, the prediction model can give a better approximation of the vibration velocities. Performing the same calculations as shown in table 5.4 for the velocities in the sand layer at depth NAP -22, but with the reduction factor $R_c = 0.10$, better results are obtained. The difference made by changing the R_c factor can be visualized in figure 5.3. The use of the new reduction factor leads to obtaining the same vibrations amplitude at 11.15 m distance from the pile. At 16.35 m distance, the predicted velocities are slightly higher than the measured ones.

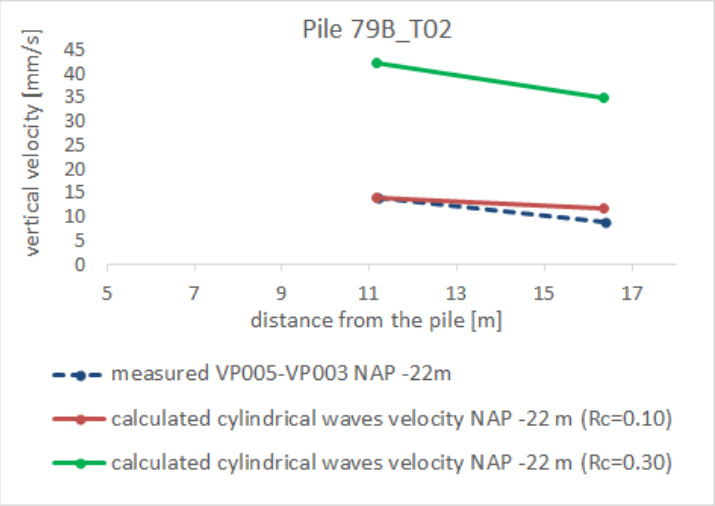

Figure 5.3: Comparison between measured vertical vibration velocities and calculated velocities using different R_c factors for the sand layer

The prediction model developed by Massarsch and Fellenius and adapted for the soil conditions in Caland Canal and for the open-ended steel tubular piles shows good results considering the main source of vibrations the cylindrical waves generated along the pile shaft. The case study dataset used by the two authors for validating the model is given for surface waves velocities. In their comparison between measurements and calculated velocities, the cylindrical waves velocities increase with increasing depth while the measured velocities at the surface level increase with increasing depth.

6 Conclusions and recommendation

6.1. Introduction

The advancement of the pile driving monitoring and electronic data acquisition systems makes it possible to gather more information about the dynamic response of the ground. During the course of completing this thesis, the recorded measurements from the field test in Caland Canal have been interpreted and analyzed. The prediction model developed by Massarsch and Fellenius [15] was adapted for open ended tubular piles and the results obtained are close to the measurement dataset. The way the prediction model was presented in this report aims to prove that the model does not need as many input parameters as discussed in the original article. However, it is not realistic to expect very few input parameters for a reliable prediction model, easy to apply in practice, that takes into account the geotechnical conditions, the hammer characteristics and the pile properties. In this chapter, the answers to the research questions are formulated based on the results provided in the previous chapters. In addition, recommendations for future research are included.

6.2. Research questions

The goal of the thesis is to provide a prediction model for sub-surface ground vibrations induced by pile driving. A literature review has been performed in order to answer the research questions stated in the first chapter. The prediction model developed by Massarsch and Felenius [15] was found in the literature. The model was adapter for open ended tubular piles and the results obtained were compared to the vibrations measured during the field test in Caland Canal. As a result, the research questions can be answered as follows:

1. *How can ground vibrations induced by pile driving be predicted at different depths?*

The amplitude of vibrations at different depths can be calculated from the propagation of driving energy through different soil layers. The amount of energy transmitted to the surrounding soil is limited by the vibrations transmission efficacy, a factor which is defined by the dynamic soil resistance and the force imparted to the pile from the impact hammer.
The results of the current research show that the main source of vibrations from impact driving of open ended tubular piles is along the pile shaft. Because of their large diameter, the piles are considered to be driven in sand in fully coring mode and the soil resistance developed at the pile tip is smaller than along the pile shaft. This approach simplifies the calculation of vibrations at different depths, as the shear waves are propagating laterally from the pile shaft and wave reflection and amplification are not taken into account. When calculating the waves propagating from the pile toe, the pile reflection has to be considered because the vibration amplitude of spherical waves is in radial direction. This effect is now considered negligible which simplifies the model.

2. *How can an existing prediction model for surface ground vibrations be modified to calculating vibrations at different depths below the surface level?*

The prediction model found in literature was not subjected to many changes, except for the assumptions related to the reduction factors used to calculate the energy transmission efficacy. The model is adapted for open ended tubular piles. This led to a decrease of the calculated particle velocity for spherical waves emitted at the pile toe, because the dynamic soil resistance at the pile toe takes into account the ratio between the area of the pile cross-section and the area delimited by the external diameter of the pile. The results are compared with velocities recorded at different depths and not at surface level, as presented by Massarsch and Fellenius [15].

3. *What are the parameters that will influence the prediction model?*

The parameters influencing the prediction model can be divided in parameters related to the soil conditions, parameters resulting from the pile geometry and parameters from the impact hammer properties. The soil related parameters are shear modulus, density, thickness of the soil layers and the empirical reduction factor for strain softening. The required properties for tubular piles are the external diameter, the wall thickness, the material density and elastic modulus. The parameters related to the hammer are the frequency of vibrations, the efficiency factor and the potential energy of the hammer.

The ground conditions have great influence on the predicted velocities. The model shows good results for the two soil layers with lower shear moduli. For the sand layer with much higher shear modulus, the model overestimates the velocity of cylindrical waves. The shear modulus is an important parameter in the model because it determines the speed of the shear waves, which is further used in calculating the dynamic soil resistance along the pile shaft and the vibrations transmission efficacy.

The thickness of the pile wall is an important parameter related to pile properties. The wall thickness at the pile toe influences the dynamic soil resistance. Together with the pile diameter and the elastic material properties of the pile, the pile thickness determines the pile impedance, which governs the transfer of vibrations in the pile and at the pile-soil interface.

6.3. Final conclusions

The prediction model shows a good correlation with the field data, considering cylindrical waves velocity as the main source of vibrations during impact pile driving. Even though the original model is focused on predicting the velocity of vibrations at surface level, the results of the current study show that the calculated velocities are a good approximation of the vibrations measured at different depths. The predicted velocities of the cylindrical waves correlate better with the measured velocities at different depths than with the measured surface waves. This is one of the main differences between the original prediction model and the one adapted for the conditions of the field study in Caland Canal.

For open ended tubular piles, if no plugging effect is considered, the soil dynamic resistance at the pile toe is considerably reduced compared to a closed ended pile. The soil dynamic resistance influences directly the velocity of the spherical waves. The results showed velocities smaller than unity for spherical waves. The cylindrical waves are the main source for ground vibrations for open ended tubular piles.

The application of the model for the field study in Caland Canal is simplified considering only the soil profile at the pile location. In reality the soil profile is more complex and the field study includes more information related to the soil profile at different locations of the sensors. Such additional information is related to the CPTs performed before and after pile installation. The relative density has been calculated based on the available CPT data, but no significant densification was noticed, limiting the use of the available data to study the effect of vibrations on densification.

6.4. Recommendations for future research

In this thesis, the prediction model is applied only for ground vibrations produced from impact driving. It is therefore recommended that future research can focus on adapting the model for vibratory pile driving. The main differences between the two driving methods that have to be taken into account are related to the hammer-pile connection and to the penetration resistance. For vibratory hammers, the connection with the pile is rigid and the energy is continuously transfered to the soil, over the entire length of the pile. The impact hammer does not have a tension connection with the pile and the energy is intermittently transmitted to the soil, over the length of the stress wave generated in the pile from the hammer-pile impact. The pile has both upwards and downwards movements during vibratory driving, influencing the development of dynamic soil resistance, considered the source of cylindrical and spherical waves.

The model could be applied for different soil conditions and pile geometry and verified against field measurements. For closed ended piles, the dynamic soil resistance at the pile toe increases, having an impact

on the spherical waves emitted from the pile toe. In this case, the wave reflections have to be considered. When driving open ended piles with smaller diameters, the chance that the pile is driven in plugging mode increases. In that case, the plug contributes to the soil resistance at the pile toe, having the same consequences on the spherical wave development as for closed ended piles .

More research can be conducted in order to find an empirical reduction factor related to the shear modulus of the soil for calculating the velocity of cylindrical waves. The results of the prediction model showed a good fit for the clay and sandy clay layer, but for the sand layer the shear modulus increases and the predicted vibrations are overestimated.

The horizontal component of cylindrical and spherical wave could be included in the model. From the field study, the measured horizontal velocities were smaller than the vertical ones, but the difference is small. For a sensitive geometry like the slope of the riverbank in the Caland Canal, the horizontal vibrations can have a high impact on slope stability.

Bibliography

[1] https://www.portofrotterdam.com/en/shipping/buoys-and-dolphins/locations-and-information-buoys-and-dolphins.

[2] P. C. Athanasopoulos G. A., Pelekis. Ground vibrations from sheetpile driving in urban environment: measurements, analysis and effects on buildings and occupants. *Soil Dynamics and Earthquake Engineering*, 19, 2000.

[3] G Baldi, R Bellotti, V Ghionna, M Jamiolkowski, and E Pasqualini. Design parameters for sands from cpt. In *Proceedings of the Second European Symposium on Penetration Testing, ESOPT*, volume 11, pages 425–432, 1982.

[4] D. D. Barkan. *Dynamics of Bases and Foundations. (translated from Russian by L. Drashevska and translation edited by G.P. Tschebotarioff.* McGraw-Hill book company Inc., N.Y., 1962.

[5] D. K. Crapps. The role of ram momentum in pile driving. In *Current Practices and Future Trends in Deep Foundations*, pages 276–309. ASCE, 2004.

[6] F. Deckner. *Ground vibrations due to pile and sheet pile driving – influencing factors, predictions and measurements.* PhD thesis, KTH, Royal Institute of Technology, 2013.

[7] P. Holscher. *Soil dynamics in urban areas.* TUDelft, 2016.

[8] K. Ishihara. *Soil Behaviour in Earthquake Geotechnics.* Clarendon Press, Oxford, Great Clarendon Street, Oxford OX2 GDP, 1996.

[9] M. Iskander. *Behavior of Pipe Piles in Sand.* Springer, 2010.

[10] T. Iwanowski and A. Bodare. On soil damping factor used in wave analysis. In *Third International Conference on Application of Stress-wave Theory to Piles, Ottawa*, pages 343–352, May 25-27, 1988.

[11] G. Jonker. Vibratory pile driving hammers for pile installations and soil improvement projects. *19th Annual Offshore Technology Conference*, 1987.

[12] M. Lidén. Ground vibrations due to vibratory sheet pile driving. 2012.

[13] T. Lunne and H. P. Christoffersen. Interpretation of cone penetrometer data for offshore sands. In *Offshore Technology Conference, 2-5 May, Houston, Texas.* Offshore Technology Conference, 1983.

[14] Bodare Massarsch, K. R. and A. A. Smekal. Effects of vibrations from railway traffic. *Banverket B01-1027/17*, 2002.

[15] K Rainer Massarsch and Bengt H Fellenius. Ground vibrations induced by impact pile driving. 2008.

[16] R. K. Massarsch. Ground vibrations caused by soil compaction. *Proceedings, International Workshop*, 2002.

[17] R. K. Massarsch and B. K. Fellenius. Deep vibratory compaction of granular soils. *Ground Improvement-Case Histories*, 2005.

[18] R. K. Massarsch and E. Westerberg. Frequency-variable vibrators and their application to foundation engineering. *Proceedings, Deep Foundation Institute, 20th Annual Conference, 14 p.*, 1995.

[19] P. Meijers. *Settlement during vibratory sheet piling.* PhD thesis, TUDelft, 2007.

[20] Nederlands Normalisatie-instituut. NEN 6740, 2006.

[21] Kyuho Paik, Rodrigo Salgado, Junhwan Lee, and Bumjoo Kim. Behavior of open-and closed-ended piles driven into sands. *Journal of Geotechnical and Geoenvironmental Engineering*, 129(4):296–306, 2003.

[22] F. Rausche, G. G. Goble, and G. E. Likins. Dynamic determination of pile capacity. In *Current Practices and Future Trends in Deep Foundations*, pages 398–417. ASCE, 2004.

[23] F. Rausche, F. Moses, and G. G. Goble. Soil resistance predictions from pile dynamics. In *Current Practices and Future Trends in Deep Foundations*, pages 418–440. ASCE, 2004.

[24] Frank Edwin Richart, John Russell Hall, and Richard D Woods. Vibrations of soils and foundations. 1970.

[25] M. S. Serdaroglu. *Nonlinear analysis of pile driving and ground vibrations in saturated cohesive soils using the finite element method*. PhD thesis, University of Iowa, 2010.

[26] M. Srbulov. *Ground vibration engineering: simplified analyses with case studies and examples*, volume 12. Springer Science & Business Media, 2010.

[27] A. Uromeihy. *Ground vibration measurements with special reference to pile driving*. PhD thesis, Durham University, 1990.

[28] A. Verruijt and S. Van Baars. *Soil mechanics*. VSSD Delft, the Netherlands, 2007.

[29] Arnold Verruijt. *An introduction to soil dynamics*, volume 24. Springer Science & Business Media, 2009.

[30] K. Viking. *Vibro-driveability - A field study of vibratory driven sheet piles in non-cohesive soils*. PhD thesis, KTH, Royal Institute of Technology, 2002.

[31] D. O. Wong. *Driveability and load transfer characteristics of vibro-driven piles*. PhD thesis, University of Houston, 1988.

[32] R. D. Woods. *Dynamic effects of pile installations on adjacent structures*, volume 253. Transportation Research Board, 1997.

A
Project data

Figure A.1: Location of the buoys and dolphins in CalandKanaal, image source: *www.portofrotterdam.comenshippingbuoys – and – dolphins*

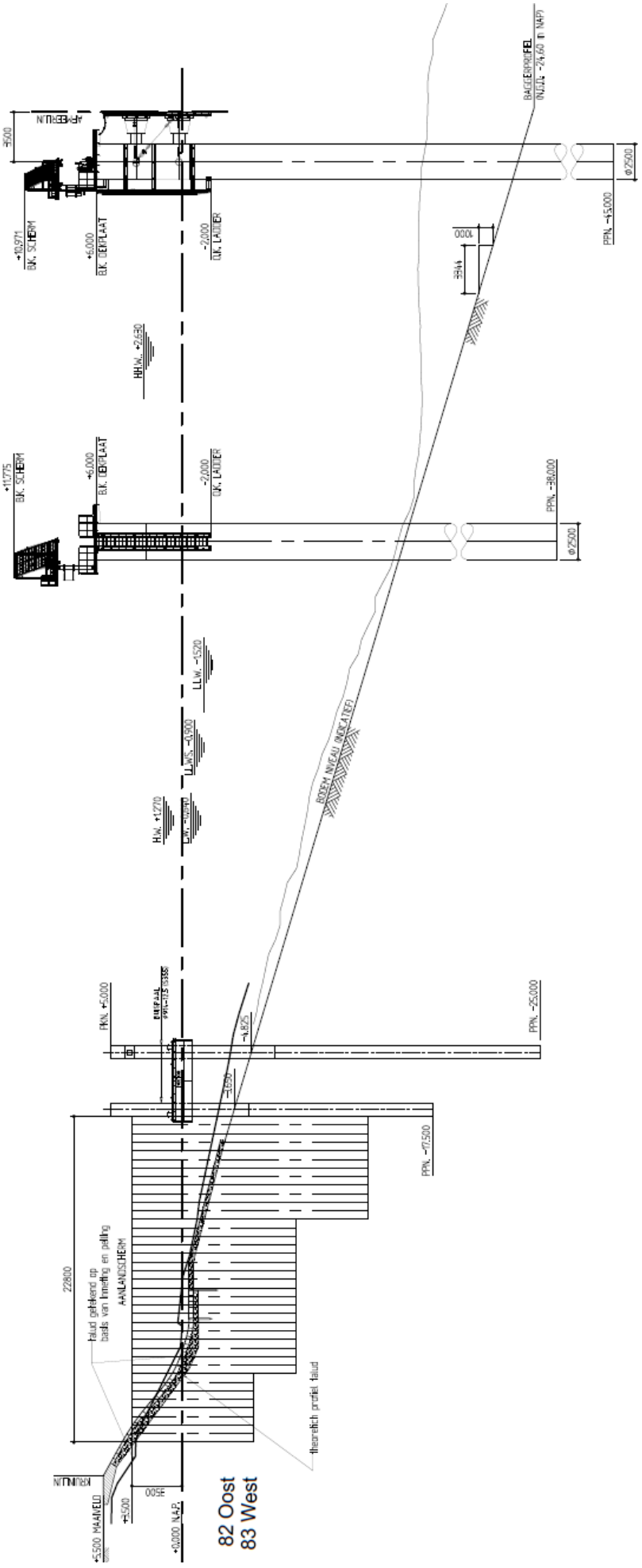

Figure A.2: Cross-section, berth 82

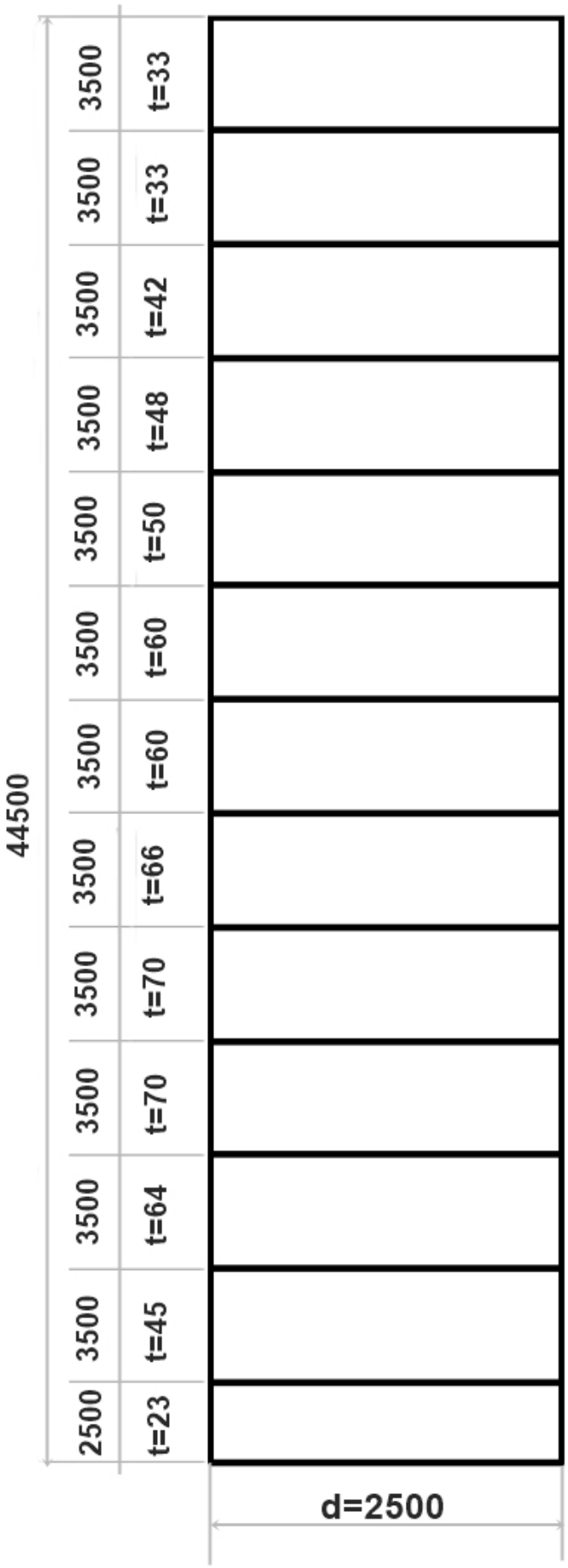

Figure A.3: Geometry of dolphin piles

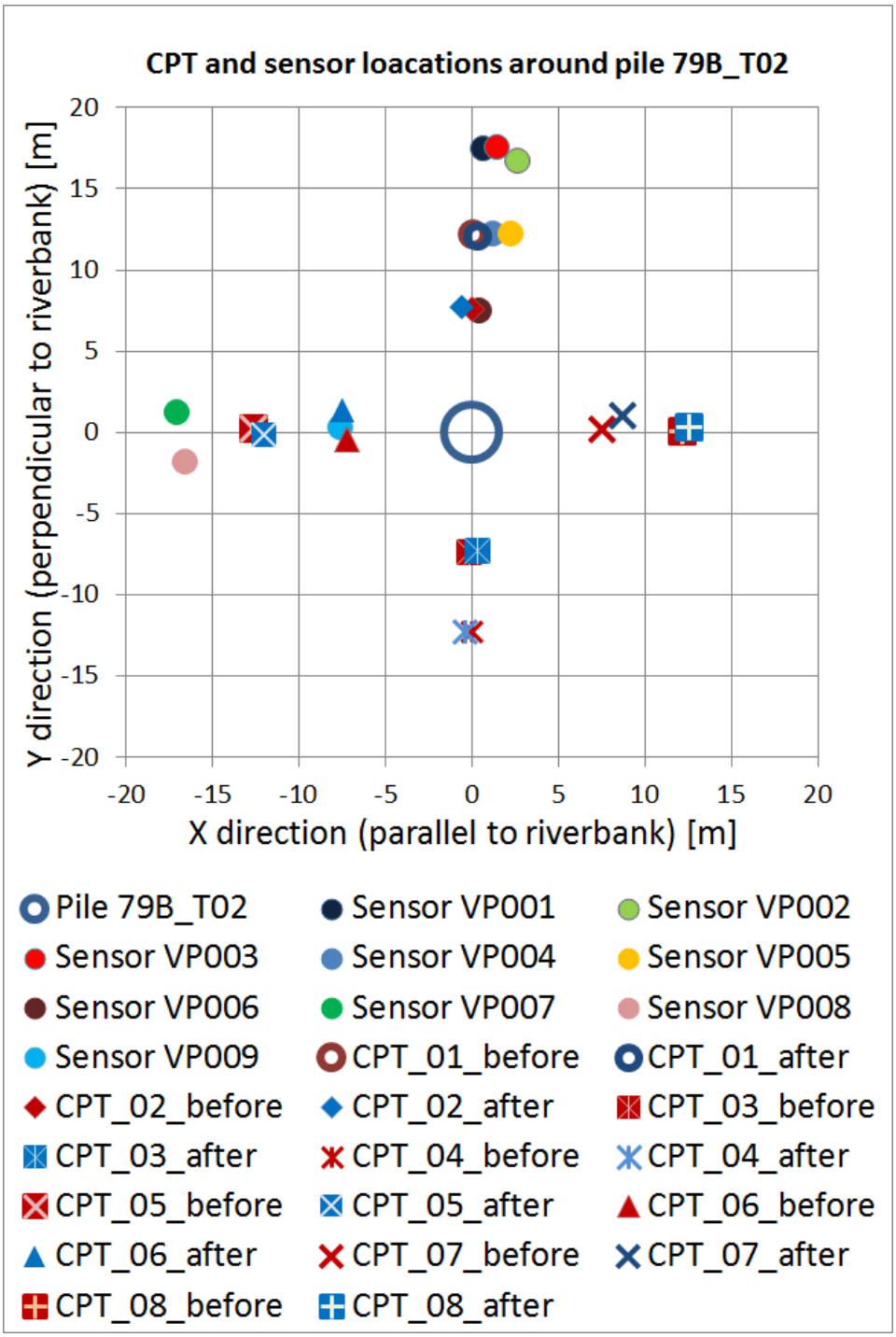

Figure A.4: Location of CPTs and sensors around pile 79B_02

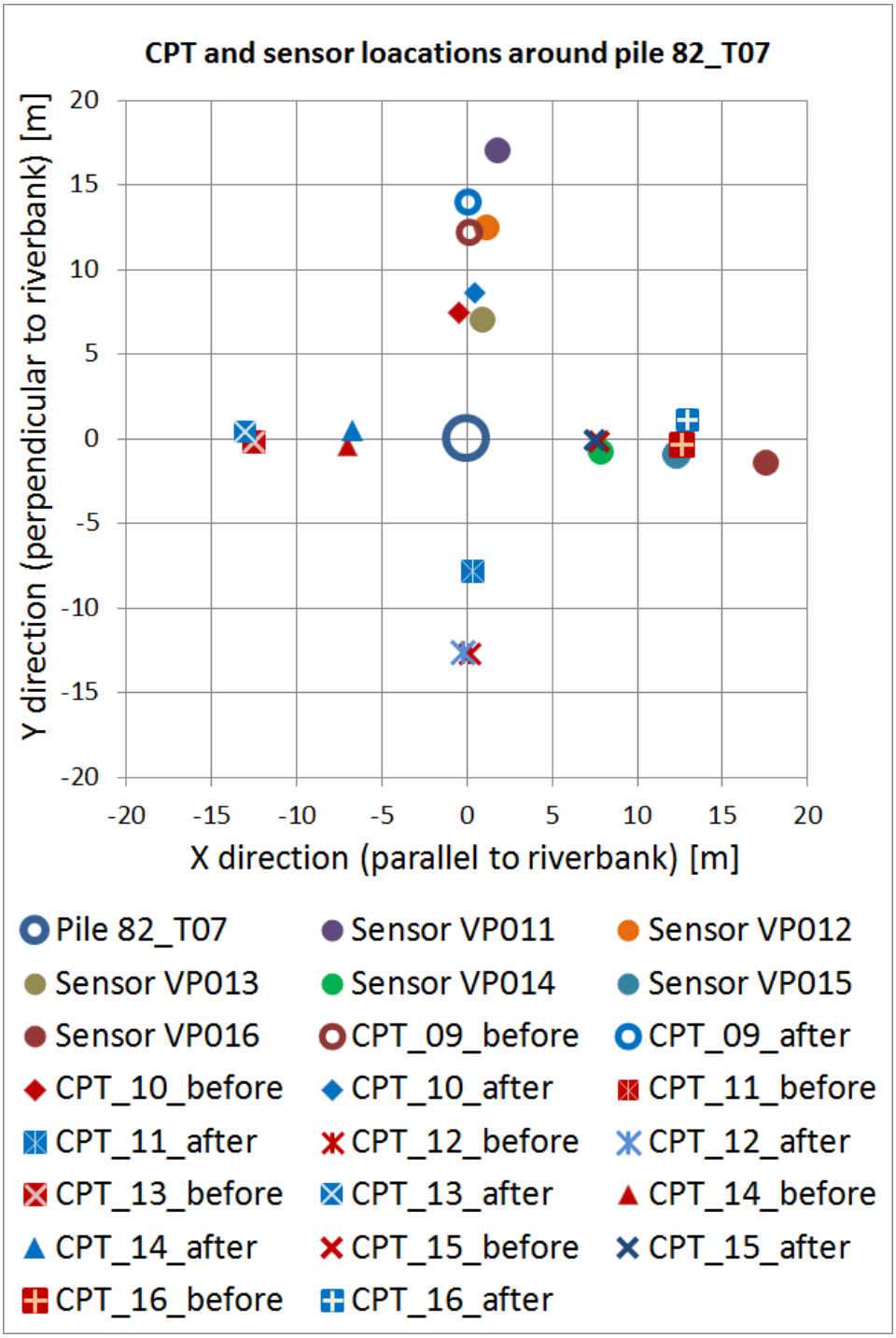

Figure A.5: Location of CPTs and sensors around pile 82_07

B

Ground velocities

Vibratory pile driving

Pile 79B_T02

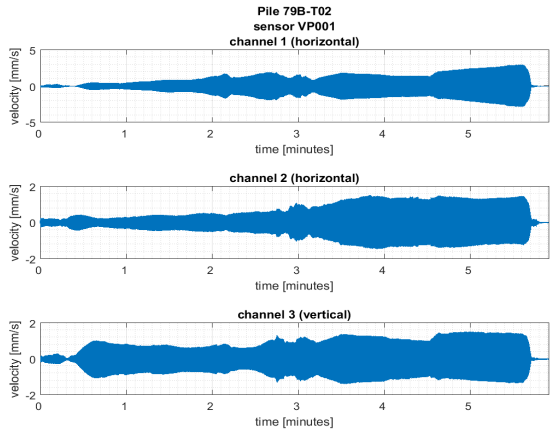

Figure B.1: Velocities recorded by sensor VP001

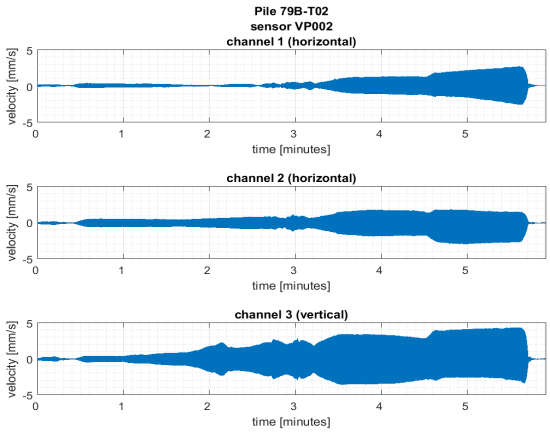

Figure B.2: Velocities recorded by sensor VP002

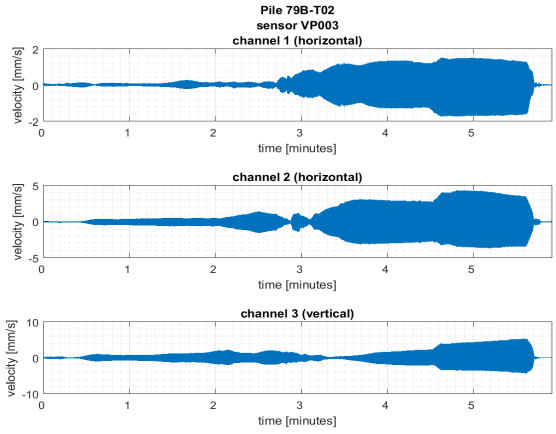

Figure B.3: Velocities recorded by sensor VP003

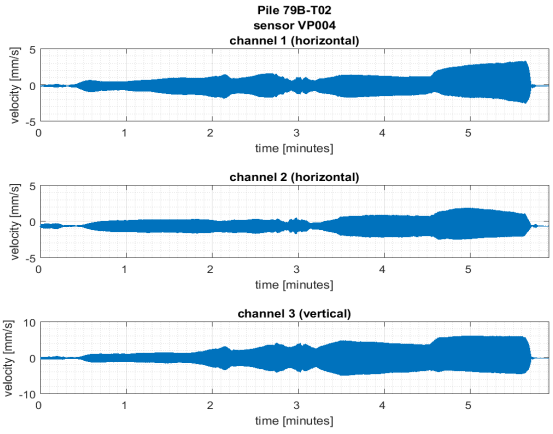

Figure B.4: Velocities recorded by sensor VP004

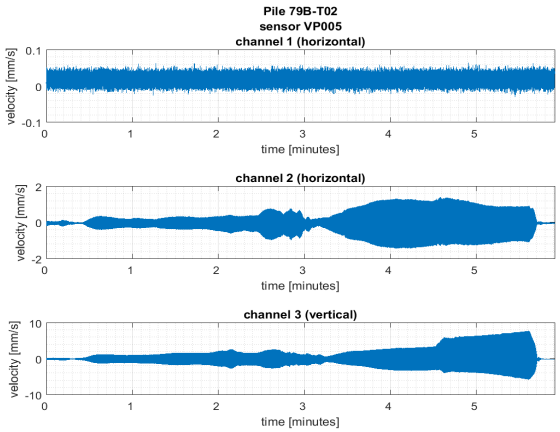

Figure B.5: Velocities recorded by sensor VP005

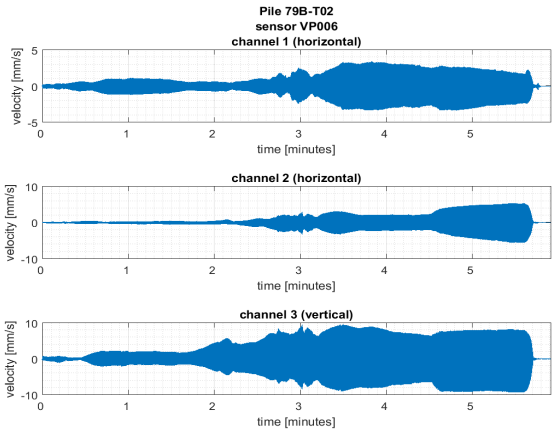

Figure B.6: Velocities recorded by sensor VP006

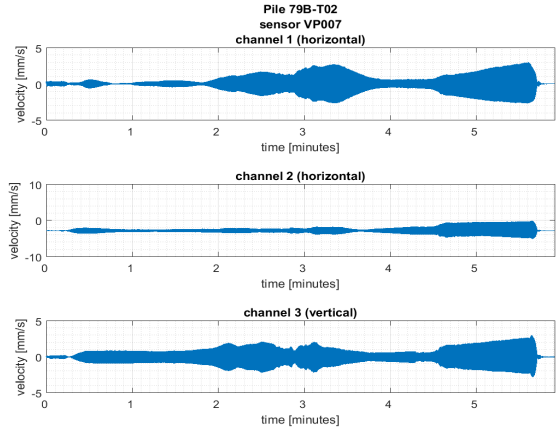

Figure B.7: Velocities recorded by sensor VP007

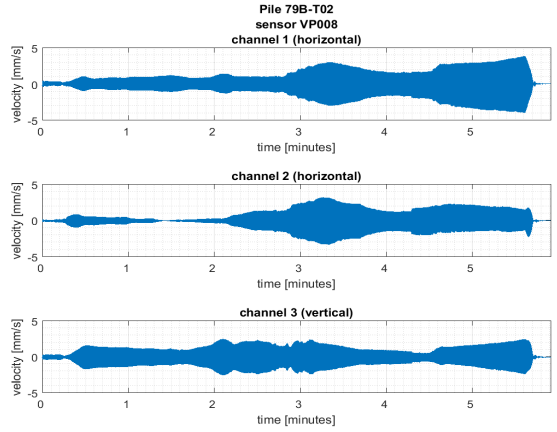

Figure B.8: Velocities recorded by sensor VP008

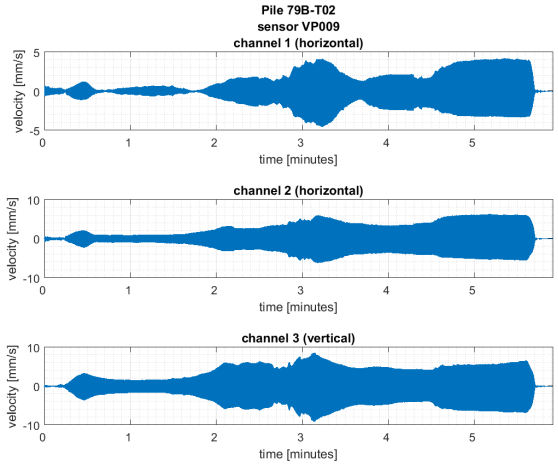

Figure B.9: Velocities recorded by sensor VP009

Pile 82_T07

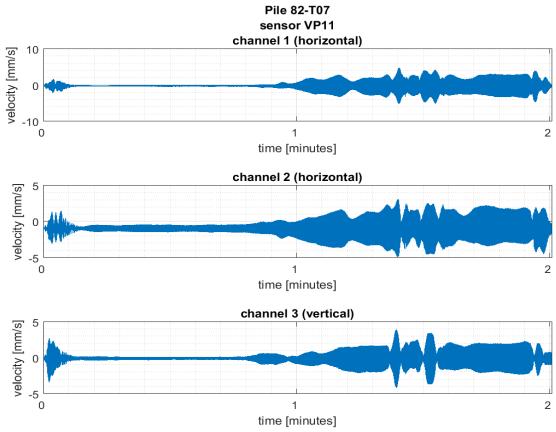

Figure B.10: Velocities recorded by sensor VP011

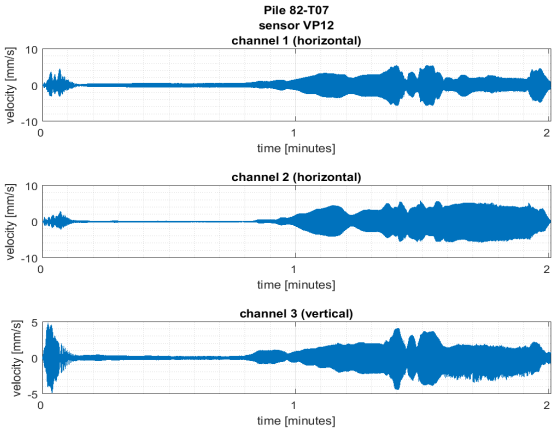

Figure B.11: Velocities recorded by sensor VP012

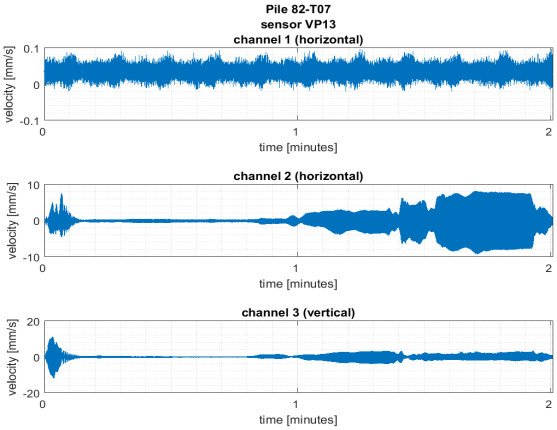

Figure B.12: Velocities recorded by sensor VP013

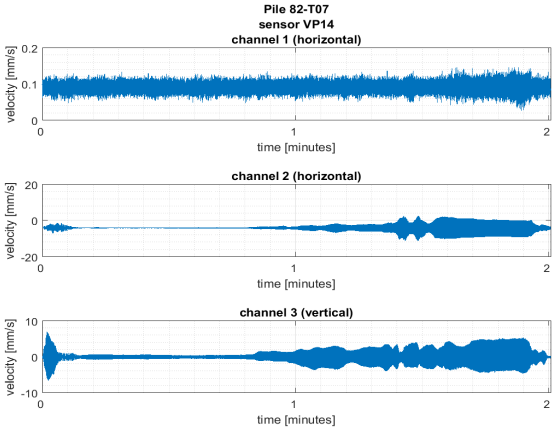

Figure B.13: Velocities recorded by sensor VP014

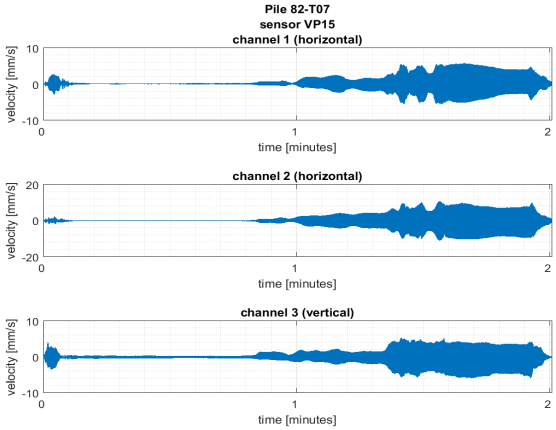

Figure B.14: Velocities recorded by sensor VP015

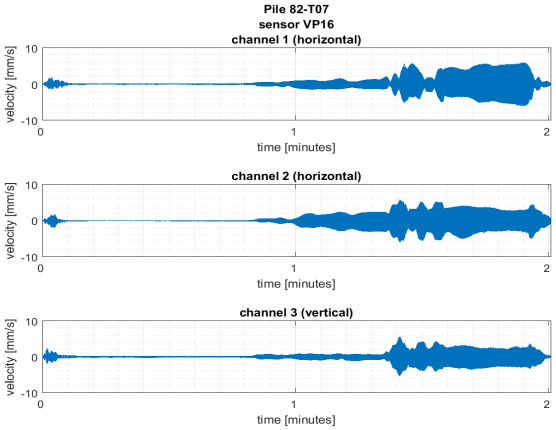

Figure B.15: Velocities recorded by sensor VP016

Impact pile driving

Pile 79B_T02

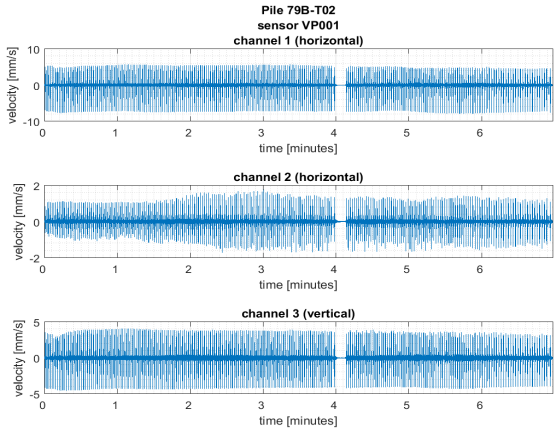

Figure B.16: Velocities recorded by sensor VP001

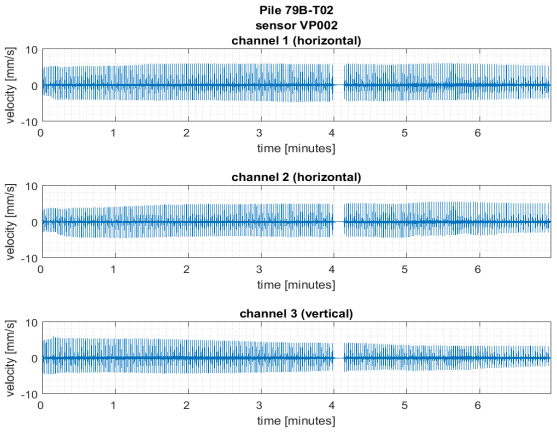

Figure B.17: Velocities recorded by sensor VP002

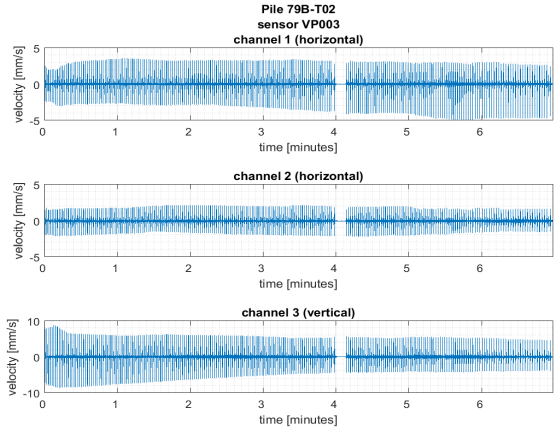

Figure B.18: Velocities recorded by sensor VP003

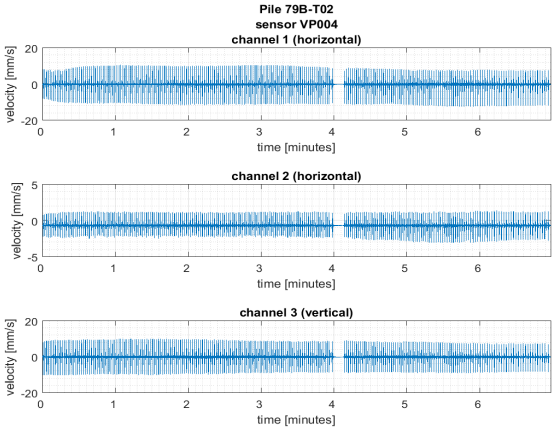

Figure B.19: Velocities recorded by sensor VP004

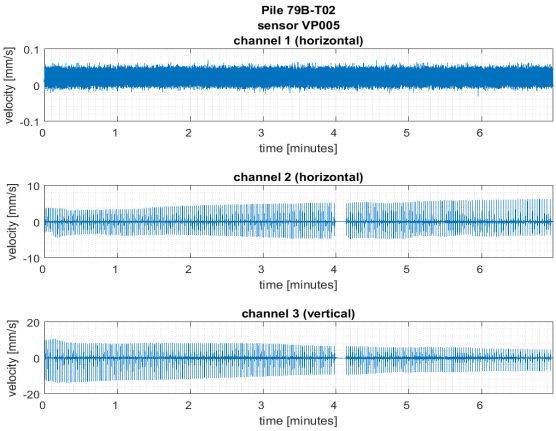

Figure B.20: Velocities recorded by sensor VP005

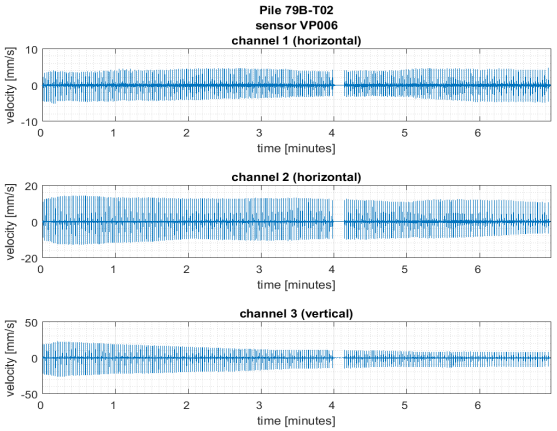

Figure B.21: Velocities recorded by sensor VP006

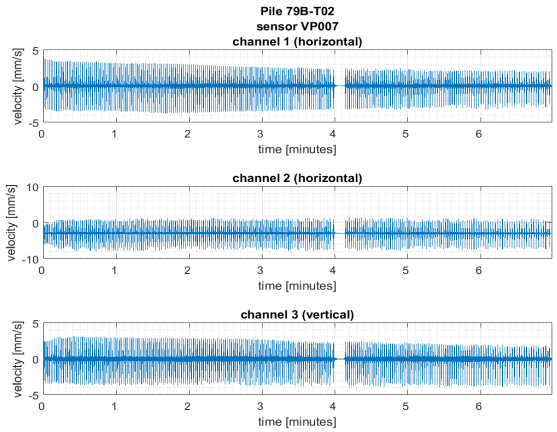

Figure B.22: Velocities recorded by sensor VP007

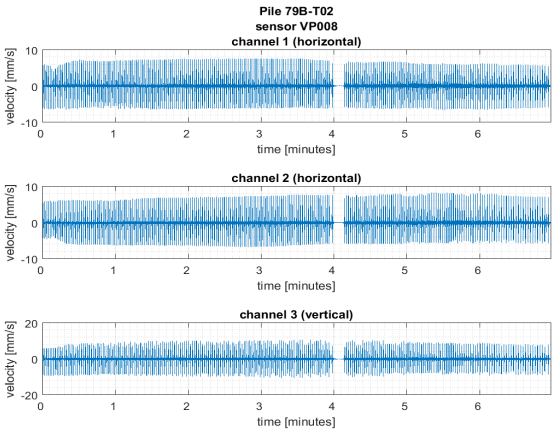

Figure B.23: Velocities recorded by sensor VP008

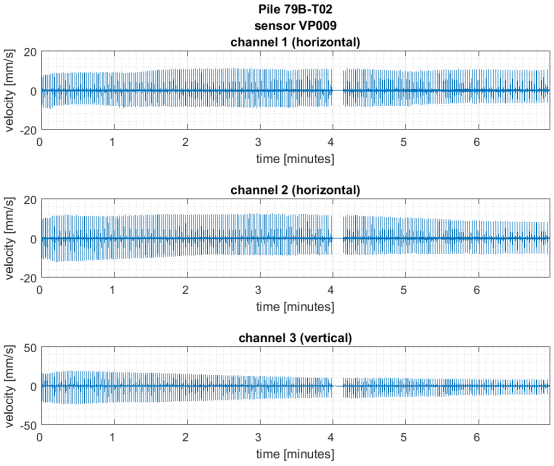

Figure B.24: Velocities recorded by sensor VP009

Pile 82_T07

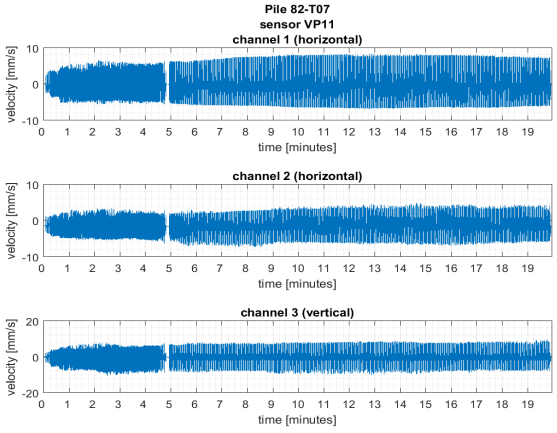

Figure B.25: Velocities recorded by sensor VP011

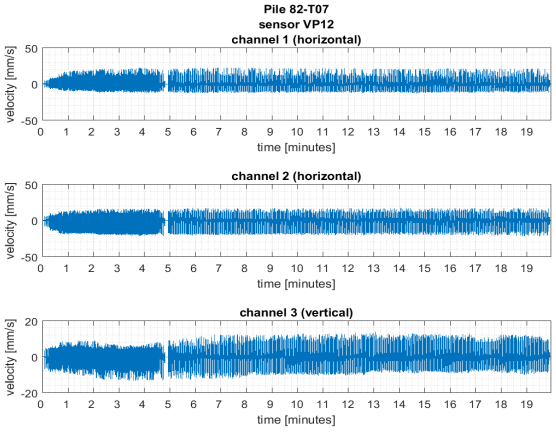

Figure B.26: Velocities recorded by sensor VP012

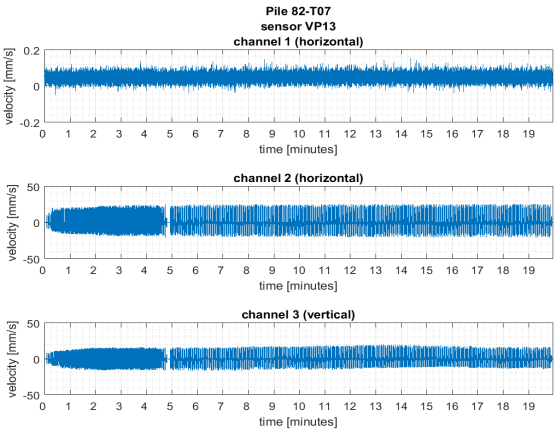

Figure B.27: Velocities recorded by sensor VP013

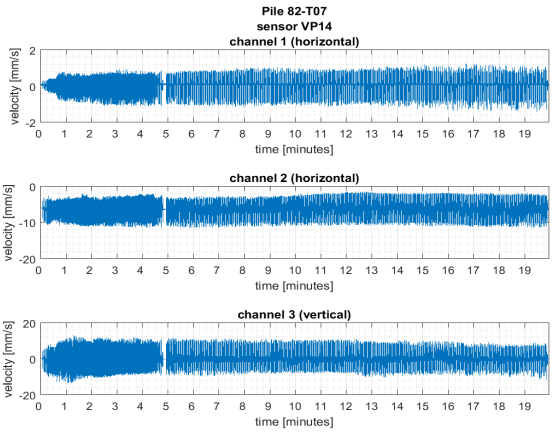

Figure B.28: Velocities recorded by sensor VP014

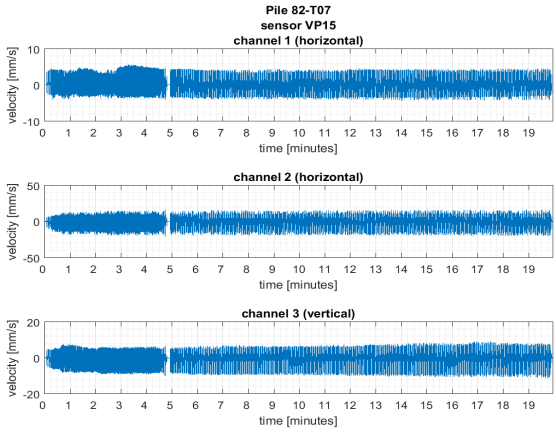

Figure B.29: Velocities recorded by sensor VP015

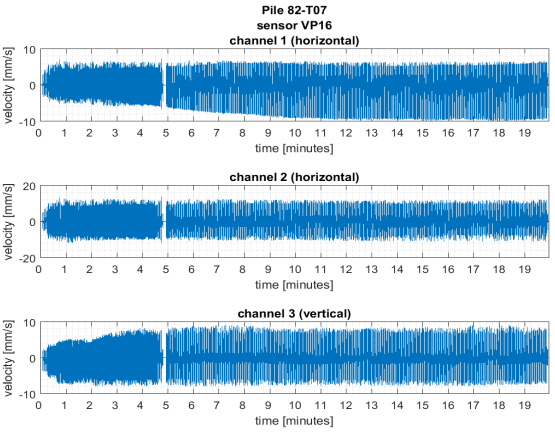

Figure B.30: Velocities recorded by sensor VP016

C

Ground accelerations

Vibratory pile driving

Pile 79B_T02

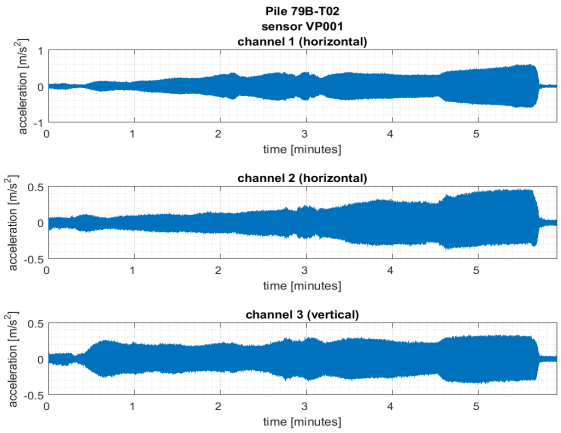

Figure C.1: Accelerations recorded by sensor VP001

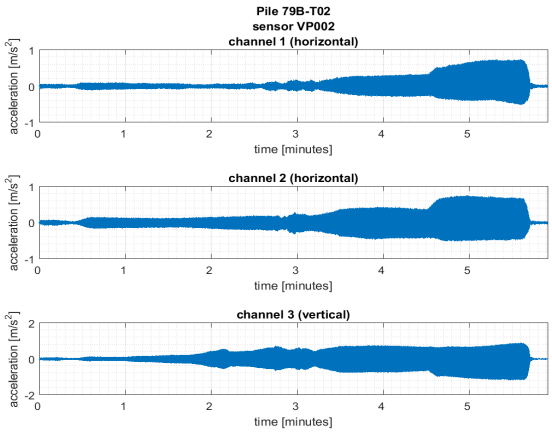

Figure C.2: Accelerations recorded by sensor VP002

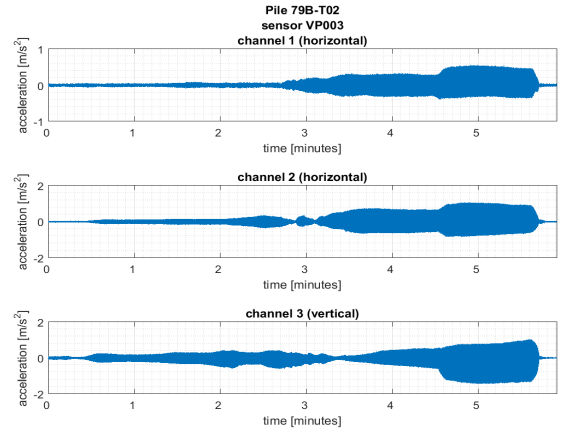

Figure C.3: Accelerations recorded by sensor VP003

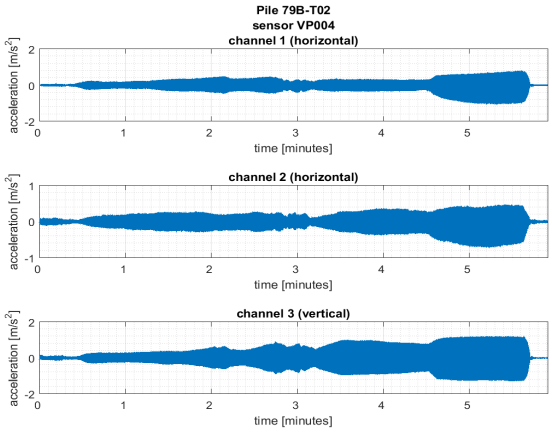

Figure C.4: Accelerations recorded by sensor VP004

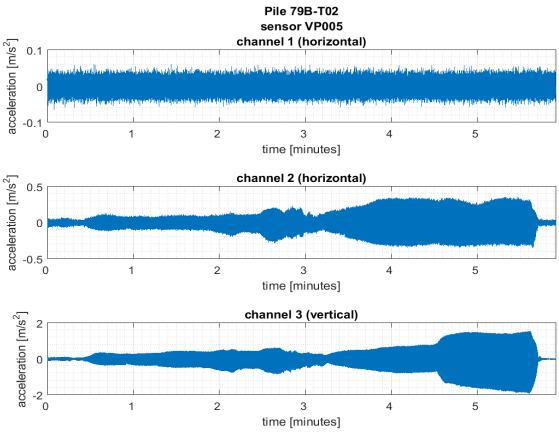

Figure C.5: Accelerations recorded by sensor VP005

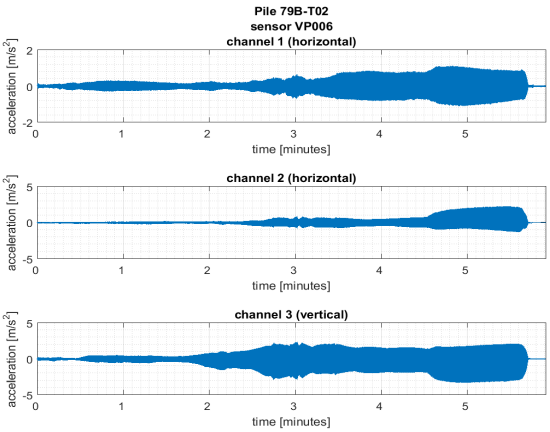

Figure C.6: Accelerations recorded by sensor VP006

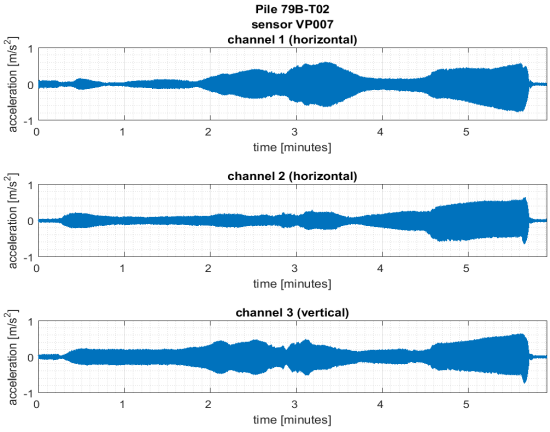

Figure C.7: Accelerations recorded by sensor VP007

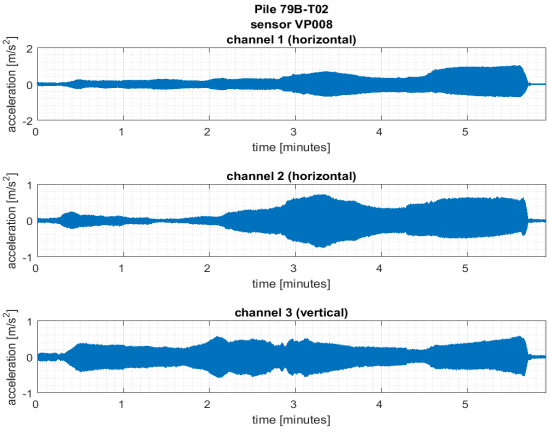

Figure C.8: Accelerations recorded by sensor VP008

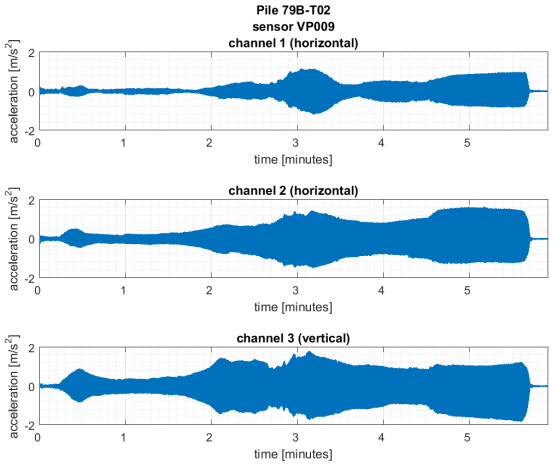

Figure C.9: Accelerations recorded by sensor VP009

Pile 82_T07

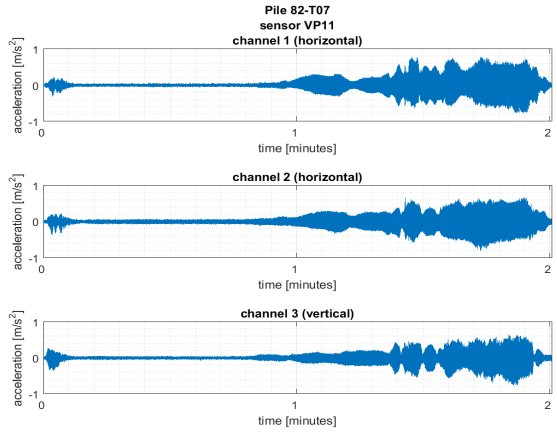

Figure C.10: Accelerations recorded by sensor VP011

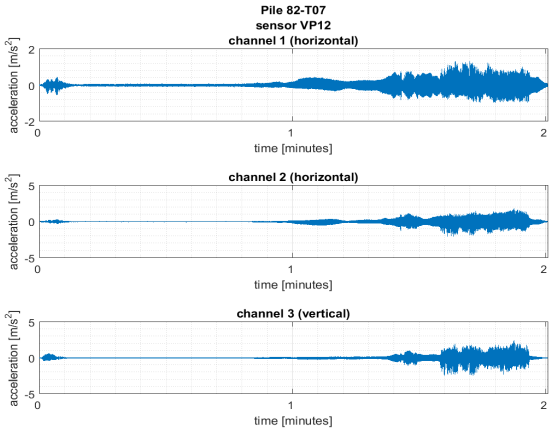

Figure C.11: Accelerations recorded by sensor VP012

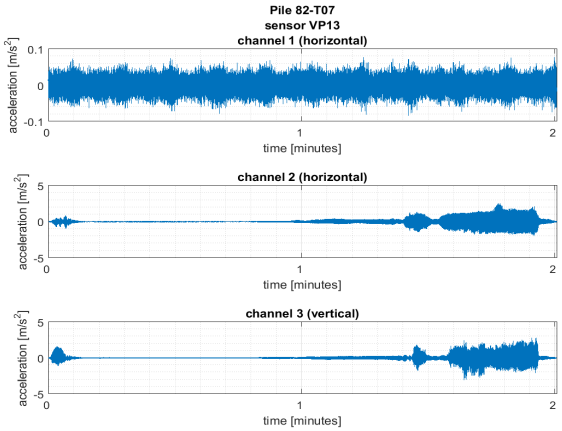

Figure C.12: Accelerations recorded by sensor VP013

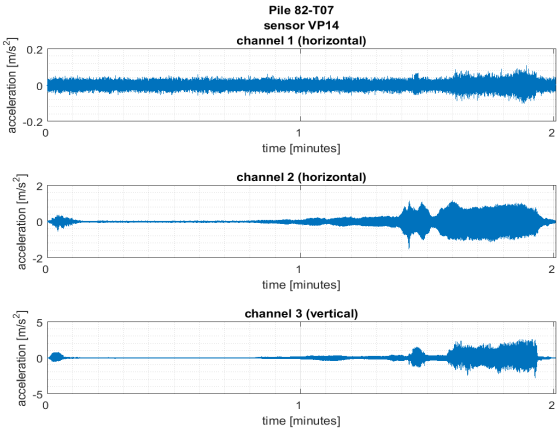

Figure C.13: Accelerations recorded by sensor VP014

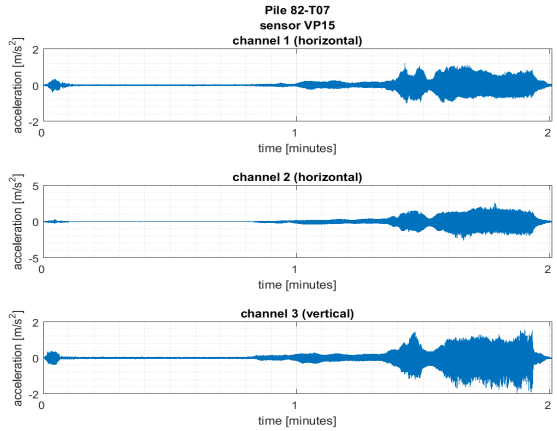

Figure C.14: Accelerations recorded by sensor VP015

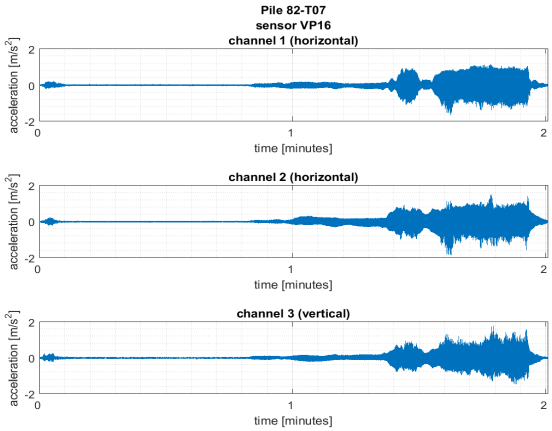

Figure C.15: Accelerations recorded by sensor VP016

Impact pile driving

Pile 79B_T02

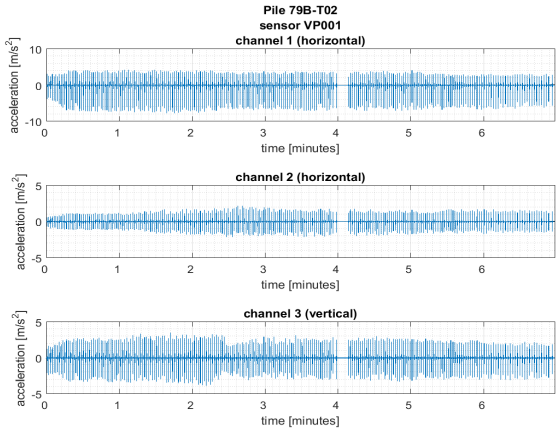

Figure C.16: Accelerations recorded by sensor VP001

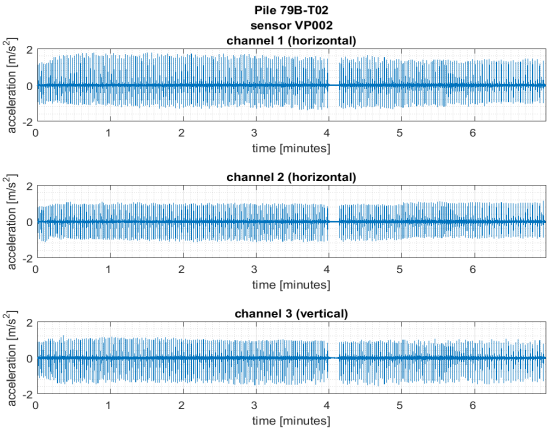

Figure C.17: Accelerations recorded by sensor VP002

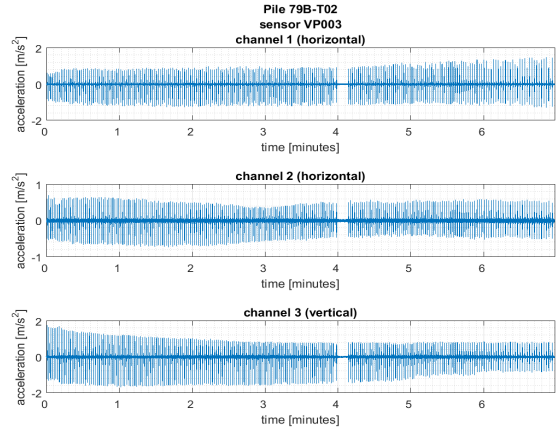

Figure C.18: Accelerations recorded by sensor VP003

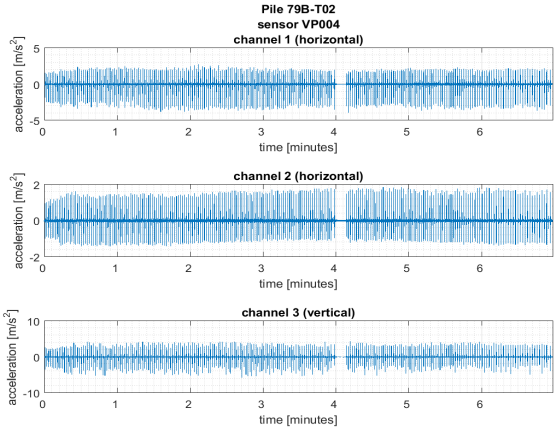

Figure C.19: Accelerations recorded by sensor VP004

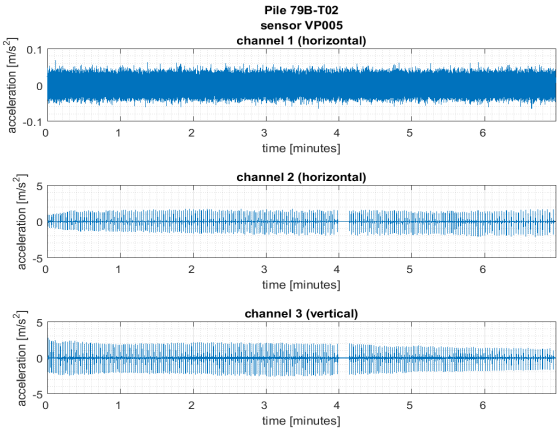

Figure C.20: Accelerations recorded by sensor VP005

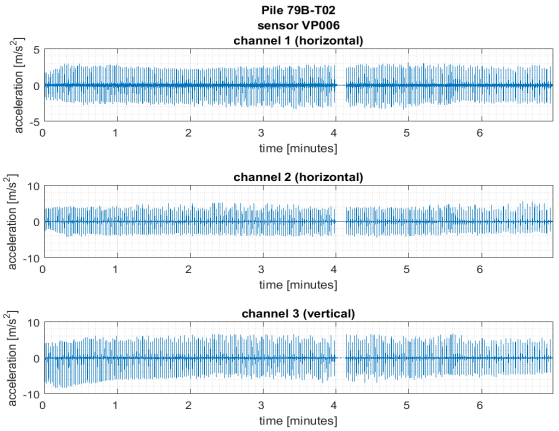

Figure C.21: Accelerations recorded by sensor VP006

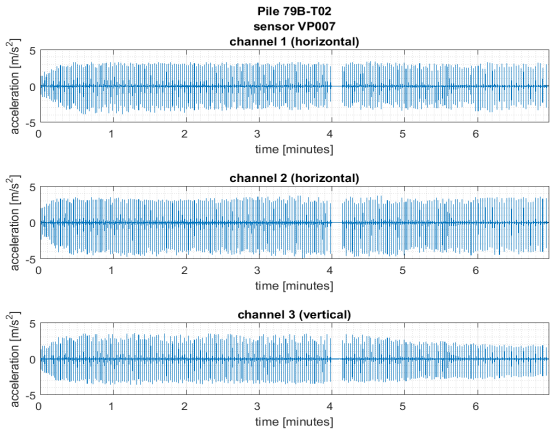

Figure C.22: Accelerations recorded by sensor VP007

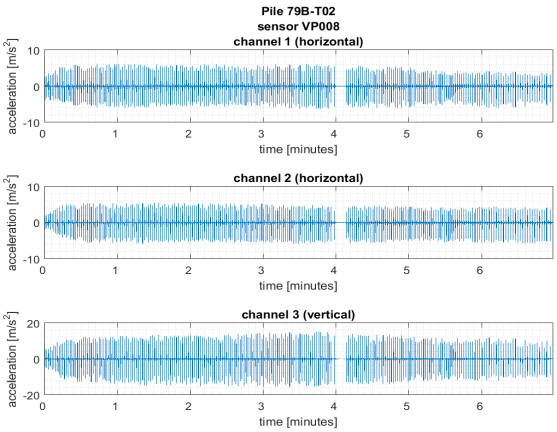

Figure C.23: Accelerations recorded by sensor VP008

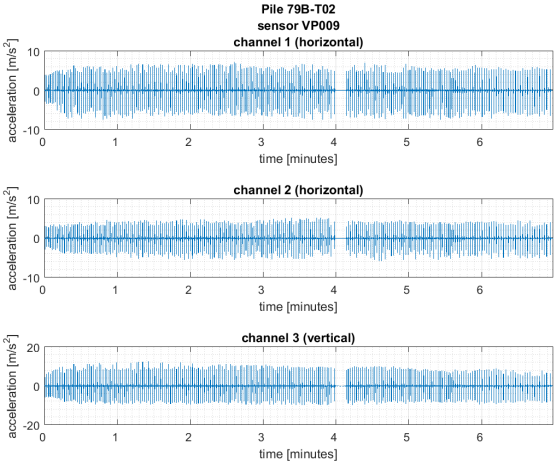

Figure C.24: Accelerations recorded by sensor VP009

Pile 82_T07

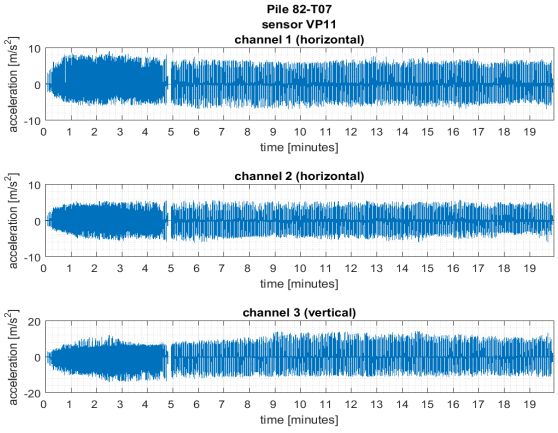

Figure C.25: Accelerations recorded by sensor VP011

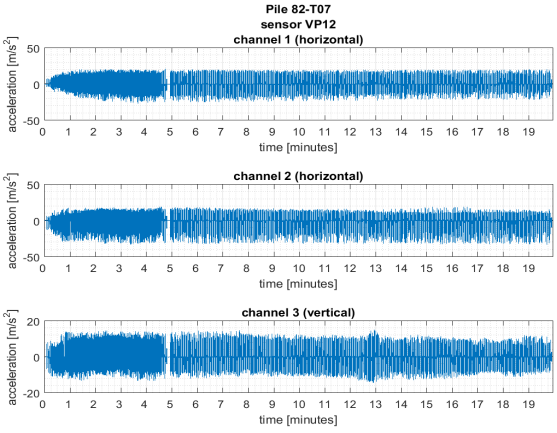

Figure C.26: Accelerations recorded by sensor VP012

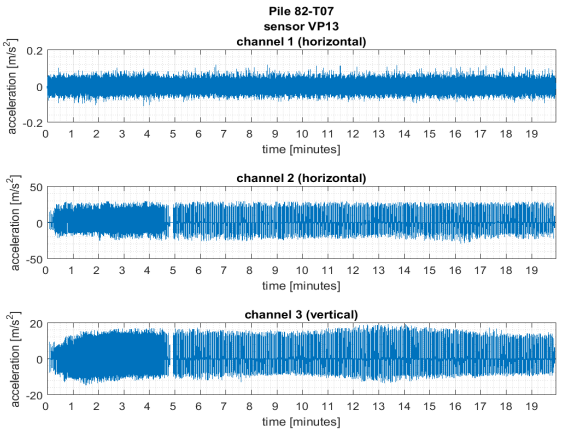

Figure C.27: Accelerations recorded by sensor VP013

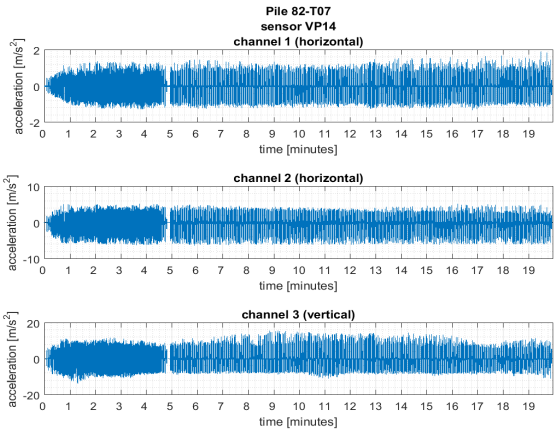

Figure C.28: Accelerations recorded by sensor VP014

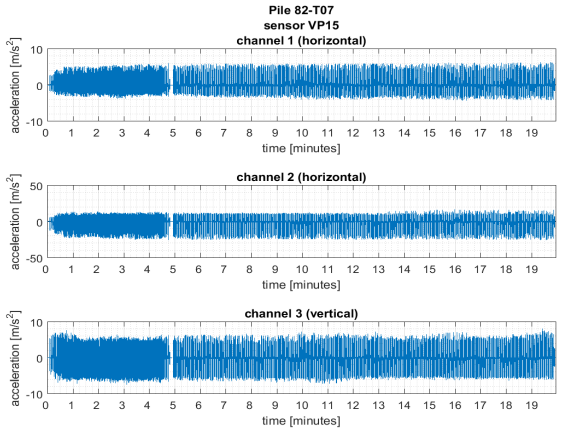

Figure C.29: Accelerations recorded by sensor VP015

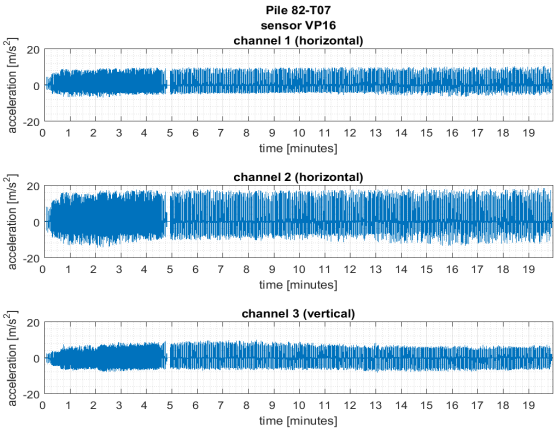

Figure C.30: Accelerations recorded by sensor VP016

D

Vibrations frequency spectra

Impact pile driving

Pile 79B_T02

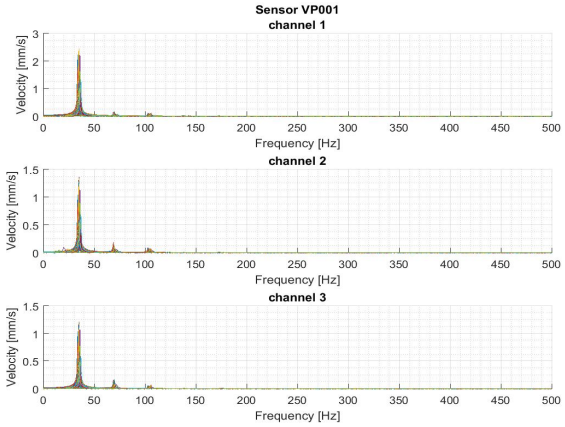

Figure D.1: Frequency domain for sensor VP001

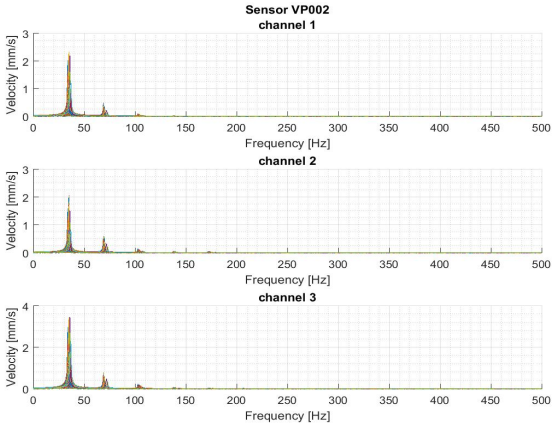

Figure D.2: Frequency domain for sensor VP002

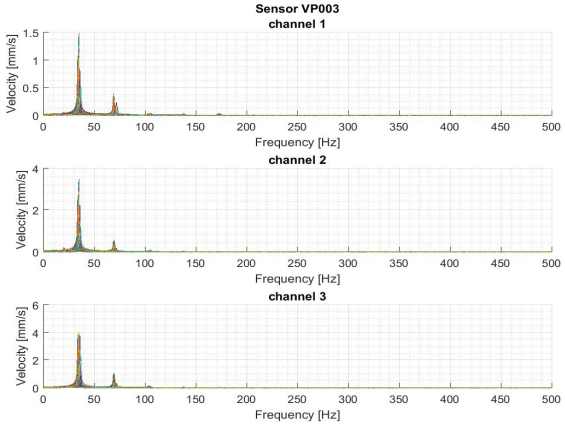

Figure D.3: Frequency domain for sensor VP003

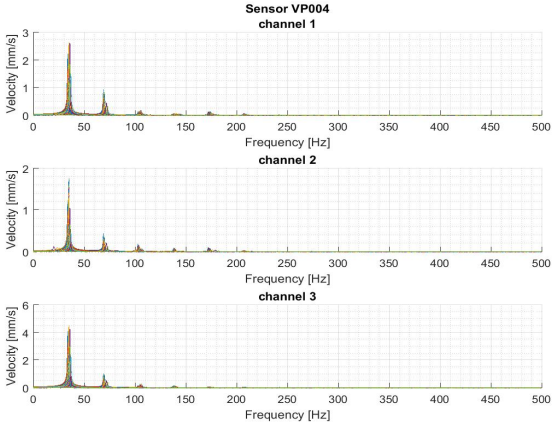

Figure D.4: Frequency domain for sensor VP004

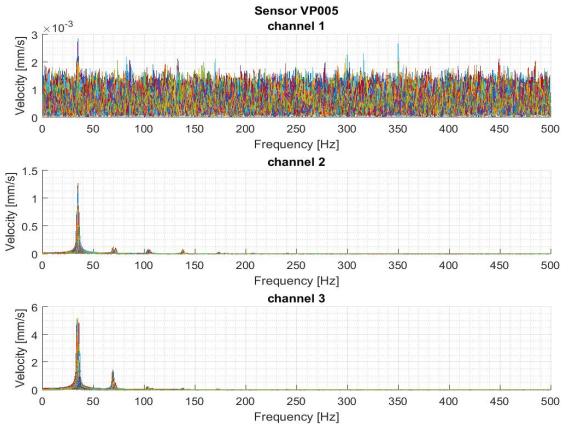

Figure D.5: Frequency domain for sensor VP005

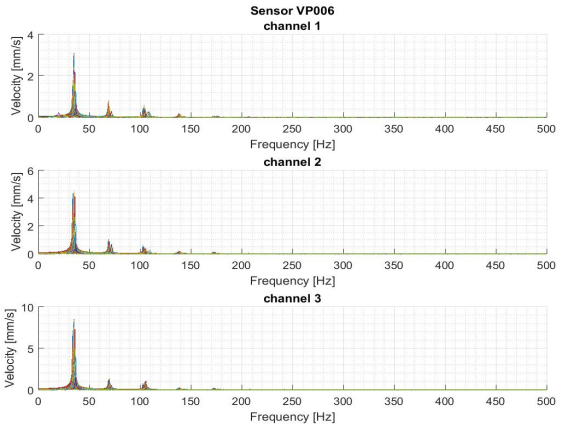

Figure D.6: Frequency domain for sensor VP006

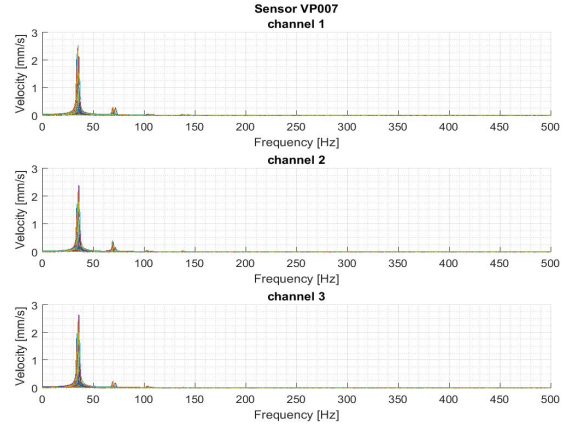

Figure D.7: Frequency domain for sensor VP007

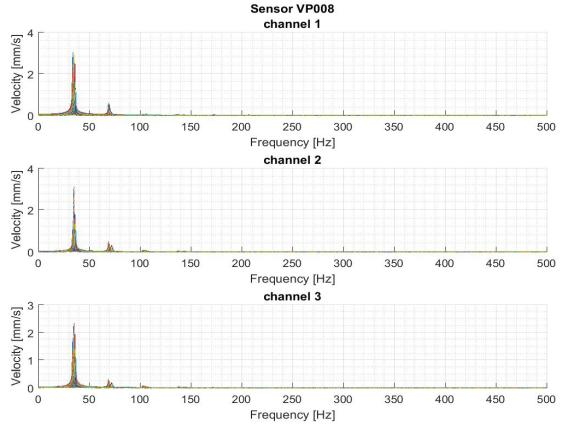

Figure D.8: Frequency domain for sensor VP008

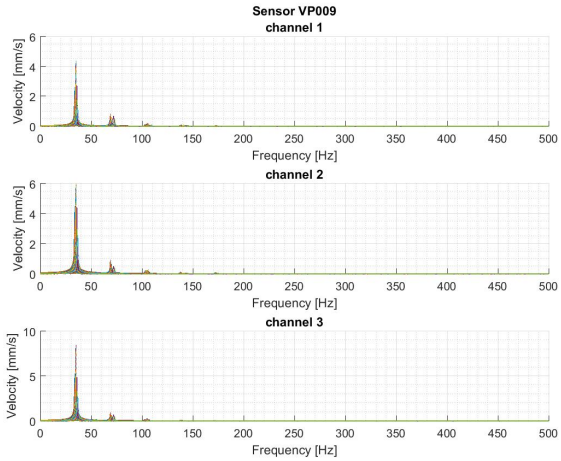

Figure D.9: Frequency domain for sensor VP009

Pile 82_T07

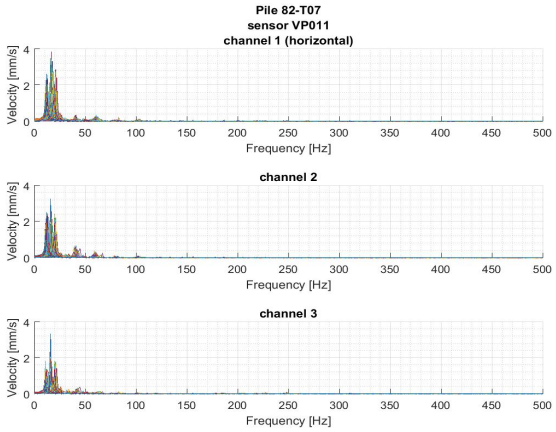

Figure D.10: Frequency domain for sensor VP011

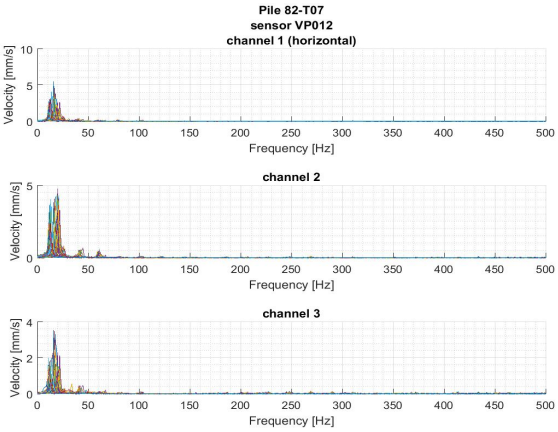

Figure D.11: Frequency domain for sensor VP012

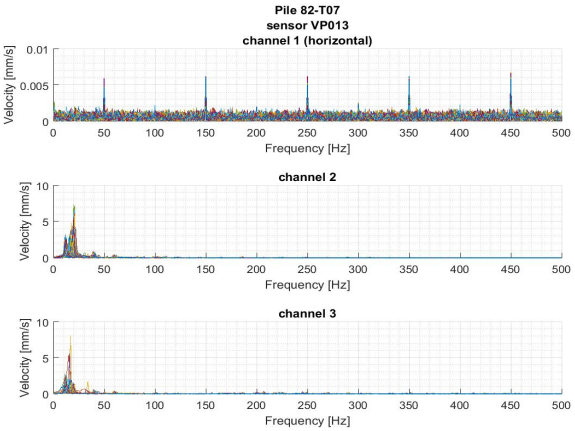

Figure D.12: Frequency domain for sensor VP013

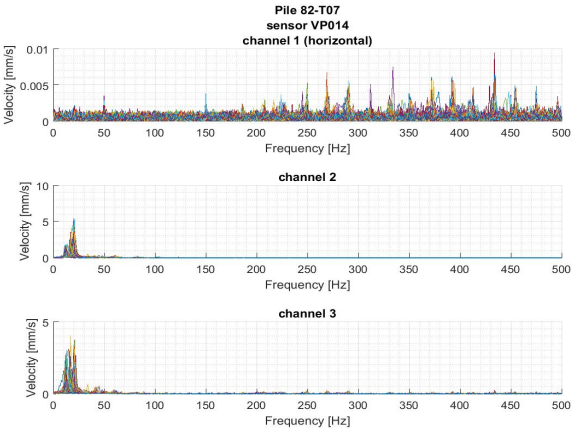

Figure D.13: Frequency domain for sensor VP014

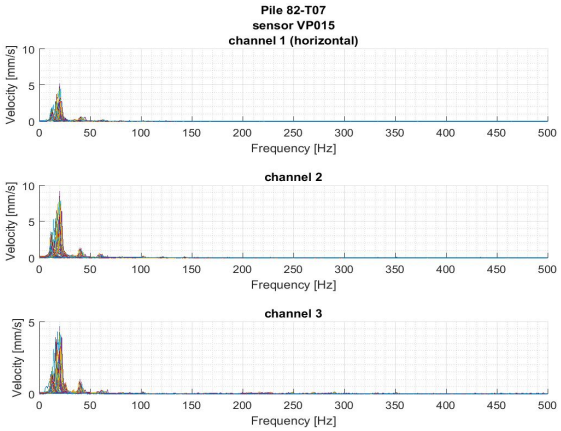

Figure D.14: Frequency domain for sensor VP015

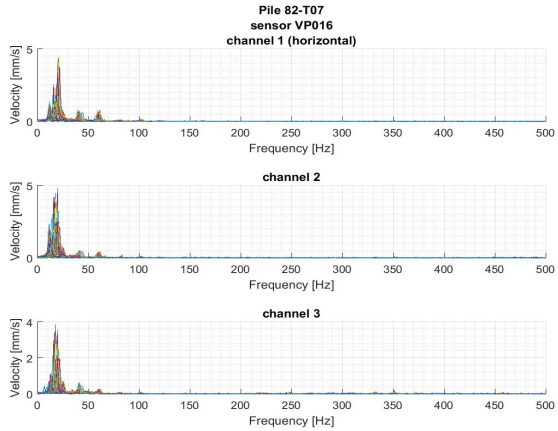

Figure D.15: Frequency domain for sensor VP016

Impact pile driving

Pile 79B_T02

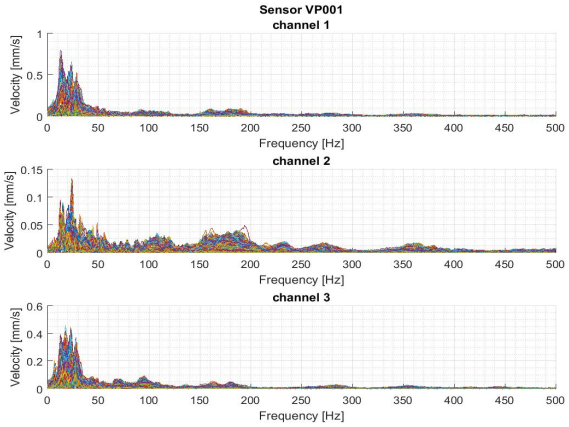

Figure D.16: Frequency domain for sensor VP001

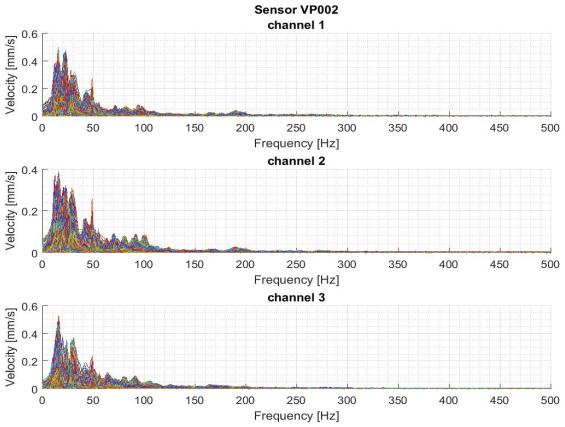

Figure D.17: Frequency domain for sensor VP002

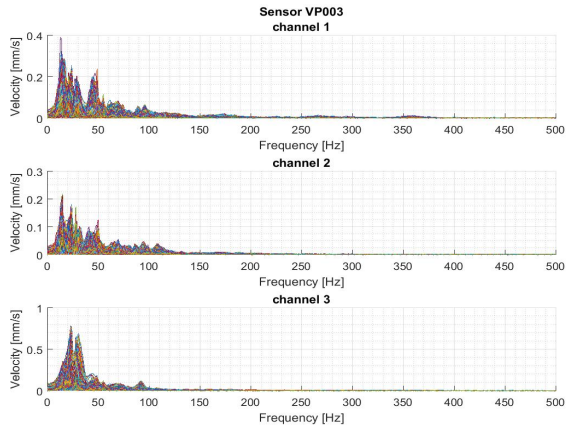

Figure D.18: Frequency domain for sensor VP003

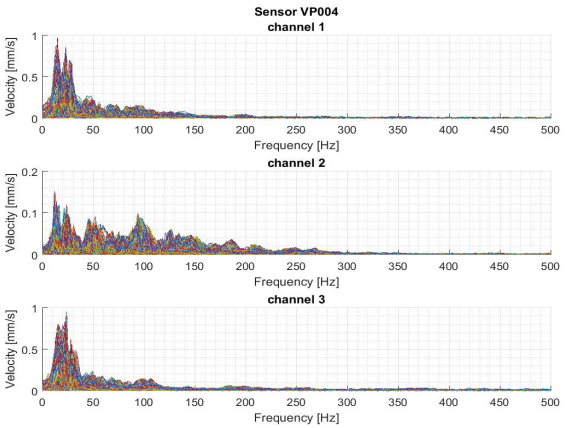

Figure D.19: Frequency domain for sensor VP004

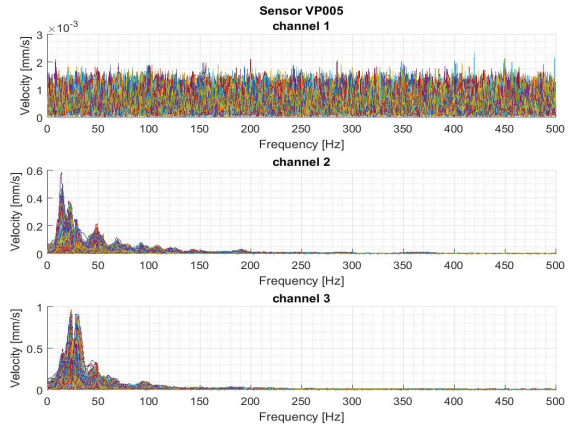

Figure D.20: Frequency domain for sensor VP005

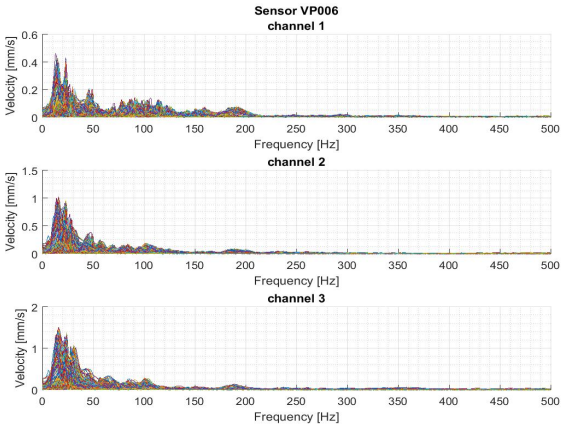

Figure D.21: Frequency domain for sensor VP006

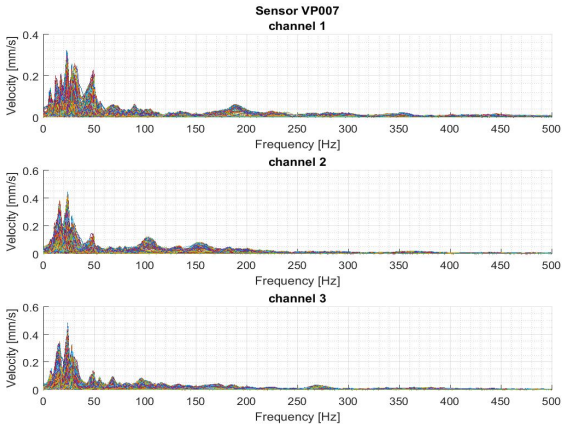

Figure D.22: Frequency domain for sensor VP007

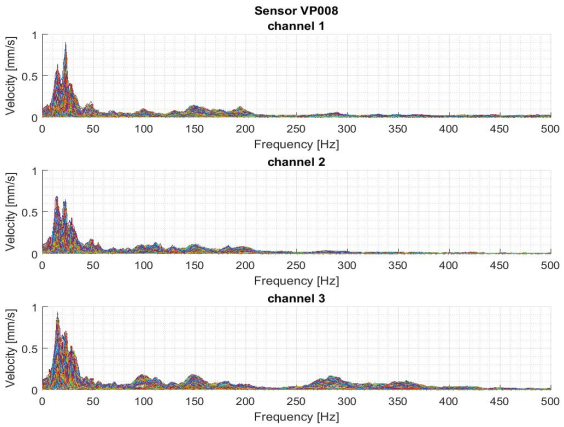

Figure D.23: Frequency domain for sensor VP008

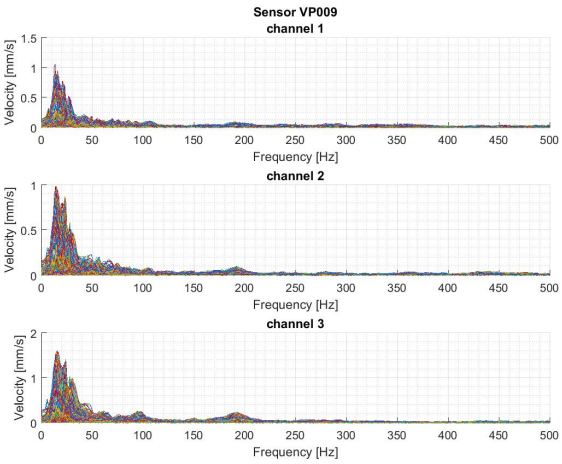

Figure D.24: Frequency domain for sensor VP009

Pile 82_T07

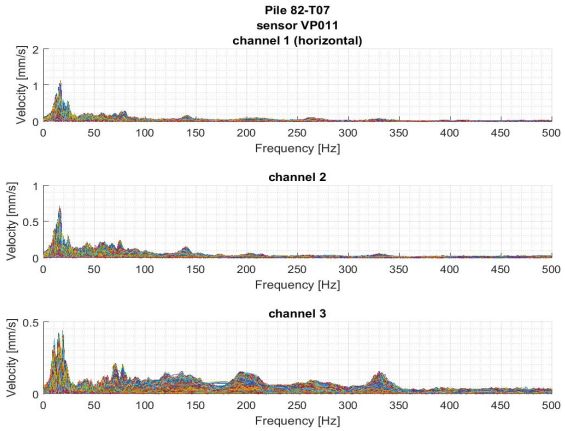

Figure D.25: Frequency domain for sensor VP011

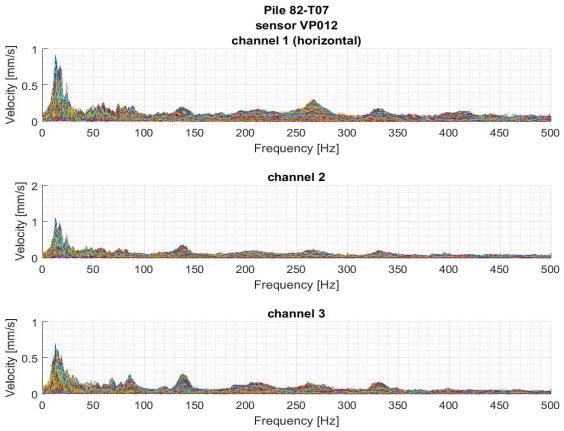

Figure D.26: Frequency domain for sensor VP012

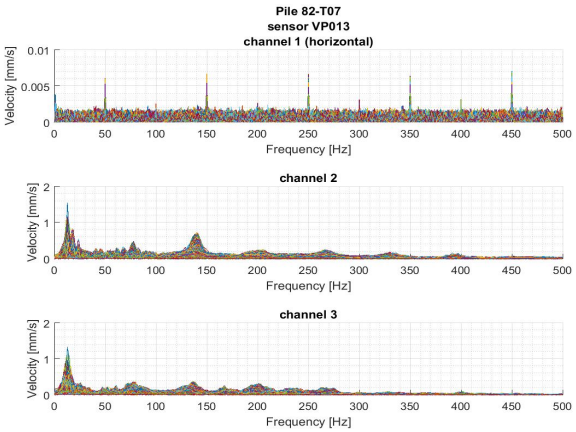

Figure D.27: Frequency domain for sensor VP013

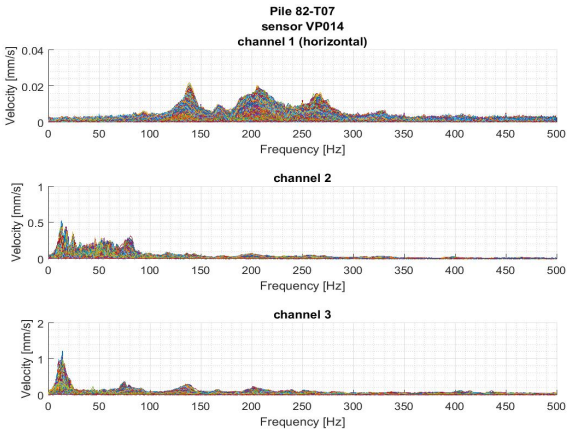

Figure D.28: Frequency domain for sensor VP014

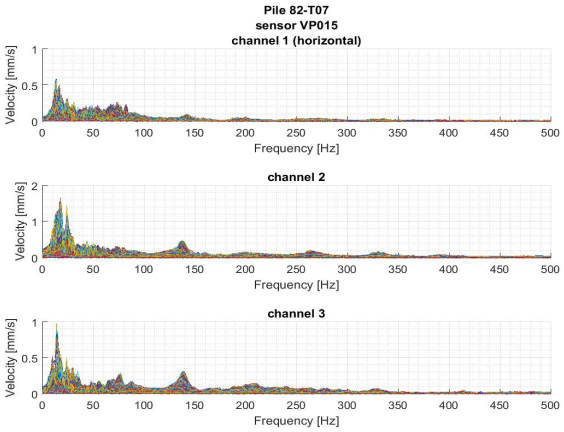

Figure D.29: Frequency domain for sensor VP015

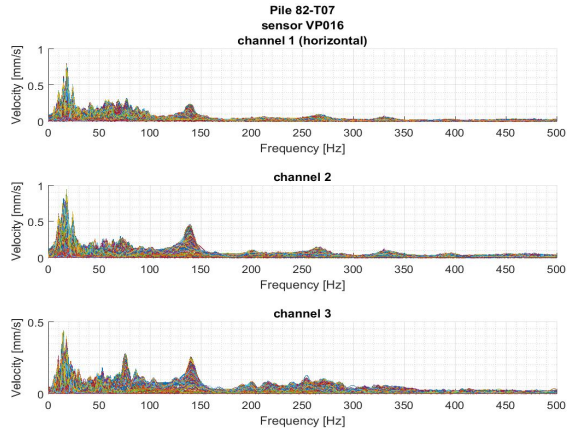

Figure D.30: Frequency domain for sensor VP016

E

CPT profiles

CPTs recorded around pile 79B_T02

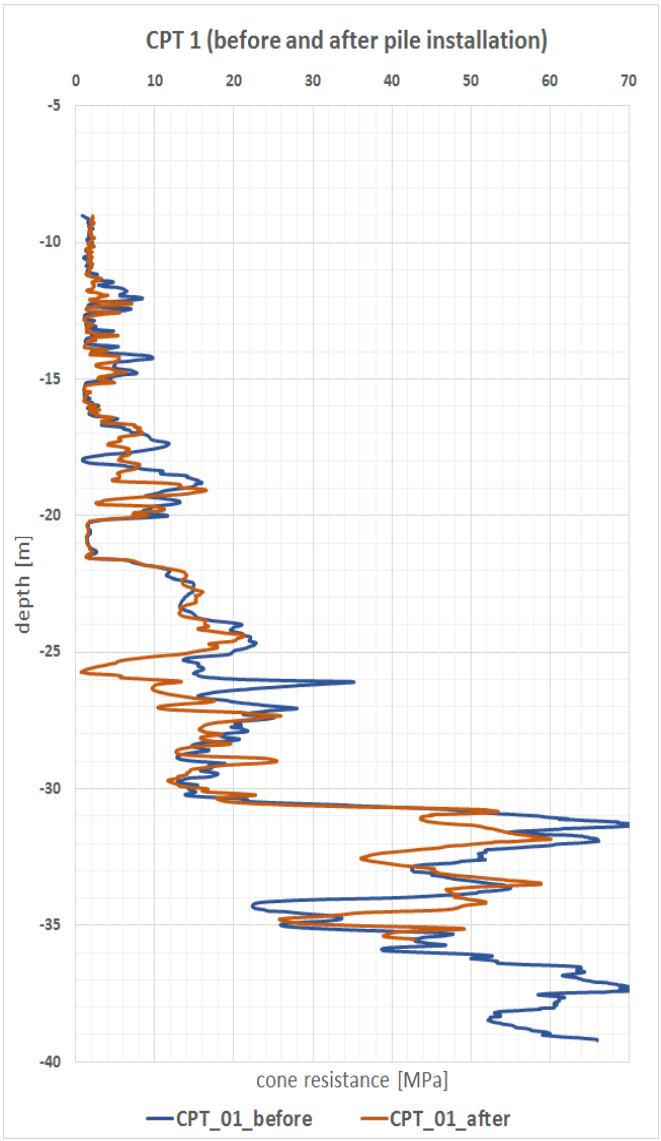

Figure E.1: CPT01 before and after pile installation

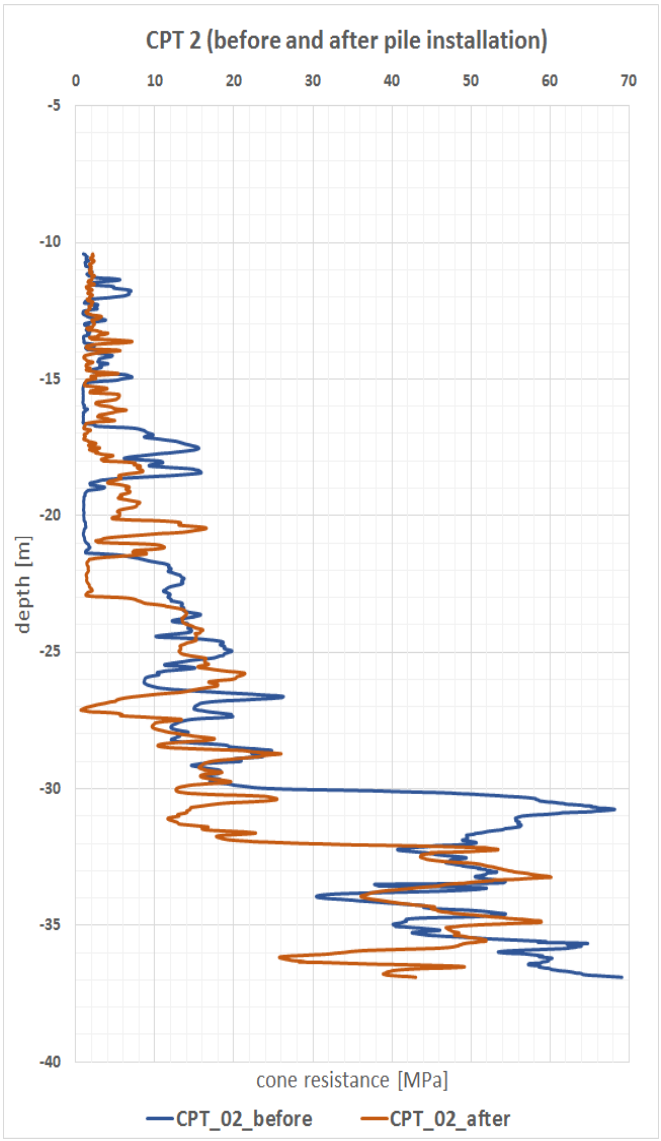

Figure E.2: CPT02 before and after pile installation

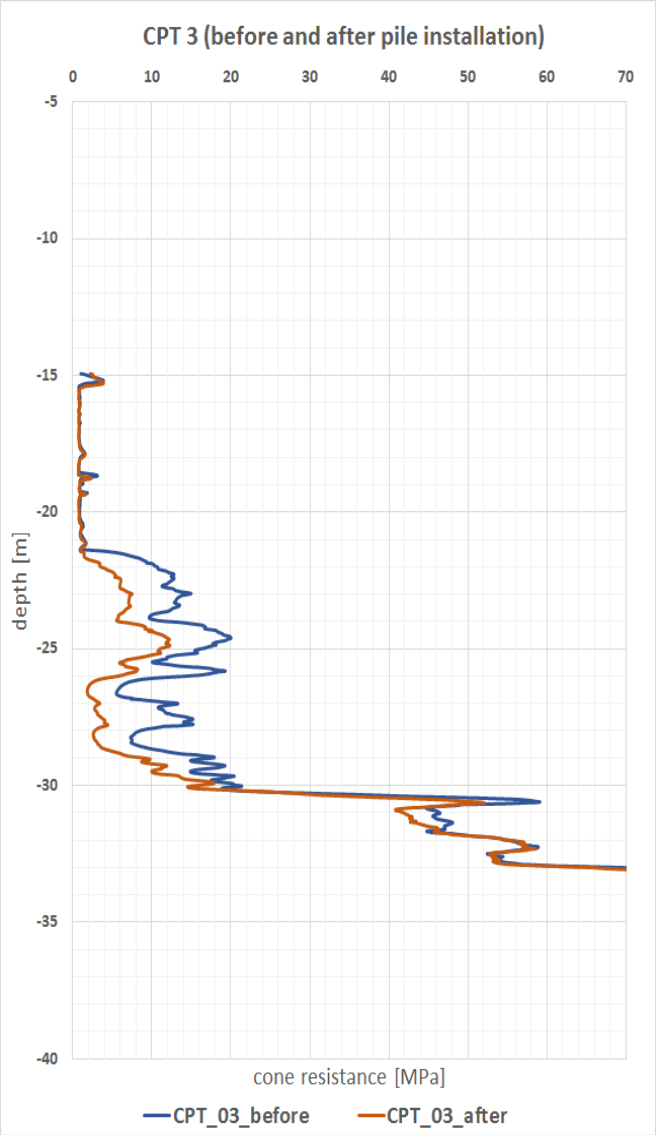

Figure E.3: CPT03 before and after pile installation

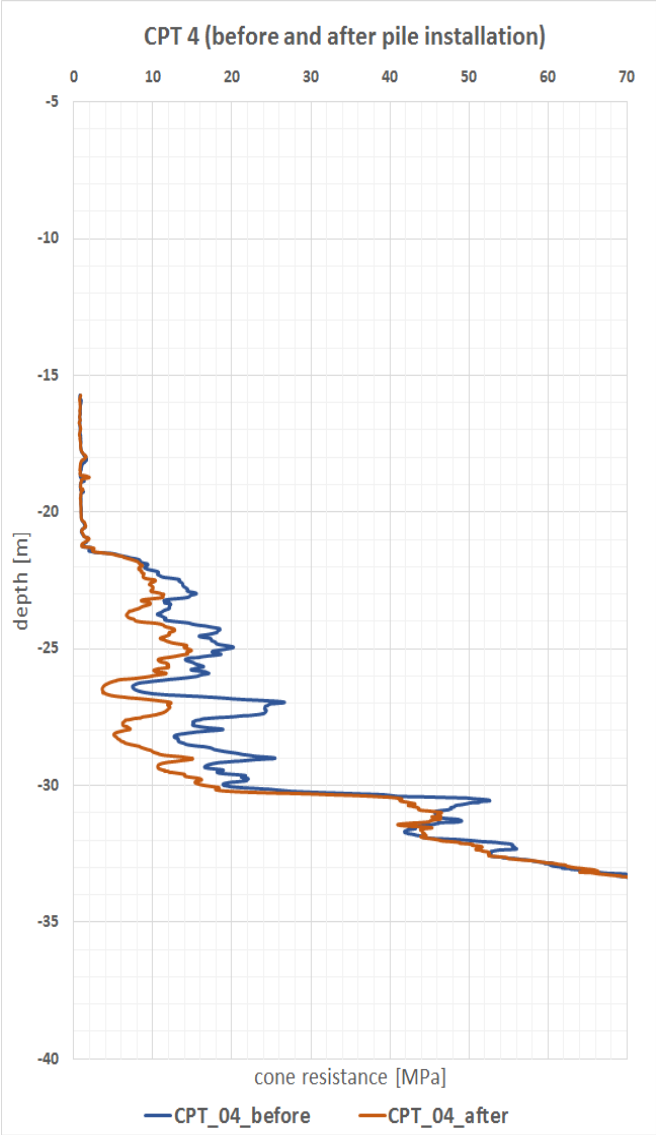

Figure E.4: CPT04 before and after pile installation

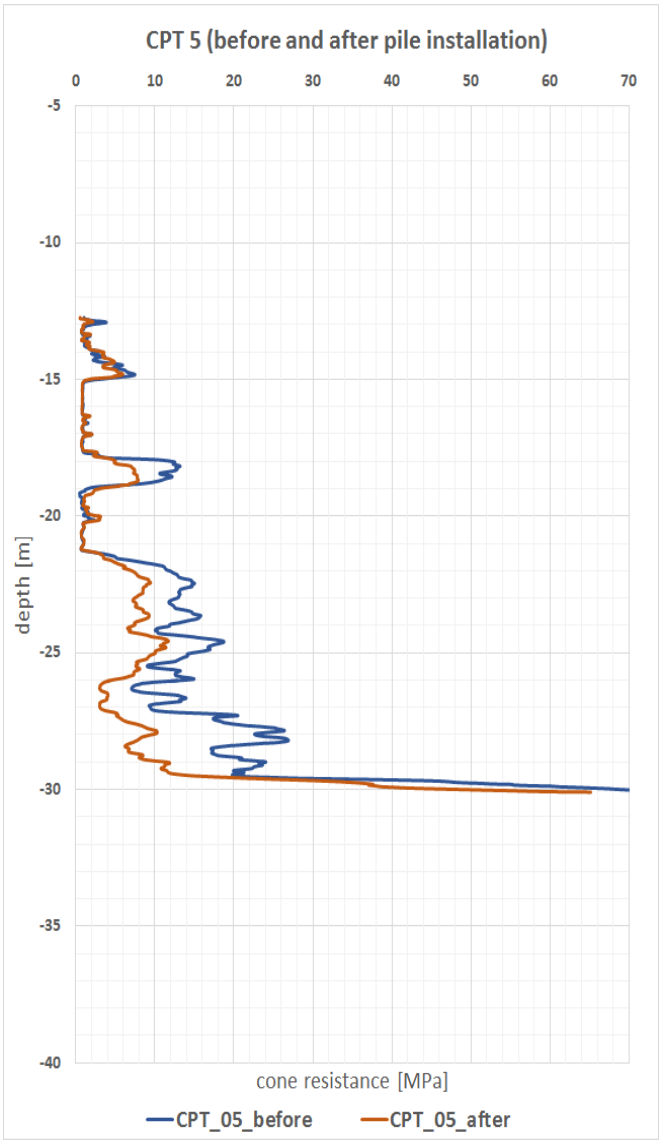

Figure E.5: CPT05 before and after pile installation

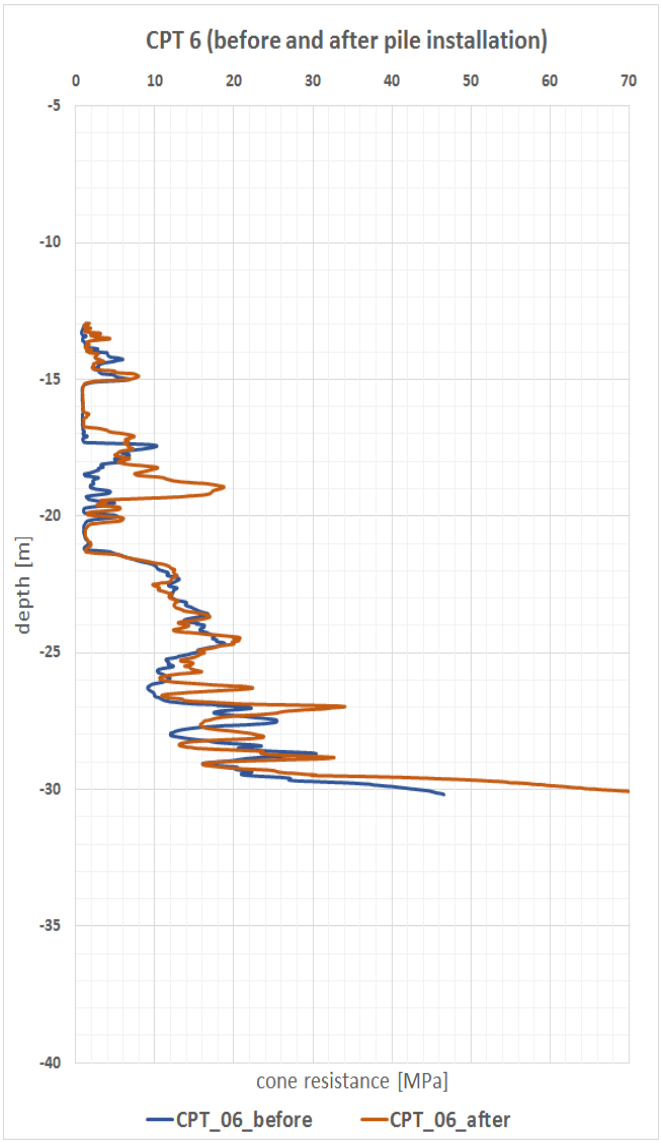

Figure E.6: CPT06 before and after pile installation

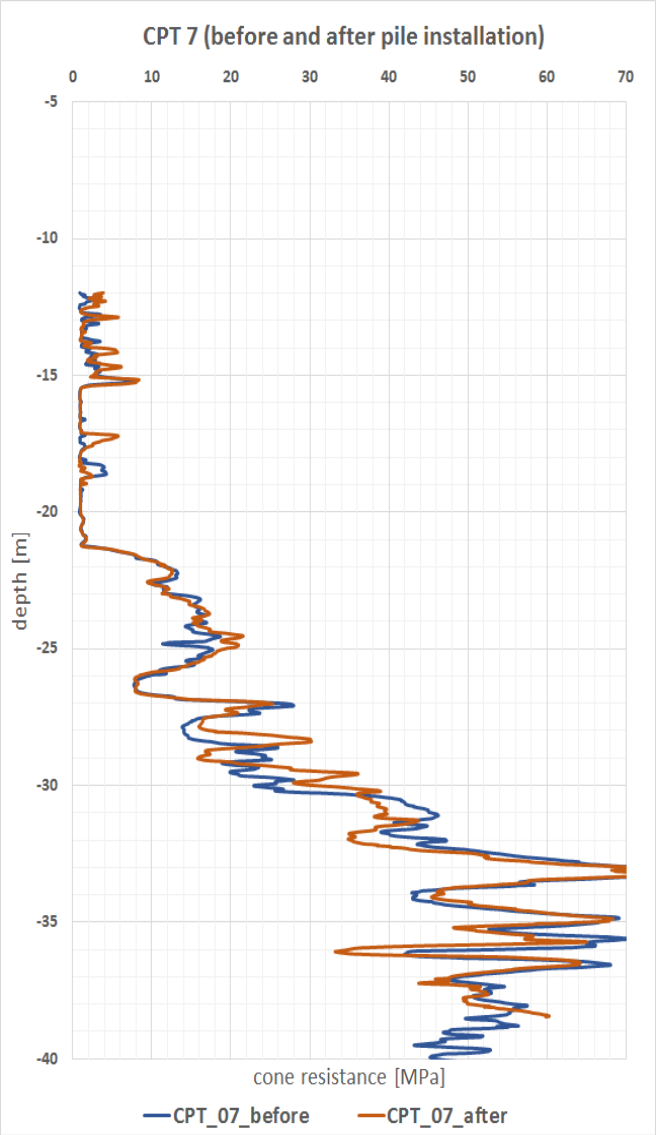

Figure E.7: CPT07 before and after pile installation

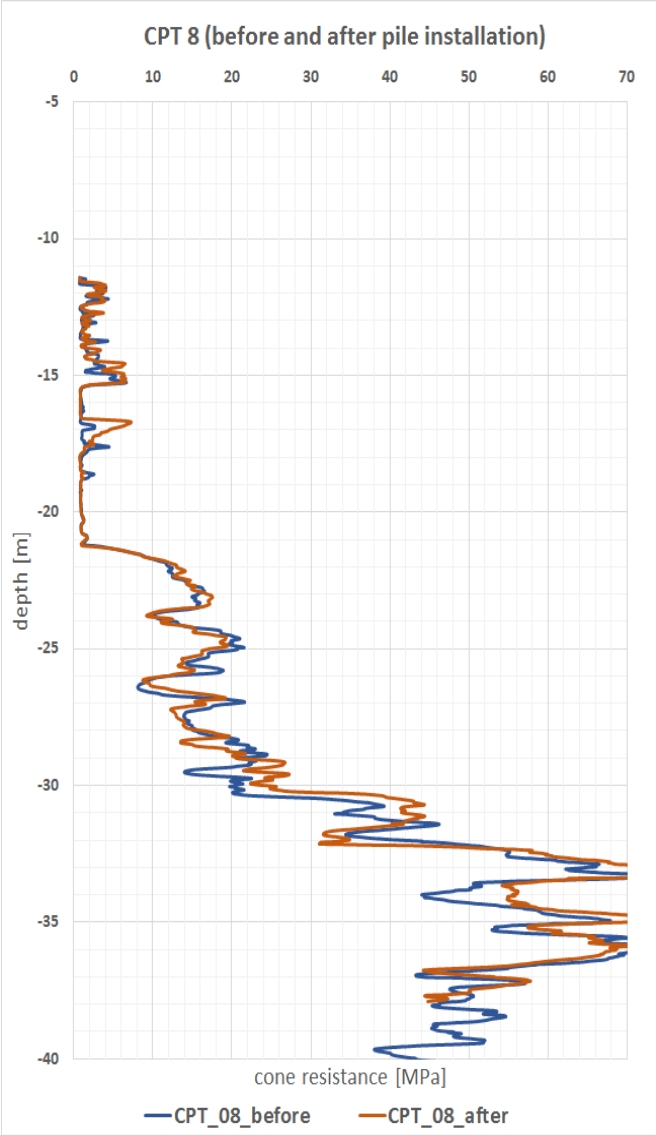

Figure E.8: CPT08 before and after pile installation

CPTs recorded around pile 82_T07

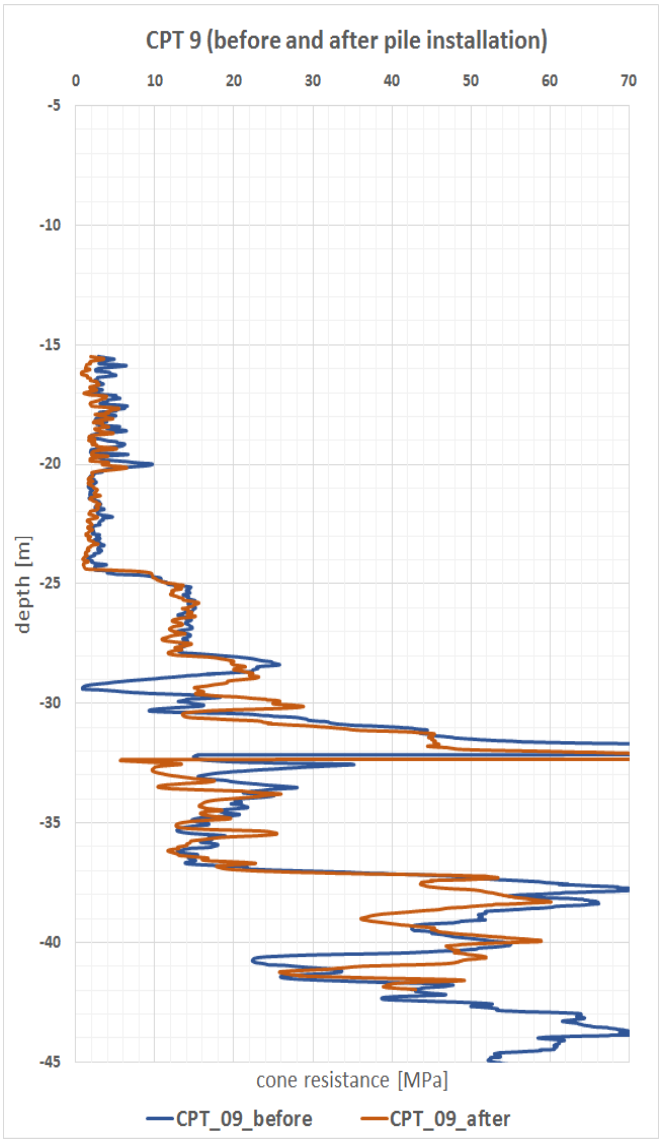

Figure E.9: CPT09 before and after pile installation

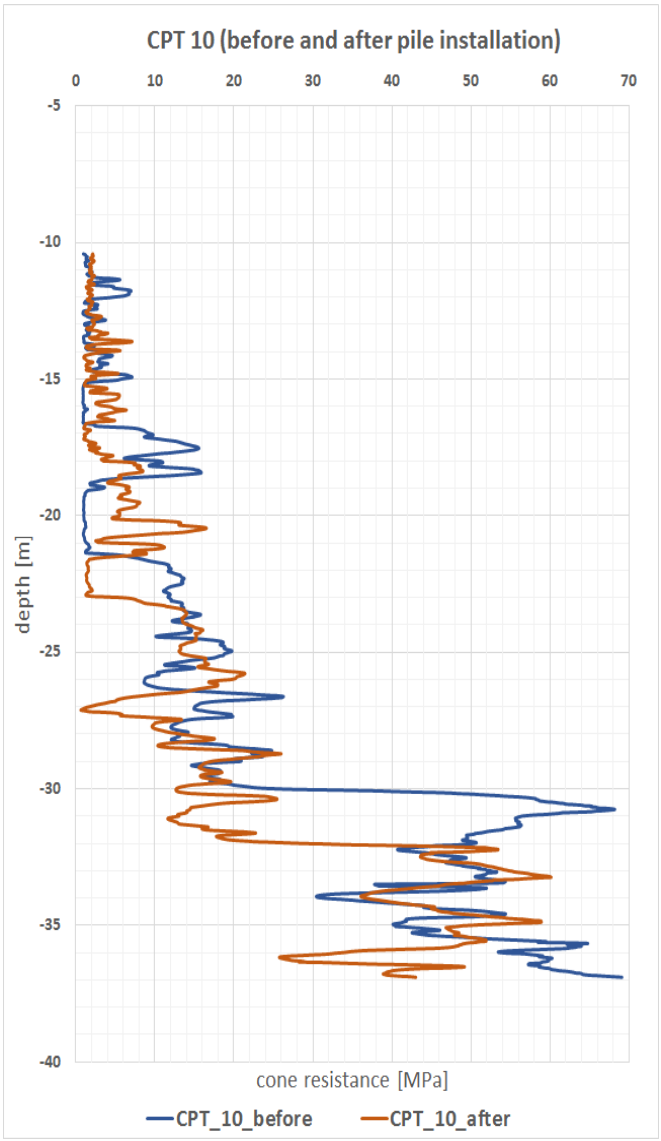

Figure E.10: CPT10 before and after pile installation

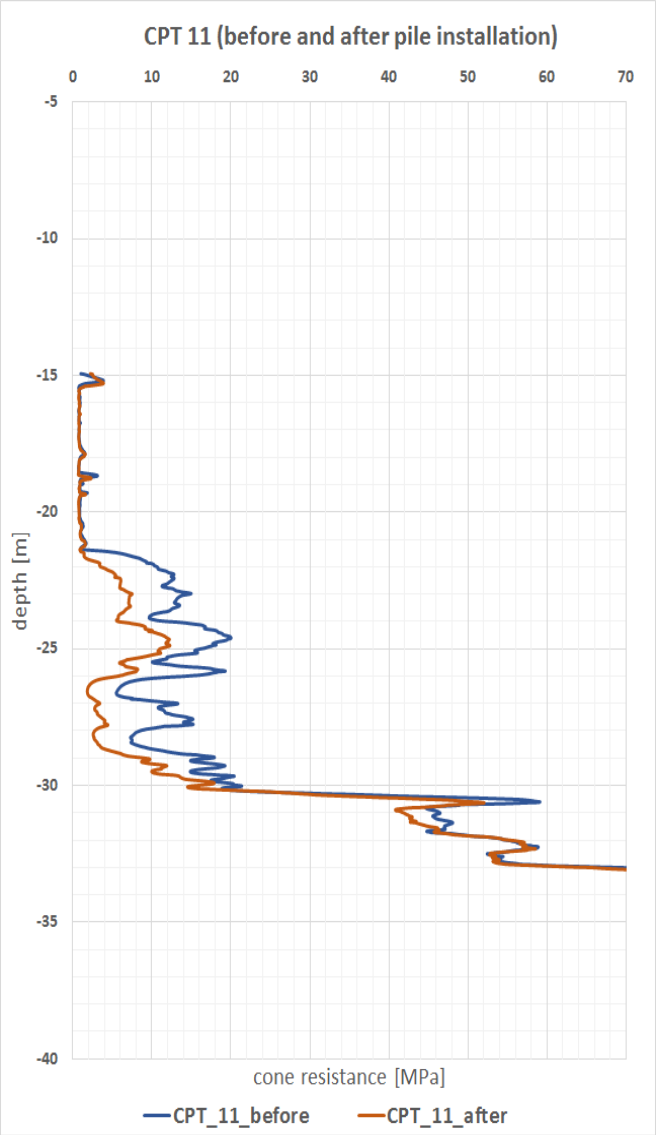

Figure E.11: CPT11 before and after pile installation

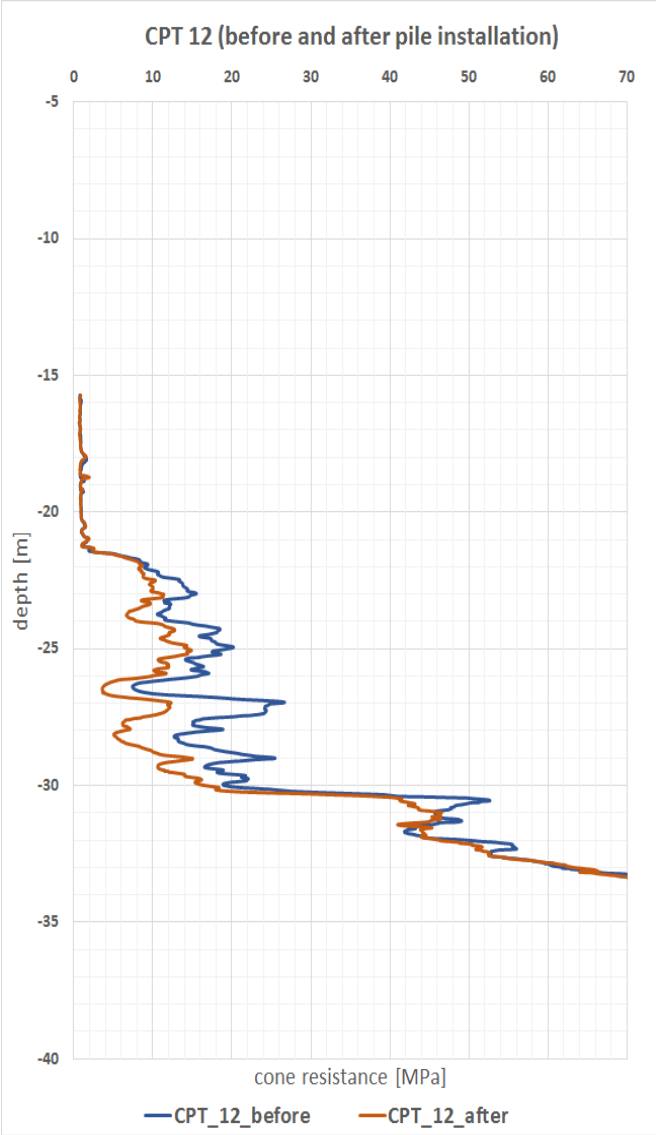

Figure E.12: CPT12 before and after pile installation

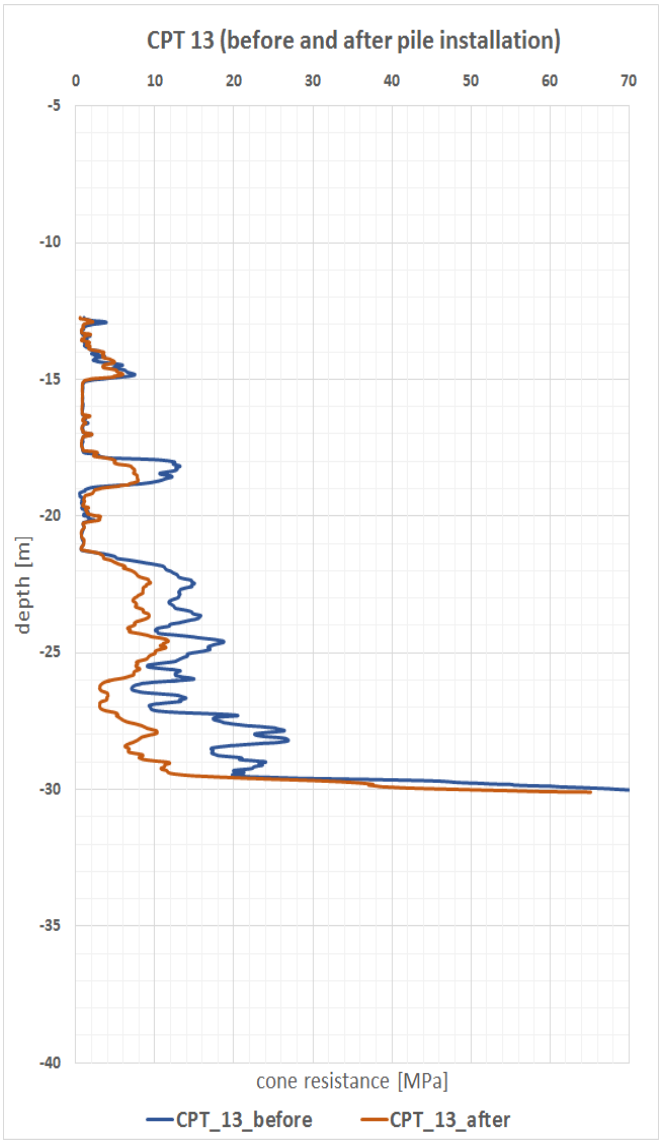

Figure E.13: CPT13 before and after pile installation

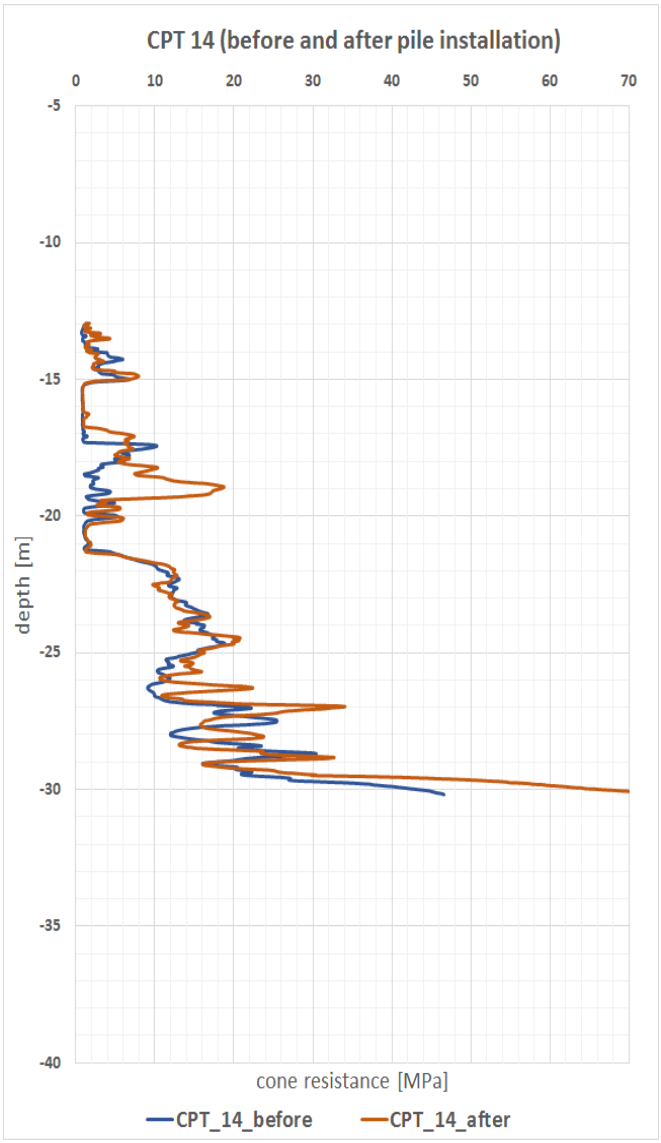

Figure E.14: CPT14 before and after pile installation

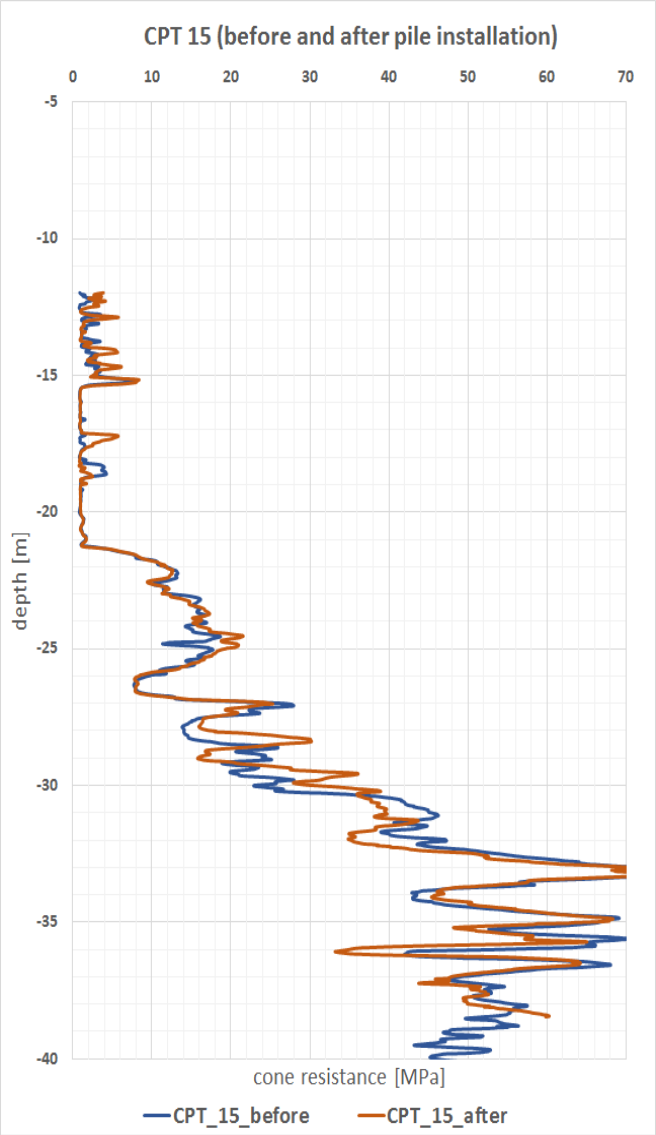

Figure E.15: CPT15 before and after pile installation

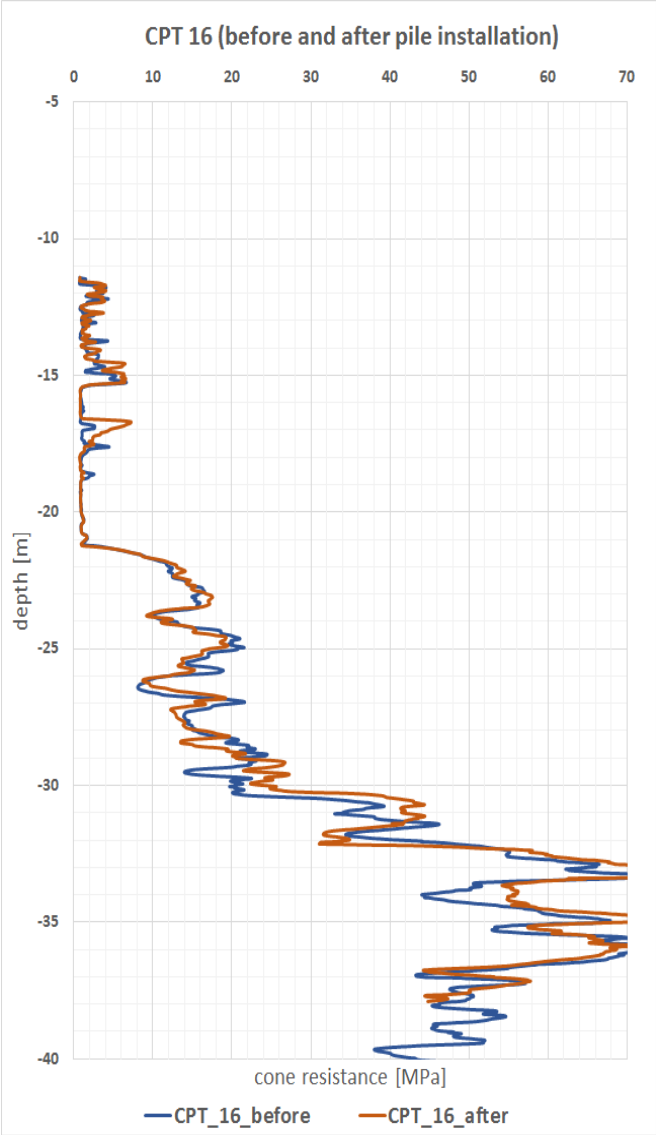

Figure E.16: CPT16 before and after pile installation

F

Relative density

Relative density calculated based on CPTs recorded around pile 79B_T02

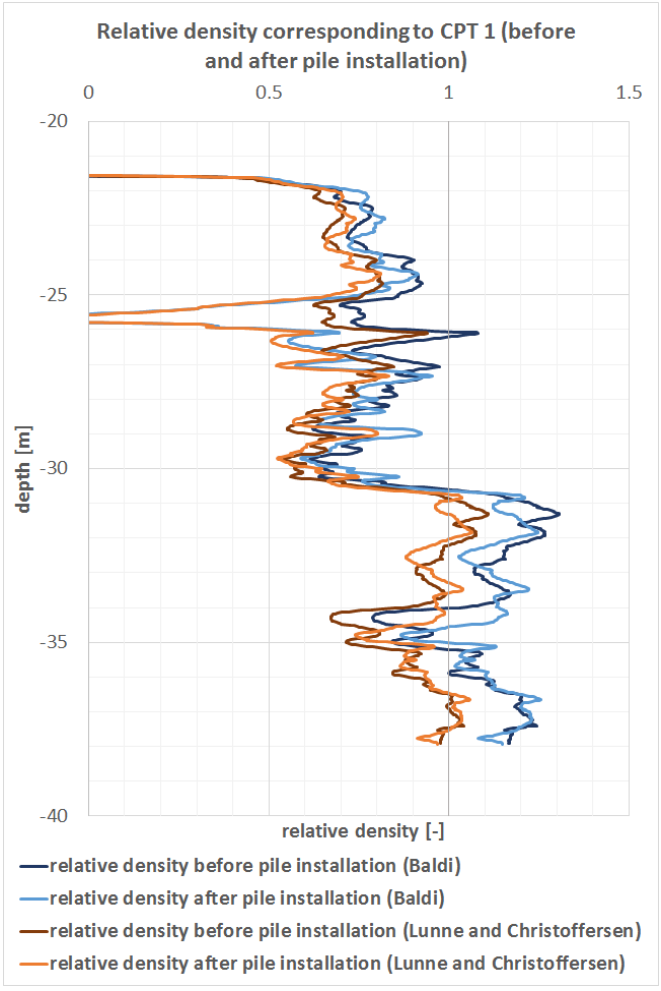

Figure F.1: Relative density calculated from CPT01 before and after pile installation

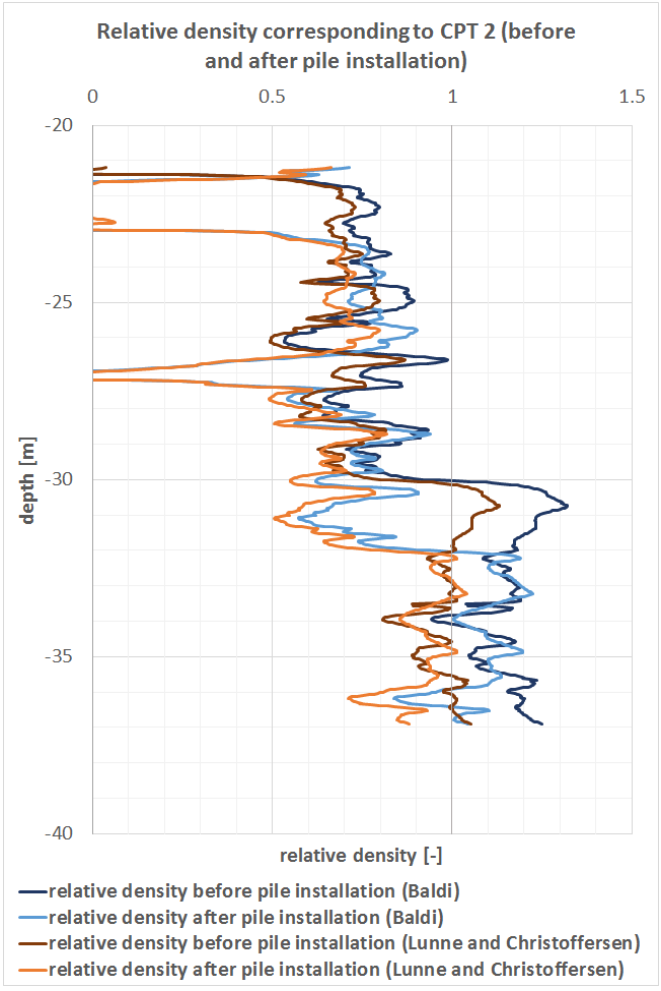

Figure F.2: Relative density calculated from CPT02 before and after pile installation

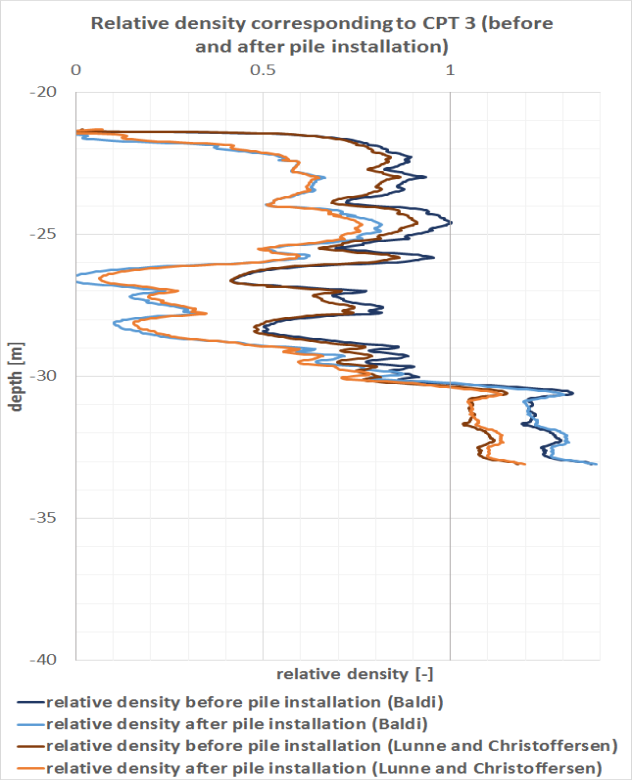

Figure F.3: Relative density calculated from CPT03 before and after pile installation

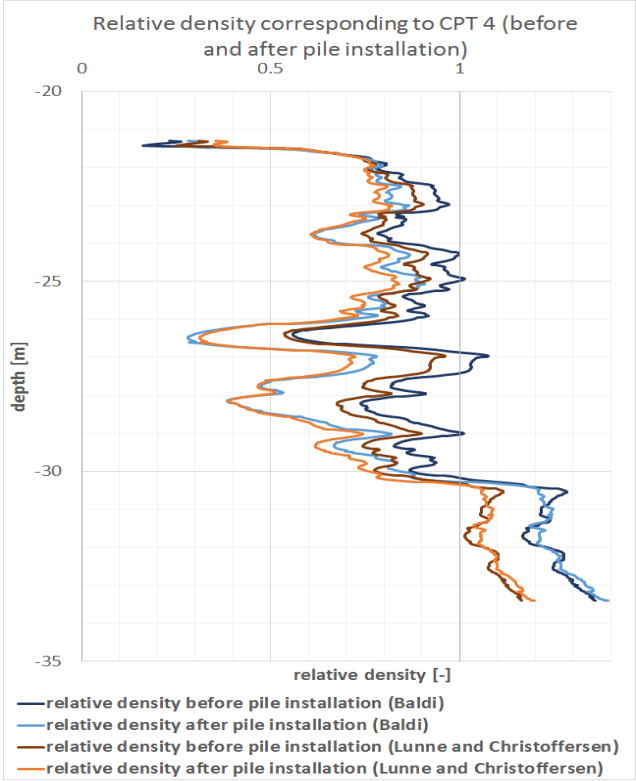

Figure F.4: Relative density calculated from CPT04 before and after pile installation

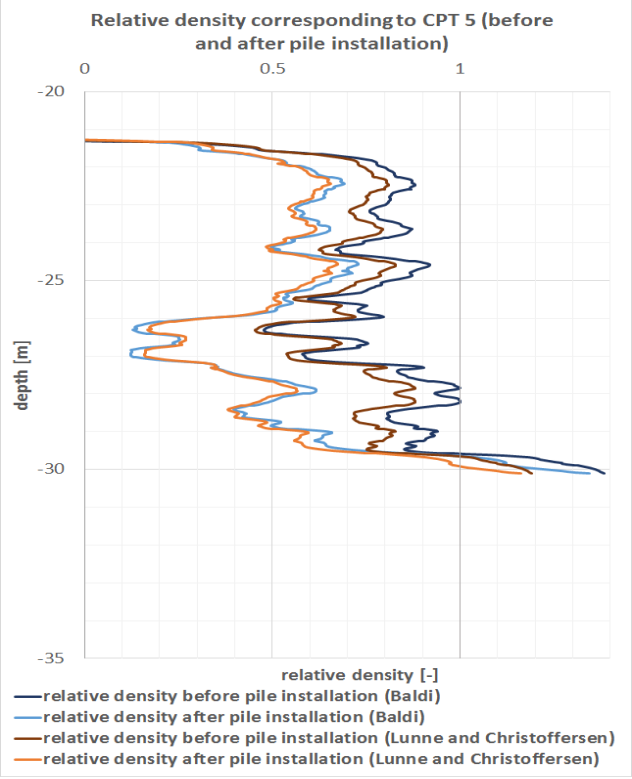

Figure F.5: Relative density calculated from CPT05 before and after pile installation

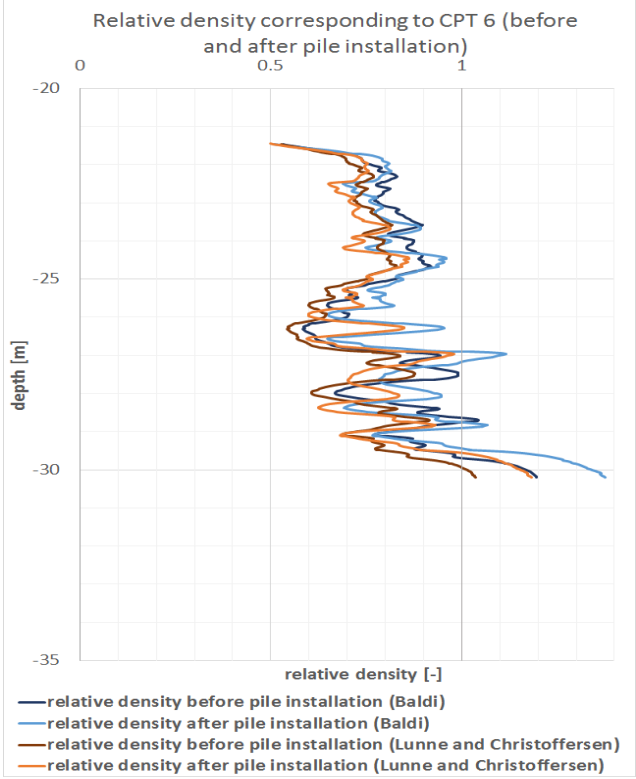

Figure F.6: Relative density calculated from CPT06 before and after pile installation

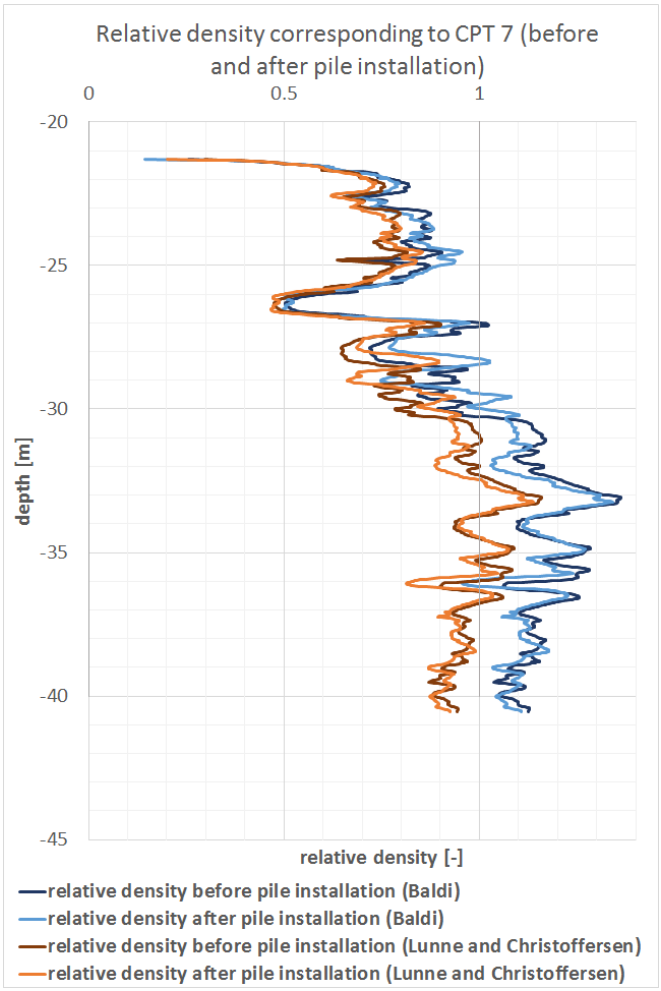

Figure F.7: Relative density calculated from CPT07 before and after pile installation

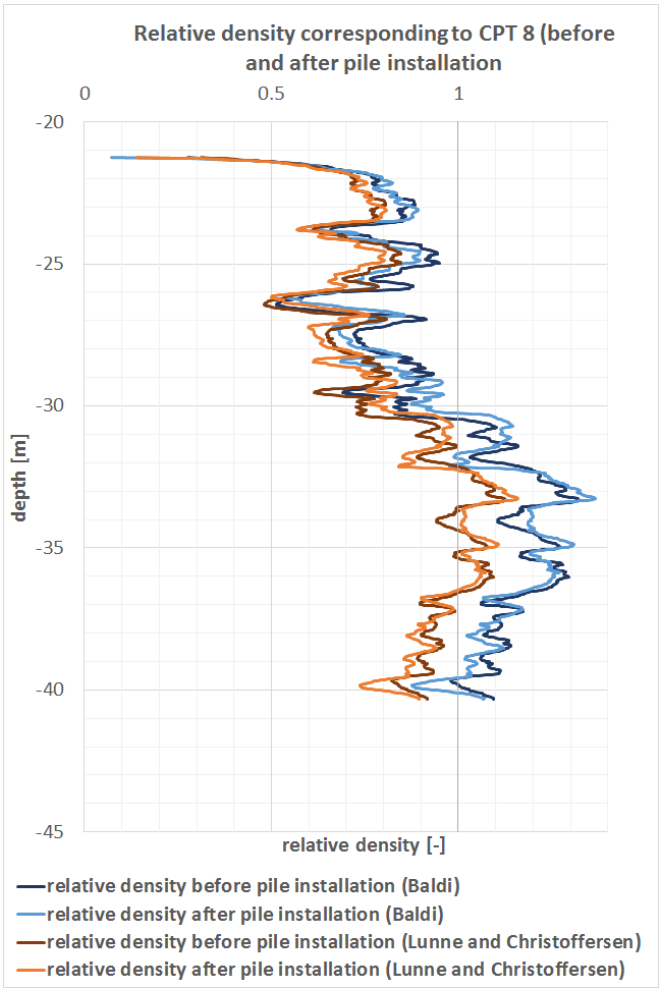

Figure F.8: Relative density calculated from CPT08 before and after pile installation

Relative density calculated based on CPTs recorded around pile 82_T07

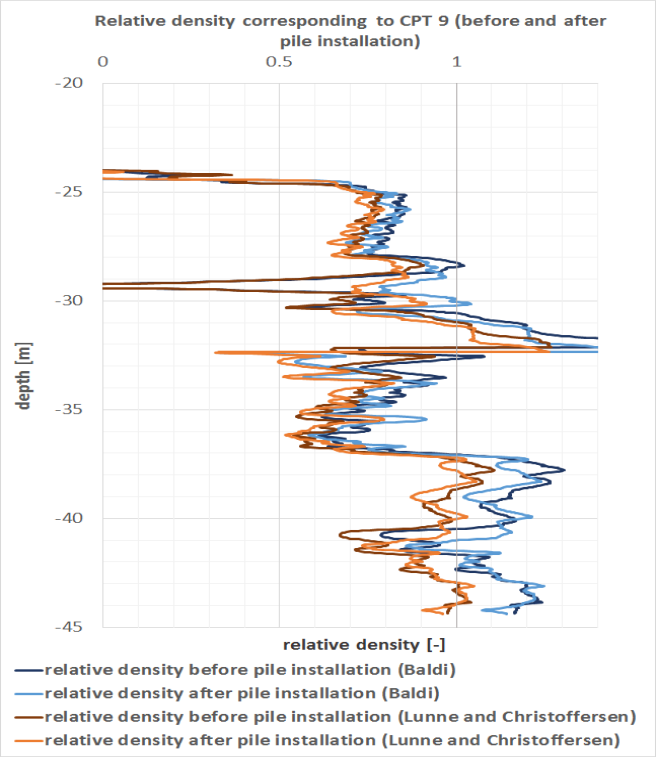

Figure F.9: Relative density calculated from CPT09 before and after pile installation

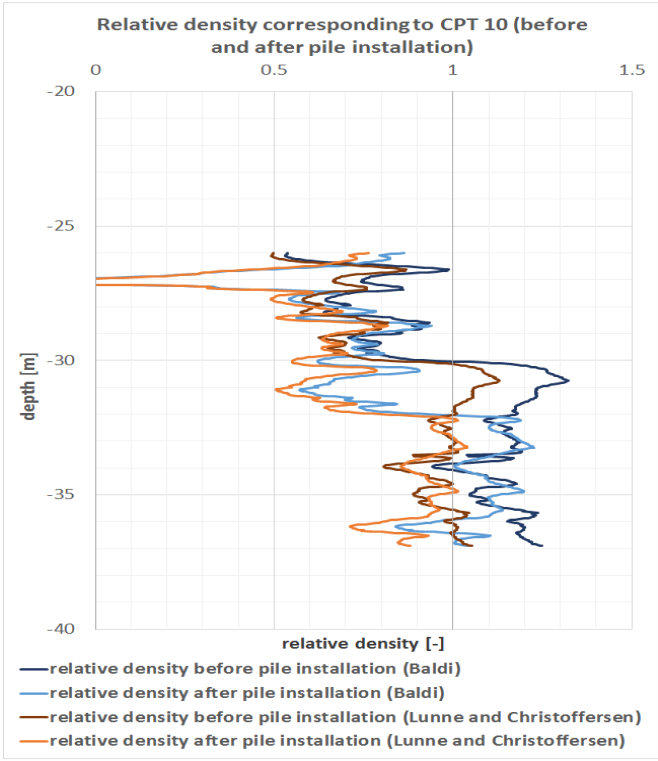

Figure F.10: Relative density calculated from CPT10 before and after pile installation

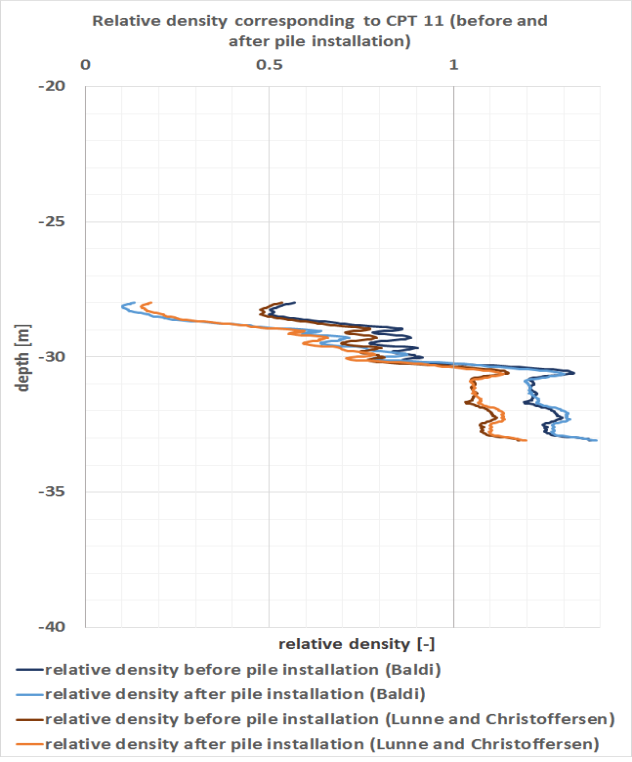

Figure F.11: Relative density calculated from CPT11 before and after pile installation

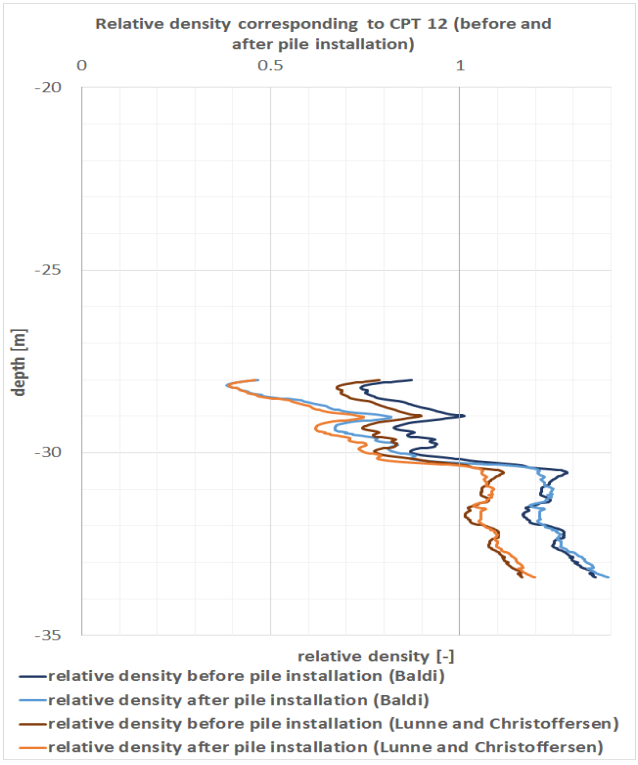

Figure F.12: Relative density calculated from CPT12 before and after pile installation

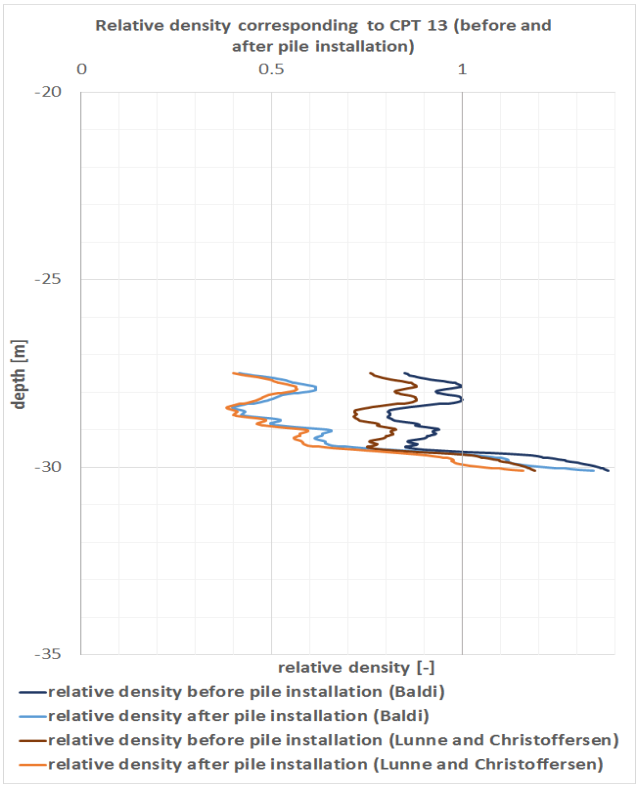

Figure F.13: Relative density calculated from CPT13 before and after pile installation

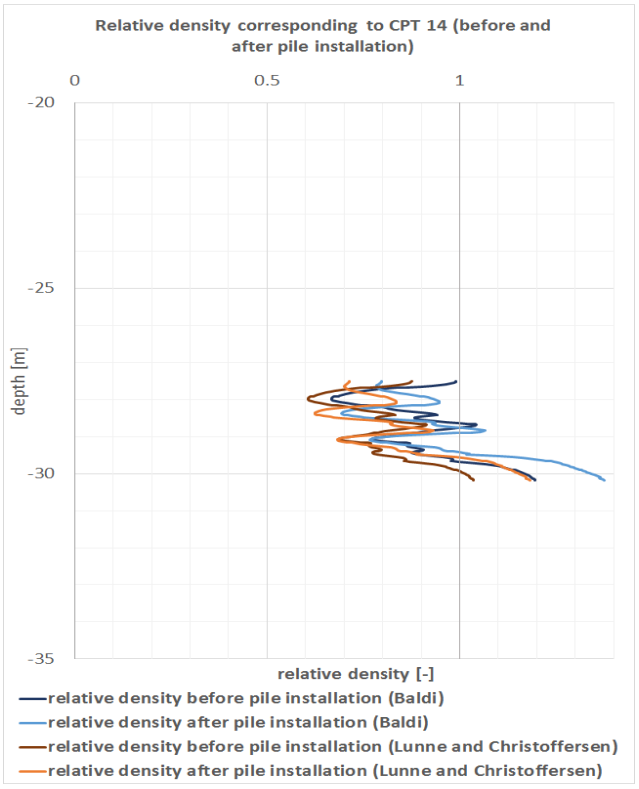

Figure F.14: Relative density calculated from CPT10 before and after pile installation

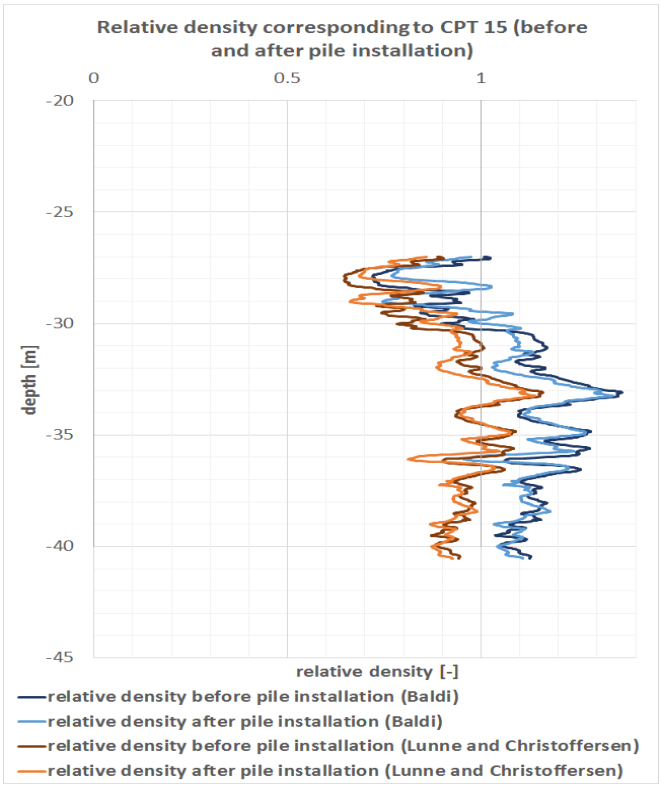

Figure F.15: Relative density calculated from CPT15 before and after pile installation

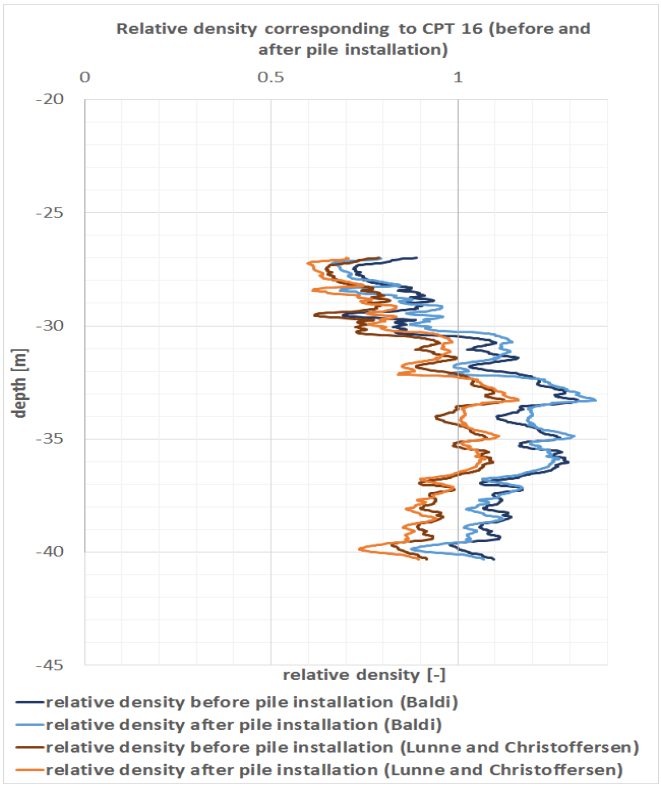

Figure F.16: Relative density calculated from CPT16 before and after pile installation